Department of Physics and Astronomy
Heidelberg University

Diploma Thesis
in Physics

submitted by
Daniel Schmidt
born in Saarbrücken
2010

Neutrinos and Dark Matter Within an Extended Zee-Babu Model

This diploma thesis was carried out by Daniel Schmidt
at the
Max-Planck-Institut für Kernphysik
Heidelberg
under the supervision of
Prof. Dr. Manfred Lindner

Fakultät für Physik und Astronomie
Ruprecht-Karls-Universität Heidelberg

Diplomarbeit
Im Studiengang Physik

vorgelegt von
Daniel Schmidt
geboren in Saarbrücken
2010

Neutrinos und Dunkle Materie in einem erweiterten Zee-Babu Model

Diese Diplomarbeit wurde von Daniel Schmidt
ausgeführt am
Max-Planck-Institut für Kernphysik
Heidelberg
unter der Betreuung von
Herrn Prof. Dr. Manfred Lindner

Neutrinos and Dark Matter Within an Extended Zee-Babu Model:

Extensions of the Zee-Babu model are investigated to find a common framework for the neutrino mass problem and the dark matter issue of the universe.
The particle content of the model is enlarged with a complex scalar singlet φ and a right-handed Majorana neutrino N_R which serves as a particle dark matter candidate. With a specific baryon (B) minus lepton (L) number for φ, the model enjoys a $U(1)_{B-L}$ symmetry.
In a first scenario, the $U(1)_{B-L}$ is gauged. To prevent $[U(1)_{B-L}]^3$ gauge anomalies, N_R is a must. In a second scenario, a $\mathbb{Z}_4$ symmetry is imposed. $U(1)_{B-L}$ is global, i.e., a Majoron enters into the theory after spontaneous symmetry breaking.
In both scenarios, light neutrino masses and the dark matter mass are generated at the $U(1)_{B-L}$ symmetry breaking scale.
The required thermal relic abundance of N_R is predominantly produced through the Higgs portal.
It is shown that N_R could be directly detected.
To complete, the verification of the model at the LHC is discussed.

Neutrinos und Dunkle Materie in einem erweiterten Zee-Babu Model:

Erweiterungen des Zee-Babu Models werden untersucht um das Problem der Neutrinomassen und der dunklen Materie im Universum in einem gemeinsamen Rahmen zu lösen.
Der Teilcheninhalt des Models wird mit einem komplexen sklaren Singlet φ und einem rechtshändigen Majorana Neutrino N_R, das als Kandidat für dunkle Materie dient, vergrößert. Infolge einer speziellen Baryon (B) minus Lepton (L) Zahl für φ hat das Model eine $U(1)_{B-L}$ Symmetrie.
In einer ersten Erweiterung wird die $U(1)_{B-L}$ Symmetrie geeicht. N_R ist notwendig um $[U(1)_{B-L}]^3$ Eichanomalien zu verhindern. In einer zweiten Erweiterung wird eine $\mathbb{Z}_4$ Symmetry eingeführt. $U(1)_{B-L}$ ist nun eine globale Symmetrie, d.h. nach spontaner Symmetriebrechung tritt ein Majoron in der Theorie auf.
In beiden Erweiterungen werden leichte Neutrinomassen und die Masse der dunklen Materie an der Skala erzeugt, an der die $U(1)_{B-L}$ Symmetrie zusammenbricht.
Die erforderliche thermische Restmenge an dunkler Materie wird überwiegend durch das Higgs Portal produziert.
Es wird gezeigt, dass N_R direkt nachgewiesen werden kann.
Abschließend wird die Bestätigung des Models am LHC diskutiert.

To My Parents

Rita & Michael Schmidt

Contents

List of Figures

List of Tables

There is a theory which states that if ever anyone discovers exactly what the Universe is for and why it is here, it will instantly disappear and be replaced by something even more bizarre and inexplicable.
-There is another theory which states that this has already happened.

(Douglas Adams, *The Restaurant at the End of the Universe*)

Chapter 1

Introduction

Based on the measured dispersion of the velocities of individual galaxies in the Coma Cluster and applying the virial theorem, the Swiss astronomer Zwicky made a surprising discovery: the mean matter density of the Coma Cluster has to be at least 400 times larger than the one resulting from observed luminous matter. Zwicky conjectured that non-luminous matter, i.e., dark matter, exists in a much larger amount in the universe than luminous matter [19].
Dark matter makes itself felt only by gravitational interactions. Its nature remains unknown. The labeling *matter* suggests that dark matter is made up of particles. But it is possible that the missing matter component of the universe does not consist of particles after all.
The Einstein field equations link the matter content of the universe with the geometry of space time. From this point of view, there are in general two possibilities to explain the missing matter component: either modify the geometry of space time, that is, modify the law of gravity, and consider only normal matter, i.e., baryonic matter, or describe the geometry as usual and change the matter content to involve a dark matter particle.
There have been proposals for modified Newtonian dynamics (MOND) to account for the measured rotation curves of galaxies: considering a galaxy and a massive object in the disk, e.g., a star with circular velocity v_c and distance r from the galactic center. In an equilibrium between the centripetal and the Newtonian gravitational force $\mathbf{F}$, one expects that v_c decreases like $\frac{1}{\sqrt{r}}$ with increasing distance to the center (compare dashed line in figure 1.1), given that the galaxy consists of baryonic matter.
Instead, figure 1.1 reveals that the observed velocity profile is nearly constant for radii r between 8 kpc and 20 kpc. This galaxy rotation problem can be solved by an acceleration constant a_0 which scales with the baryonic mass: if for the absolute value a of the gravitational acceleration $\mathbf{a}$ the relation $a \ll a_0$ holds, then Newton's second law becomes

$$m\mathbf{a} = \frac{a_0}{a}\mathbf{F} \quad , \tag{1.0.1}$$

producing a constant profile at large distances.
However, this theory in its original form [20] is only valid on galactic scales. It fails to describe structure formations on larger scales. For example, figure 1.2, the Bullet Cluster 1E 0657-558, shows the merger of two galaxy clusters.
During a merger of two clusters, the galaxies, modelled as collisionless particles, decouple from the X-ray emitting intracluster plasma, which slows down by ram pressure felt in the fluid-like intergalactic medium. If there were no dark matter mass compo-

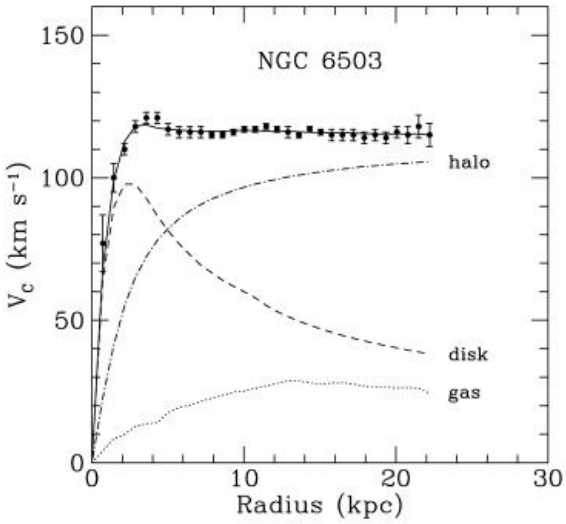

Figure 1.1: Rotation curve for the spiral galaxy NGC 6503. The points are the measured circular rotation velocities as a function of distance from the center of the galaxy. The dashed and dotted curves are the contribution to the rotational velocity due to the observed disk and gas, respectively, and the dot-dash curve is the contribution from the dark halo. Figure from [1].

Figure 1.2: The Bullet Cluster 1E 0657-558. The X-Ray emitting intracluster plasma is in red. The gravitational field determined from weak gravitational lensing is in blue. Figure borrowed from the *CHANDRA X-Ray Observatory* (`http://chandra.harvard.edu/`).

nent, the plasma would contribute the largest amount to the total mass of the system and therefore the gravitational field should be peaked between the two clusters, where the luminous mass is located. Instead, weak gravitational lensing verifies an offset between the peaks of the gravitational field and the visible mass distribution: the gravitational field is not peaked where the plasma is, it is peaked at the positions of the galaxies. Non standard gravitational forces that scales with baryonic mass cannot explain this offset *without* an unseen matter contribution [21]. The view that the missing matter component of the universe is dark matter, which is indeed composed of massive weakly interacting particles dominating the total mass of the clusters, is more reasonable; such particles would follow the movement of the galaxies and induce the gravitational field observed. Furthermore, particle dark matter explains constant rotation curves with a dark matter halo density $\rho(r) \propto r^{-2}$ for distances r between 8 kpc and 20 kpc. The dot-dash curve in figure 1.1 shows the contribution to the rotational velocity due to the dark halo.
In this work, we explain the missing matter component without modifying the law of gravity. We hold the view that dark matter is made up of particles.
Any theory of particle dark matter merges the two pillars of astroparticle physics, namely astrophysics and particle physics. Astrophysics confirms Zwicky's conjecture: we infer from the combined cosmic microwave background signal, the baryon acoustic oscillation data and supernovae surveys that the baryonic matter accounts for just 17 % of the matter content of the universe, the dominant part being dark matter. The Standard Model of Particle Physics, which describes very well the baryonic matter component, has no candidate for particle dark matter. Besides this, there is no mass term for neutrinos in the Standard Model Lagrangian for obvious reasons: a Dirac mass term relies on right-handed neutrinos which are absent in the Standard Model particle spectrum. A Majorana mass term violates the Standard Model global baryon minus lepton number symmetry by two units. But we have learned from neutrino flavor oscillation experiments [22, 23, 24, 25] that there are at least two massive neutrinos. The two main problems of astroparticle physics can thus be summarized in the sentence

Neutrinos have mass and the Universe has dark matter [26].

Our aim is to juggle both of these shortcomings of the Standard Model within one theory. We proceed as follows:
In section 2, we start with a review of the Electroweak theory. Special emphasis is attached to the mass generation of fermions and gauge bosons. For the neutrino mass generation, which is beyond the physics of the Standard Model, we briefly present the realizations of the seesaw mechanism and then concentrate on radiatively generated neutrino masses. In this class of models, the Standard Model neutrinos remain massless at tree level. Masses are induced at loop level. Each loop is suppressed with a factor $\frac{1}{16\pi^2}$, which in turn suppresses the scale Λ at which physics beyond the Standard Model emerges. Gauging the Standard Model global baryon minus lepton number symmetry, gauge anomaly conditions motivate the introduction of a right handed Majorana neutrino N_R which will become our particle dark matter candidate.

Dark matter is enlightened in section 3. Having surveyed the Standard Model of Cosmology, we show how the amount of dark matter is determined. Given that this amount has a thermal origin, the Boltzmann equations predict the relic density of dark matter (see equation (3.3.20)) to be

$$\Omega_{DM}h^2 \approx \frac{3 \cdot 10^{-27}\ \mathrm{cm}^3\ \mathrm{s}^{-1}}{\langle \sigma_{1+2\leftrightarrow 3+4}\, v_r \rangle} \quad .$$

The calculated relic density matches the observations if the thermal average of the annihilation cross section times the relative velocity, $\langle \sigma_{1+2\leftrightarrow 3+4}\, v_r \rangle$, is of order $\mathcal{O}(1\ \mathrm{pb})$, which is the strength of electroweak scale interactions. That means that a stable massive particle associated with new physics at the electroweak scale can contribute the dark matter relic density. Apart from the correct relic abundance, we further address the issue of structure formation setting constraints on any model of dark matter. In addition, we list strategies to learn about the nature of dark matter. These are direct and indirect detection experiments, and production at colliders. Positive signals in direct detection experiments would give us a glimpse into the non-gravitational interactions of dark matter and could therefore provide hints about its couplings to Standard Model particles. At colliders, the effect of Standard Model annihilations into dark matter particles would be missing energy. From measurements of the detected missing energy the mass of the dark matter particles can be reconstructed. These three aspects, namely the correct relic abundance, constraints from structure formation and the experimental verification will serve as a three-point test which a particle dark matter model has to pass.
Finally, we set up our model in section 4. The input is the Zee-Babu model [27], which generates masses for two Standard Model neutrinos at two-loop level with charged scalars h^+ and k^{++} running in the loops. We add a right-handed Majorana neutrino N_R with mass at the electroweak scale as particle dark matter candidate and a complex Higgs singlet scalar φ to the particle spectrum. In comparision to other models with right-handed neutrinos as dark matter particles, e.g. [28], we do not need more than one right-handed neutrino because in our model the right-handed neutrino is not related to the mass generation of light neutrinos. The new Higgs singlet φ mixes with the Standard Model Higgs doublet ϕ allowing the particle dark matter to couple to the Standard Model through the Higgs portal [29]. Two scenarios are investigated: in Scenario 1, we extend the Standard Model gauge group to contain a local $U(1)_{B-L}$ and a dark matter stabilization $\mathbb{Z}_2$ symmetry. In this framework, the right-handed Majorana neutrino N_R is a natural candidate for particle dark matter due to gauge anomaly conditions. The $(B-L)$ violating μ term of the Zee-Babu model needed to produce neutrino masses is generated dynamically. In Scenario 2, we enlarge the Standard Model gauge group with a $\mathbb{Z}_4$ symmetry. Altough this enlargement is more economic compared to Scenario 1, N_R is now an ad-hoc candidate for particle dark matter. With spontaneous symmetry breakdown of $U(1)_{B-L}$, which is now a global symmetry, a Majoron enters into the theory. We point out how the Majoron can lead to invisible Higgs decays and briefly discuss the self interaction of dark matter particles mediated by Majoron exchange. To reconcile both scenarios with neutrino oscillation

data, the scale Λ of new physics determined by the masses of the scalars h^+ and k^{++} and the $(B-L)$ breaking constant μ has to be the TeV scale. Since we generate the μ term dynamically, the scale for spontaneous symmetry breaking of $U(1)_{B-L}$ is at order $\mathcal{O}(1\text{ TeV})$. The Majorana mass of N_R is then naturally at order $\mathcal{O}(1\text{ TeV})$, too. For these two scenarios, we show that our model passes the three-point test.
In addition, we discuss the verification of our model at the LHC.

Chapter 2

Motivation for a Right-Handed Majorana Neutrino

This chapter deals with particle physics. We begin with a review of the Lagrangian of the Standard Model in section 2.1. The mechanism of spontaneous symmetry breaking, which gives masses to almost all Standard Model fermions and gauge bosons, is explained in section 2.2.1. We emphasize *almost* because the photon is massless due to the remaining $U(1)_{em}$ symmetry of electromagnetic interactions and for neutrinos, there are no mass terms in the Standard Model. However, it is now an experimental fact that neutrinos are massive. In section 2.3, we present the global fit of the neutrino oscillation data, which reveal that at least two neutrinos carry small masses relative to all other massive particles. We then briefly describe pathways to naturally small neutrino masses by introducing right-handed neutrinos. Having discussed the axial vector current anomaly in section 2.4, we show in section 2.5 that a right-handed Majorana neutrino N_R is a must in an extended Standard Model with a gauged $U(1)_{B-L}$ in order to prevent gauge anomalies. N_R will become our dark matter candidate.

2.1 The Lagrangian of the Electroweak Theory

The Standard Model of Particle Physics is a relativistic quantum field theory with the gauge symmetry group $G^{(SM)} = SU(3)_C \times SU(2)_L \times U(1)_Y$. It characterizes leptons and quarks as the fundamental building blocks of ordinary matter and describes their non-gravitational interactions through the exchange of gauge bosons.
Since the temperature of the universe, which we take as the temperature of the photons, cools down due to expansion (see equation (3.3.8)), there are phase transitions between gauge symmetries realized by spontaneous symmetry breaking. After the grand unified phase transition when the photons and all other particles still in thermal equilibrium with the photons had a temperature of 10^{14} GeV to 10^{16} GeV [30], the remaining symmetry is $SU(2)_L \times U(1)_Y$ which governs electroweak interactions.
The fundamental representation of an $SU(N)$ group is the N dimensional complex vector. The fundamental representation of $SU(2)_L$ is generated by the weak isospin operators ${\mathbf{I_W}}^a$ [31] which are equal to the three Pauli matrices σ^a, σ^b, σ^c (see appendix B) multiplied by a factor $\frac{1}{2}$. The corresponding gauge fields are $W^a_\mu(x)$ and the gauge coupling constant is g. a, b, c are $SU(2)_L$ gauge indices. The factor $\frac{1}{2}$ in the definition of ${\mathbf{I_W}}^a$ is needed to fulfill the Lie algebra of $SU(2)_L$: $[{\mathbf{I_W}}^a, {\mathbf{I_W}}^b] = i\epsilon^{abc}{\mathbf{I_W}}^c$ with the antisymmetric ϵ tensor being the structure constant of $SU(2)_L$ [32]. The commutator

satisfies the canonical normalization condition $\mathrm{tr}[\mathbf{I_W}^a, \mathbf{I_W}^b] = \frac{1}{2}\delta^{ab}$.
The generator of $U(1)_Y$ is the hypercharge unit matrix $\mathbf{Y_W}$ with corresponding gauge field $B_\mu(x)$ and gauge coupling constant g'. The electromagnetic charge Q is obtained from the hypercharge Y and the third component I_W^3 of the weak isospin according to the charge-hypercharge relation

$$Q = I_W^3 + Y \quad .$$

The chiral fermions (see appendix B) of the theory are arranged into left-handed doublets $\Psi_L^{(i)}$ and right-handed singlets $\Psi_R^{(i)}$ under $SU(2)_L$.
There are $i = 1, 2, 3$ flavor copies for the doublet and singlet representation. In each representation, the flavor copies have the same hypercharge (see table 2.1).
The leptons are the doublets $\Psi_L^{(i)}$ with hypercharge $q_Y = -\frac{1}{2}$ and singlets $\Psi_R^{(i)}$ with hypercharge $q_Y = -1$:

$$\Psi_L^{(1)} = \begin{pmatrix} \nu_e \\ e^- \end{pmatrix}_L \ , \ \Psi_L^{(2)} = \begin{pmatrix} \nu_\mu \\ \mu^- \end{pmatrix}_L \ , \ \Psi_L^{(3)} = \begin{pmatrix} \nu_\tau \\ \tau^- \end{pmatrix}_L \ .$$

$$\Psi_{R,i} = e_R, \mu_R, \tau_R \ .$$

Observe that there are no right-handed neutrinos.
The quarks are the doublets $\Psi_{L,q}^{(i)}$ with hypercharge $q_Y = \frac{1}{6}$ and singlets $\Psi_{R,u}^{(i)}$ and $\Psi_{R,d}^{(i)}$ with hypercharges $q_{Y,u} = \frac{2}{3}$ and $q_{Y,d} = -\frac{1}{3}$:

$$\Psi_{L,q}^{(1)} = \begin{pmatrix} u \\ d' \end{pmatrix}_L \ , \ \Psi_{L,q}^{(2)} = \begin{pmatrix} c \\ s' \end{pmatrix}_L \ , \ \Psi_{L,q}^{(3)} = \begin{pmatrix} t \\ b' \end{pmatrix}_L \ ,$$

$$\Psi_{R,u}^{(i)} = u_\mathrm{R}, c_\mathrm{R}, t_R \quad \Psi_{R,d}^{(i)} = d_\mathrm{R}, s_\mathrm{R}, b_R \ .$$

For quarks, there are two types of Yukawa terms (see below): the one which forms a mass term for the upper component of the doublets (Yukawa coupling y_u) and the one which forms a mass term for the lower component (Yukawa coupling y_d). So there are two corresponding mass matrices, however, they can not be diagonalized at the same time. In general, each type mixes the flavors of the doublets and the singlets. We choose the doublets in such a way that the upper components are the mass eigenstates. Then the lower components are a linear combination of lower doublet flavor fields, indicated by a prime:

$$\begin{pmatrix} d' \\ s' \\ b' \end{pmatrix} = \begin{pmatrix} V_{ud} & V_{us} & V_{ub} \\ V_{cd} & V_{cs} & V_{cb} \\ V_{td} & V_{ts} & V_{tb} \end{pmatrix} \begin{pmatrix} d \\ s \\ b \end{pmatrix} \equiv \mathbf{V} \begin{pmatrix} d \\ s \\ b \end{pmatrix} \quad . \tag{2.1.1}$$

This means that in the quark sector there is a flavor mixing expressed by the 3×3 unitary Cabibbo [33]-Kobayashi-Maskawa-matrix [34] $\mathbf{V}$.
Clearly, for leptons, there is only the mass term for the lower component of the doublet because neutrinos are massless in the Standard Model. Therefore, transitions in a

Particle	q_C	q_L	q_Y	q_{B-L}	$\mathbb{Z}_2$	$\mathbb{Z}_4$
Standard Model						
$\Psi_L^{(i)}$	1	2	$-\frac{1}{2}$	-1	+1	α
$\Psi_R^{(i)}$	1	1	-1	-1	+1	α
$\Psi_{L,q}^{(i)}$	3	2	$\frac{1}{6}$	$\frac{1}{3}$	+1	1
$\Psi_{R,u}^{(i)}$	3	1	$\frac{2}{3}$	$\frac{1}{3}$	+1	1
$\Psi_{R,d}^{(i)}$	3	1	$-\frac{1}{3}$	$\frac{1}{3}$	+1	1
ϕ	1	2	$\frac{1}{2}$	0	+1	1
Extension						
φ	1	1	0	2	+1	α^2
N_R	1	1	0	-1	-1	α^3
h^+	1	1	1	2	+1	α^2
k^{++}	1	1	2	2	+1	α^2

Table 2.1: Particle content

lepton doublet mediated by the exchange of $W_\mu^a(x)$ gauge bosons are flavor conserving. In the Standard Model, the electroweak symmetry breaking is driven by the complex Higgs doublet $\phi(x)$. In the neighborhood of its vacuum expectation value w, $\phi(x)$ can be written as

$$\phi(x) = \frac{1}{\sqrt{2}} \begin{pmatrix} 0 \\ H(x) + w \end{pmatrix} \tag{2.1.2}$$

with $\langle 0|\phi(x)|0\rangle = \frac{w}{\sqrt{2}}$.
In (2.1.2), we use the unitary gauge in which the unphysical degrees of freedom (see equation (4.2.3)) are absorbed into the gauge transformation. The complex scalar field $H(x)$ parametrizes fluctuations about w with $\langle 0|H(x)|0\rangle = 0$.
The prefactor $\frac{1}{\sqrt{2}}$ in (2.1.2) originates from the minimization of the potential (2.2.1).
The charge assignments are listed in table 2.1, where q_C denotes the charge under $SU(3)_C$, q_L the charge under $SU(2)_L$, q_Y the charge under $U(1)_Y$ and q_{B-L} the charge under $U(1)_{B-L}$. $\mathbb{Z}_2$ and $\mathbb{Z}_4$ indicate the transformation behavior of the fields under the abelian discrete symmetries $\mathbb{Z}_2$ and $\mathbb{Z}_4$ with $\alpha = e^{\frac{\mathrm{i}2\pi}{4}}$.
The full Lagrangian of the theory can be split into separate parts:

$$\mathcal{L}_{EWSM} = \mathcal{L}_{cov} + \mathcal{L}_{gauge} + \mathcal{L}_{Yukawa} + V(\phi)\ . \tag{2.1.3}$$

In the following analysis we suppress the flavor indices. Each term containing $\overline{\Psi}$ and Ψ represents a sum over flavor indices in the form of $\overline{\Psi}^{(i)}\Psi^{(j)}\delta^{(ij)}$. Recall that the lower components of quark doublets are mixtures of the corresponding flavor fields. $SU(2)_L$ gauge indices are shown only when needed.

The part containing the covariant derivative terms of the fields listed in table 2.1 is

$$\begin{aligned}\mathcal{L}_{cov} &= \mathrm{i}\overline{\Psi}_{L,q}\not{\mathcal{D}}\Psi_{L,q} + \mathrm{i}\overline{\Psi}_{R,u}\not{\mathcal{D}}\Psi_{R,u} + \mathrm{i}\overline{\Psi}_{R,d}\not{\mathcal{D}}\Psi_{R,d} \\ &\quad + \mathrm{i}\overline{\Psi}_{L}\not{\mathcal{D}}\Psi_{L} + \mathrm{i}\overline{\Psi}_{R}\not{\mathcal{D}}\Psi_{R} \\ &\quad + (\mathcal{D}_\mu\phi)^\dagger(\mathcal{D}^\mu\phi) \ . \end{aligned} \tag{2.1.4}$$

The generators of the covariant derivative $\mathcal{D}_\mu$ are in the representation to which the corresponding field belongs, e.g., for $SU(2)_L$ doublet fields the Standard Model covariant derivative $\mathcal{D}_\mu^{(SM)}$ is in its fundamental representation:

$$\mathcal{D}_\mu^{(SM)} = \partial_\mu - \mathrm{i}g\mathbf{I_W^a}W_\mu^a - \mathrm{i}g'\mathbf{Y_W}B_\mu \ . \tag{2.1.5}$$

Furthermore, there are the gauge kinetic terms

$$\mathcal{L}_{gauge} = -\frac{1}{4}F_{1,\mu\nu}(x)F_1^{\mu\nu}(x) - \frac{1}{4}F_{2,\mu\nu}^a(x)F_2^{a,\mu\nu}(x) \ , \tag{2.1.6}$$

with $U(1)_Y$ field strength tensor

$$F_{1,\mu\nu}(x) = \partial_\mu B_\nu(x) - \partial_\nu B_\mu(x) \ ,$$

and $SU(2)_L$ field strength tensor

$$F_{2,\mu\nu}^a = \partial_\mu W_\nu^a(x) - \partial_\nu W_\mu^a(x) + g\epsilon^{abc}W_\mu^b(x)W_\nu^c(x) \ .$$

Observe that $F_{2,\mu\nu}^a$ involves an additional term compared to $F_{1,\mu\nu}(x)$ which accounts for the fact that $SU(2)_L$ is non-abelian whereas $U(1)_Y$ is abelian. The Yukawa terms are

$$\mathcal{L}_{Yukawa} = -y_d\overline{\Psi}_{L,q}\phi\Psi_{R,d} - y_u\overline{\Psi}_{L,q}\tilde{\phi}\Psi_{R,u} - y_L\overline{\Psi}_L\phi\Psi_R \tag{2.1.7}$$

with $\tilde{\phi} \equiv i\sigma^2\phi^*$ and $\overline{\Psi}_L^{(1)} \equiv (\overline{\nu} \ \ \overline{e})_L$.
The potential is

$$V(\phi) = \frac{\lambda}{4}\left(\phi^\dagger\phi\right)^2 - \mu_2^2\phi^\dagger\phi \ . \tag{2.1.8}$$

The parameter μ_2 in the potential (2.1.8) with mass dimension 2 is the only dimensionful parameter of the electroweak Lagrangian (2.1.3). Observe that the signs chosen in (2.1.8) are crucial: only if there is a relative minus sign between the $|\phi|^2$ and the $|\phi|^4$ terms, the minima of (2.1.8) occur at $\phi = \phi_0 \neq 0$. The extremum at $\phi = 0$ is unstable. This means that if the field ϕ is initially zero, it will make a transition to the stable state ϕ_0. The degeneracy of ϕ_0 is essential for spontaneous symmetry breaking (see section 2.2.1).
All terms of the Lagrangian (2.1.3) enjoy a $U(1)$ symmetry which can be either global or local. This is due to the fact that in the Standard Model, all interactions preserve lepton number L and baryon number B and hence also $(B-L)$ number. Therefore, the $U(1)$ symmetry can be $U(1)_{B-L}$.

2.2 Mass Terms of the Electroweak Theory

2.2.1 Fermions

Writing Dirac mass terms m_D for the chiral fermions in the Lagrangian (2.1.3) violates the gauge symmetry of the theory. Consider, for example, the Dirac mass term for the electron: $m_D^{(e)} = m_e \overline{e}_L e_R$. The tensor product of an $SU(2)_L$ doublet $\overline{e}_L$ and an $SU(2)_L$ singlet e_R does not contain an $SU(2)_L$ singlet in its direct sum and is thus not gauge invariant under $SU(2)_L$. Besides, the expression $\overline{e}_L e_R$ has a remaining hypercharge $q_Y = +\frac{1}{2} - 1 = -\frac{1}{2} \neq 0$.
The Standard Model mechanism to obtain Dirac mass terms for chiral fermions is spontaneous symmetry breaking . To put spontaneous symmetry breaking into action, we have to introduce the complex Higgs doublet

$$\phi(x) = \begin{pmatrix} \phi^+(x) \\ \phi^0(x) \end{pmatrix} \quad .$$

The charge assignments of its components are a consequence of its hypercharge $Y_W = \frac{1}{2}$ and the charge-hypercharge relation. All the Yukawa terms in (2.1.7) transform as scalars under $SU(2)_L \times U(1)_Y$.
The potential (2.1.8) is equivalent to

$$V(|\phi|^2) = \frac{\lambda}{4}\left(|\phi|^2\right)^2 - \mu_2^2 |\phi|^2 \; . \tag{2.2.1}$$

Since $|\phi|^2 = \phi^\dagger \phi$ is invariant under $\phi(x) \to \phi'(x) = e^{\mathrm{i}\alpha(x)}\phi(x)$, (2.2.1) is invariant under a local $U(1)$ transformation with phase $\alpha(x)$. Setting the first derivative of V with respect to $|\phi|^2$ to zero, (2.2.1) shows that the potential (2.1.8) takes its minima for

$$0 \neq |\phi_0|^2 = \frac{2\mu_2^2}{\lambda} \equiv \frac{w^2}{2} \; .$$

These minima also exhibit a local $U(1)$ symmetry. But if the potential is in a certain minimum ϕ_0 with vacuum expectation value $w = \frac{2}{\sqrt{\lambda}}\mu$ and a definite phase α_0, then the potential does not possess the full original symmetry: the symmetry is spontaneously broken. With spontaneous breaking of a continuous global symmetry, massless scalar degrees of freedom, the Goldstone modes , enter the theory. But with spontaneous breaking of a continous local symmetry, the Goldstone modes have no physical significance. For example, in unitary gauge , they can be absorbed into a local transformation of $\phi(x)$.
Demanding $\mathbf{Q}\phi_0 \stackrel{!}{=} 0$ for an electrically neutral vacuum, where the charge operator $\mathbf{Q}$ for the Higgs field reads

$$\mathbf{Q} = \frac{1}{2}\sigma^{\mathbf{3}} + \frac{1}{2}\mathbf{1} = \begin{pmatrix} 1 & 0 \\ 0 & 0 \end{pmatrix} \quad ,$$

we see that ϕ_0 is given by

$$\phi_0 = \begin{pmatrix} 0 \\ \frac{1}{\sqrt{2}} w \end{pmatrix} \quad .$$

Since the lower component of the Higgs doublet is electrically neutral as mentioned above, the minimum ϕ_0 is invariant under $U(1)_{em}$ transformations.
Hence, the complex Higgs field $\phi(x)$ introduced at the end of section 2.1 accomplishes the phase transition $SU(2)_L \times U(1)_Y \to U(1)_{em}$. After this symmetry breakdown, the Yukawa terms (2.1.7) transform into Dirac mass terms for the chiral fermions, which are still invariant under $U(1)_{em}$. An important fact is that the Dirac mass cannot be larger than the symmetry breaking scale set by w.
Dirac mass terms connect the left-handed projection of a Dirac spinor Ψ with its right-handed projection (see appendix B), i.e., they have the form $m_D\overline{\Psi}_L\Psi_R$. Majorana mass terms connect a fermion with its Majorana conjugate (see B.3), i.e., they have the form $m_M\overline{\Psi^C}\Psi$. Majorana mass terms do in general not rely on spontaneous symmetry breaking. This means that the tensor product $\overline{\Psi^C}\Psi$ itself has to be gauge invariant, in contrast to the Standard Model Dirac mass terms, which arise from gauge invariant Yukawa terms *after* spontaneous symmetry breaking and are therefore not gauge invariant under $SU(2)_L \times U(1)_Y$. To be gauge invariant, the tensor product $\overline{\Psi^C}\Psi$ has to contain a singlet in its decomposition (compare to the beginning of this section). That means that Ψ has to transform either trivially under the gauge group, i.e., as a singlet, or in a real representation. A representation r of a Lie algebra is real if r is equivalent to its conjugate $\overline{r}$. So for Ψ transforming in a real representation r, the tensor product in the Majorana mass term is $r \times r$, which contains a singlet in its decomposition for any real r and thus is gauge invariant. The adjoint representation, for which the generators are given by the structure constants, is a real representation because the structure constants are real. In summary, for a gauge invariant Majorana mass term $m_M\overline{\Psi^C}\Psi$, the field Ψ has to be a singlet or it has to transform in a real representation, for example, in the adjoint. In our proposed model, Ψ is a singlet.

2.2.2 Gauge Bosons

The covariant derivative (2.1.5) acting on the Higgs doublet is expanded into

$$\mathcal{D}_\mu = \partial_\mu - \frac{\mathrm{i}g}{2}\begin{pmatrix} W_\mu^3 & W_\mu^1 - \mathrm{i}W_\mu^2 \\ W_\mu^1 + \mathrm{i}W_\mu^2 & -W_\mu^3 \end{pmatrix} - \frac{\mathrm{i}g'}{2}\begin{pmatrix} B_\mu & 0 \\ 0 & B_\mu \end{pmatrix} \quad .$$

With the definition $W_\mu^\pm \equiv \frac{1}{\sqrt{2}}\left(W_\mu^1 \mp \mathrm{i}W_\mu^2\right)$, the covariant derivative term for the Higgs doublet becomes

$$\begin{aligned} \left(\mathcal{D}_\mu\phi\right)^\dagger\left(\mathcal{D}^\mu\phi\right) &= \frac{1}{4}g^2W_\mu^-W^{\mu+}\left(H^2(x) + 2wH(x) + w^2\right) \\ &\quad + \frac{1}{8}\left(H^2(x) + 2wH(x) + w^2\right) \\ &\quad \cdot \left(g^2W_\mu^3W^{\mu 3} - gg'W_\mu^3B^\mu - gg'B_\mu W^{\mu 3} + g'B_\mu B^\mu\right) \\ &\quad + \frac{1}{2}\partial_\mu H(x)\partial^\mu H(x)\,. \end{aligned} \tag{2.2.2}$$

The terms proportional to w^2 are

$$\frac{1}{4}g^2w^2W_\mu^-W^{\mu+} \text{ and } \frac{1}{8}w^2(gW_\mu^3 - g'B_\mu)(gW^{\mu 3} - g'B^\mu)\,. \tag{2.2.3}$$

The first term of (2.2.3) reveals that $W^{\pm}$ are the electrically charged eigenstates with mass $m_{W_\mu^\pm} = \frac{1}{2}gw$.
The second term of (2.2.3) is equivalent to

$$\frac{1}{8}w^2 \left(B_\mu \; W_\mu^3\right) \cdot \mathbf{M^2} \cdot \begin{pmatrix} B^\mu \\ W^{\mu 3} \end{pmatrix} \tag{2.2.4}$$

with

$$\mathbf{M^2} = \begin{pmatrix} g'^2 & -g'g \\ -g'g & g^2 \end{pmatrix} \quad . \tag{2.2.5}$$

$\mathbf{M^2}$ is diagonalized by the orthogonal matrix

$$\mathbf{O} = \begin{pmatrix} \frac{g}{\sqrt{g'^2+g^2}} & \frac{g'}{\sqrt{g'^2+g^2}} \\ -\frac{g'}{\sqrt{g'^2+g^2}} & \frac{g}{\sqrt{g'^2+g^2}} \end{pmatrix} \equiv \begin{pmatrix} \cos\Theta_W & \sin\Theta_W \\ -\sin\Theta_W & \cos\Theta_W \end{pmatrix} \tag{2.2.6}$$

with the weak mixing angle Θ_W.

Inserting (2.2.6) as unit matrix $\mathbf{O^T O} = \mathbf{1}$ into (2.2.4),

$$\frac{1}{8}w^2 \left(B_\mu \; W_\mu^3\right) (\mathbf{O^T O}) \cdot \mathbf{M^2} \cdot (\mathbf{O^T O}) \begin{pmatrix} B^\mu \\ W^{\mu 3} \end{pmatrix} ,$$

and defining

$$\begin{pmatrix} A_\mu \\ Z_\mu \end{pmatrix} \equiv \mathbf{O} \begin{pmatrix} B_\mu \\ W_{\mu 3} \end{pmatrix} ,$$

(2.2.4) simplifies to

$$\frac{1}{8}w^2 \left(A_\mu \; Z_\mu\right) \begin{pmatrix} 0 & 0 \\ 0 & g'^2+g^2 \end{pmatrix} \begin{pmatrix} A^\mu \\ Z^\mu \end{pmatrix} = \frac{1}{2} \cdot \frac{1}{4}w^2(g'^2+g^2) Z_\mu Z^\mu \; . \tag{2.2.7}$$

(2.2.7) reveals that the electrically neutral mass eigenstates are A_μ and Z_μ with masses $m_{A_\mu} = 0$ and $m_{Z_\mu} = \frac{1}{2}w\sqrt{g'^2+g^2} = \frac{1}{\cos\Theta_W} m_{W_\mu^\pm}$.
So, in the Standard Model, the masses of the $W^{\pm}$ and Z_μ boson obey the relation

$$\rho \equiv \frac{m^2_{W_\mu^\pm}}{m^2_{Z_\mu} \cos^2\Theta_W} = 1 \quad . \tag{2.2.8}$$

Deviations of ρ from 1 are induced by radiative corrections (see end of section 4.2.1).
The covariant derivative term (2.2.2) for the Higgs doublet expressed in mass eigenstates then reads:

$$\begin{aligned} (\mathcal{D}_\mu\phi)^\dagger (\mathcal{D}^\mu\phi) \;\; = \;\; & \frac{1}{4}g^2 W_\mu^- W^{\mu +} \left(H^2(x) + 2wH(x) + w^2\right) \\ & + \frac{1}{8}\left(g'^2+g^2\right) Z_\mu Z^\mu \left(H^2(x) + 2wH(x) + w^2\right) \\ & + \frac{1}{2}\partial_\mu H(x) \partial^\mu H(x) \; . \end{aligned} \tag{2.2.9}$$

2.3 Masses for Neutrinos

2.3.1 The Problem

The particle spectrum of the Standard Model does not contain a right-handed neutrino. So there is no Dirac mass m_D for neutrinos. A Majorana mass m_M violates the global $U(1)_{B-L}$ symmetry by two units. Besides this, Majorana mass terms are only allowed for singlet fields with singlets zero hypercharges or for fields transforming in a real representation, for example in the adjoint (see section 2.2.1). This special transformation behavior also accounts for the charge conjugation operation **C**: by definition, a Majorana field has to satisfy $\Psi^C = \Psi$. But in the Standard Model, all fermions are charged under $U(1)_Y$ and there are no $SU(2)$ triplet fields which corresponds to the adjoint representation. Therefore, in the framework of the Standard Model, neutrinos are massless.
Experiments have measured neutrino oscillations. The propability $P^t_{\alpha\beta}$ for the flavor eigenstate ν_α to make the transition to the flavor eigenstate ν_β during a time interval t must therefore be different from zero. It can be shown [35] that $P^t_{\alpha\beta}$ is proportional to the term

$$\sum_{i,j} \sin^2\left(\frac{(m_i^2 - m_j^2)L}{4E}\right) \quad , \tag{2.3.1}$$

where i and j index mass eigenstates, L is the distance which the propagating mass eigenstates travel during the time t and E is the energy of the neutrinos.
The term (2.3.1) is different from zero only if $m_i^2 - m_j^2 \neq 0$. Thus neutrinos must be massive in order to explain the observed oscillations. Note that for three generations there are two independent mass differences.
Hence the flavor eigenstates $\nu_e\,, \nu_\mu\,, \nu_\tau$ are linear combinations of the mass eigenstates $\nu_1\,, \nu_2\,, \nu_3$:

$$\begin{pmatrix} \nu_e \\ \nu_\mu \\ \nu_\tau \end{pmatrix} \equiv \mathbf{U} \begin{pmatrix} \nu_1 \\ \nu_2 \\ \nu_3 \end{pmatrix} \quad , \tag{2.3.2}$$

$$\mathbf{U} = \overbrace{\underbrace{\begin{pmatrix} 1 & 0 & 0 \\ 0 & c_{23} & s_{23} \\ 0 & -s_{23} & c_{23} \end{pmatrix}}_{\Theta_{23}}}^{\text{Atmospheric}} \cdot \overbrace{\underbrace{\begin{pmatrix} c_{13} & 0 & s_{13}e^{-i\delta} \\ 0 & 1 & 0 \\ -s_{13}e^{-i\delta} & 0 & c_{13} \end{pmatrix}}_{\Theta_{13}}}^{\text{Cross-Mixing}}$$
$$\cdot \overbrace{\underbrace{\begin{pmatrix} c_{12} & s_{12} & 0 \\ -s_{12} & c_{12} & 0 \\ 0 & 0 & 1 \end{pmatrix}}_{\Theta_{12}}}^{\text{Solar}} \cdot \overbrace{\begin{pmatrix} e^{\frac{i\alpha_1}{2}} & 0 & 0 \\ 0 & e^{\frac{i\alpha_2}{2}} & 0 \\ 0 & 0 & 1 \end{pmatrix}}^{\text{Majorana phases}} \quad ,$$

where the Pontecorvo-Maki-Nakagawa-Sakata matrix **U** expresses the lepton mixing [36].
For n generations the $n \times n$ unitary mixing matrix **U** has $(n-1)^2$ free parameters because $(2n-1)$ parameters are absorbed into the relative phases between the n neutrino flavor eigenstates and the n neutrino mass eigenstates. $(n-1)^2$ equals

$$(n-1)^2 = \underbrace{\frac{1}{2}n(n-1)}_{\text{mixing angles}} + \underbrace{\frac{1}{2}(n-1)(n-2)}_{\text{CP violating phases}} .$$

Thus for $n = 3$ there are three mixing angles Θ_{12}, Θ_{13}, Θ_{23} and one CP violating phase δ.
We use the abbreviations $c_{ij} = \cos\Theta_{ij}$, $s_{ij} = \sin\Theta_{ij}$ and α_i are the Majorana phases which do not enter into the oscillation phenomena.
According to (2.3.1), only differences of mass squares can be measured in oscillation experiments and there are the possible cases of normal mass hierarchy with $m_1 < m_2 < m_3$ and inverted mass hierarchy with $m_3 < m_1 < m_2$. The current global fit of the oscillation data is [37]:

$$\begin{aligned}
&\Delta m^2_{sol} = m_2^2 - m_1^2 = (7.59 \pm 0.20) \times 10^{-5}\ \text{eV}^2, \\
&\Delta m^2_{atm} = m_3^2 - m_1^2 = \begin{cases} (-2.36 \pm 0.11) \times 10^{-3}\ \text{eV}^2 & \text{for Inverted Hierarchy} \\ (+2.46 \pm 0.12) \times 10^{-3}\ \text{eV}^2 & \text{for Normal Hierarchy} \end{cases}, \\
&\sin^2\theta_{12} = 0.319 \pm 0.016, \quad \sin^2\theta_{23} = 0.462^{+0.082}_{-0.050}, \quad \sin^2\theta_{13} = 0.0095^{+0.013}_{-0.007} .
\end{aligned}$$

There are three additional measurable quantities which are formed of the neutrino mass eigenvalues m_i [38]: the kinematic mass $m_\beta = \sqrt{\sum |U_{ei}|^2\, m_i^2}$ measured in beta decay experiments, e.g., with KATRIN [39], and currently limited by $m_\beta \leq 2.3$ eV [40]; the effective mass $\langle m \rangle = |\sum U_{ei}^2\, m_i|$ measured in neutrinoless double beta decay ($0\nu\beta\beta$) experiments and limited from above by 0.5 to 1 eV assuming light neutrino exchange for $0\nu\beta\beta$ [38]; and the sum $\Sigma \equiv \sum m_i$ of neutrino masses limited by cosmic microwave background (CMB) data: $\Sigma < 1.3$ eV [41].
We see how particle physics and cosmology cooperate: From particle physics experiments one can get information about the neutrino mixing, from cosmological observations one can learn about the sum of the neutrino mass eigenvalues.
In summary, at least two neutrinos carry masses that are small relative to all other particle masses.

2.3.2 Pathways to Naturally Small Neutrino Masses

The problem about the neutrino mass encountered in the previous section indicates that only physics beyond the Standard Model can create neutrino masses.
Majorana neutrino masses can be generated through the unique dimension five operator [42]

$$\Lambda^{-1}\phi\phi\nu_i\nu_j \tag{2.3.3}$$

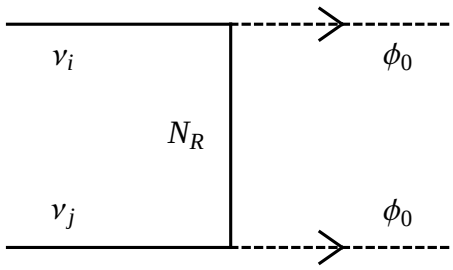

Figure 2.1: Tree-level realization of the effective operator (2.3.3) with a heavy right-handed Majorana neutrino N_R

with left-handed neutrino flavor states $\nu_{i,j}$.
One possibility to obtain the operator (2.3.3) at tree level is to start with a completed theory which has heavy right-handed Majorana neutrinos N_R with masses m_{N_R} as Standard Model singlet particles and the renormalizable interactions $f_i \nu_i N_R \phi$ leading to Dirac mass terms $f_i w \nu_i N_R$ with $m_D^i = f_i w$. The relevant parts in the corresponding Lagrangian are symbolically

$$\mathcal{L} = f_i \nu_i N_R \phi - m_{N_R} N_R N_R \,.$$

N_R fulfills the classical Euler-Lagrange equations of motion if

$$\partial_\mu \frac{\partial \mathcal{L}}{\partial_\mu N_R} - \frac{\partial \mathcal{L}}{\partial N_R} = 0 \Leftrightarrow f_i \nu_i \phi = 2 m_{N_R} N_R \Leftrightarrow N_R = \frac{1}{2 m_{N_R}} f_i \nu_i \phi \quad . \tag{2.3.4}$$

Integrating out the spinor N_R from the t-channel exchange processes depicted in figure 2.1, i.e., replacing N_R in the vertex $f_j \nu_j N_R \phi$ with equation (2.3.4), the effective operator (2.3.3) emerges with $\Lambda^{-1} = \frac{f_i f_j}{2 m_{N_R}}$ and the neutrino mass matrix becomes $\frac{m_D^i m_D^j}{m_{N_R}}$. Assuming the coupling constants f_i of order $\mathcal{O}(0.1)$, the mass m_{N_R} has to be of order $\mathcal{O}(10^{12})$ GeV to produce the light neutrino mass of order $\mathcal{O}(0.1)$ eV. Note that compared to chiral fermions, m_{N_R} is not limited from above by the electroweak scale w, it can be arbitrarily large. There are two more tree-level realizations of the operator (2.3.3) [43]. All tree-level realizations rely on heavy extra particles and lead to the known Type I, II and III seesaw mechanism : Type I is just the described case in which a fermion singlet is exchanged, whereas in Type II seesaw models scalar triplets produce the light neutrino masses and in Type III models fermion triplets are responsible for the neutrino masses.
The operator (2.3.3) can also be realized at loop-level with additional particles running in the loop [43]. The extra particles in models which generate neutrino masses radiatively need not be heavy due to additional loop suppression factors and could be in reach of upcoming experiments.
In section 4.1 we will present a model with radiatively generated neutrino masses.

2.4 The Axial Vector Current Anomaly

In this section, we present the condition for the conservation of the axial vector current in a quantum field theory. The result is needed in the following section to motivate the introduction of a right-handed Majorana neutrino N_R in an extended Standard Model with a gauged $U(1)_{B-L}$.
In appendix B, the axial vector current is defined as:

$$j^{\mu 5}(x) = \overline{\Psi(x)}\gamma^\mu\gamma^5\Psi(x) \quad . \tag{2.4.1}$$

In view of Noether's theorem, the axial vector current is a symmetry current which follows from the chiral transformation $\Psi(x) \to \Psi'(x) = (1 + \mathrm{i}\alpha\gamma^5)\Psi(x)$.
Observe that due to the anticommutation relations of the γ matrices, we have the equality

$$\overline{(1 + \mathrm{i}\alpha\gamma^5)\Psi} = (\Psi^\dagger - \mathrm{i}\alpha\Psi^\dagger\gamma^5)\gamma^0 = \overline{\Psi} + \mathrm{i}\alpha\overline{\Psi}\gamma^5 = \overline{\Psi}(1 + \mathrm{i}\alpha\gamma^5) \quad .$$

The chiral transformation is a symmetry tranformation of the Dirac Lagrangian (B.2.1) if $m = 0$:

$$\begin{aligned}
\overline{\Psi'}(\mathrm{i}\partial\!\!\!/ - m)\Psi' &= \overline{\Psi}(1 + \mathrm{i}\alpha\gamma^5)\mathrm{i}\gamma^\mu\partial_\mu(1 + \mathrm{i}\alpha\gamma^5)\Psi - m\overline{\Psi}(1 + \mathrm{i}\alpha\gamma^5)(1 + \mathrm{i}\alpha\gamma^5)\Psi \\
&= \overline{\Psi}\mathrm{i}\gamma^\mu\partial_\mu\Psi + \overline{\Psi}\mathrm{i}\gamma^\mu\partial_\mu(\mathrm{i}\alpha\gamma^5\Psi) + \overline{\Psi}\mathrm{i}\alpha\gamma^5 i\gamma^\mu\partial_\mu\Psi \\
&\quad - \overline{\Psi}m\Psi - 2\mathrm{i}m\alpha\overline{\Psi}\gamma^5\Psi + \mathcal{O}(\alpha^2) \\
&= \overline{\Psi}\mathrm{i}\gamma^\mu\partial_\mu\Psi - \overline{\Psi}\mathrm{i}\alpha\gamma^5\mathrm{i}\gamma^\mu\partial_\mu\Psi + \overline{\Psi}\mathrm{i}\alpha\gamma^5\mathrm{i}\gamma^\mu\partial_\mu\Psi \\
&\quad - \overline{\Psi}m\Psi - 2\mathrm{i}m\alpha\overline{\Psi}\gamma^5\Psi + \mathcal{O}(\alpha^2) \\
&= \overline{\Psi}(\mathrm{i}\partial\!\!\!/ - m)\Psi - 2\mathrm{i}m\alpha\overline{\Psi}\gamma^5\Psi + \mathcal{O}(\alpha^2)\,.
\end{aligned}$$

In fact, using the classical Euler-Lagrange equations (B.2.2) and (B.2.3), we see that $j^{\mu 5}$ is conserved

$$\partial_\mu j^{\mu 5} = 2\mathrm{i}m\overline{\Psi}\gamma^5\Psi = 0 \tag{2.4.2}$$

for massless fermions Ψ.
However, the conservation of the axial vector current relies on the classical equations of motion. A conservation law and thus a symmetry which exists on the classical level need not hold automatically after promoting the classical theory to a quantum field theory. If the resulting quantum field theory does not possess the original symmetry of the classical theory, it is said to be anomalous. Local, i.e., gauge symmetries are of special importance because with a gauge choice one can remove the unphysical degrees of freedom in a theory, compare, for example, to the Goldstone modes which can be absorbed in a unitary gauge . A consistent quantum field theory has therefore to be free of gauge anomalies .
To see how anomalies arise in a quantum field theory, we begin with an abelian gauge symmetry to simplify the argumentation. Consider the process in which an axial vector current $j^{\mu 5}(x)$ creates two photons from the vacuum state $|0\rangle$ with momenta and four-vector components (p, ν) and (k, λ), respectively. We write the matrix element which

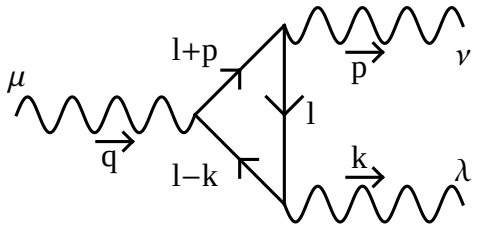

Figure 2.2: Triangle diagram

we have to study for this process as

$$\langle p,\nu;k,\lambda|j^{\mu 5}(x)|0\rangle \quad . \tag{2.4.3}$$

The initial state is the vacuum state $|0\rangle$ and the final state is the two particle state $\langle p,\nu;k,\lambda|$. The transition operator is the axial vector current $j^{\mu 5}(x)$.
To apply the momentum space Feynman rules we have to Fourier transform (2.4.3). Then we obtain

$$\begin{aligned}\langle p,\nu;k,\lambda|\tilde{j}^{\mu 5}|0\rangle &= \int d^4x\, e^{-\mathrm{i}qx}\langle p,\nu;k,\lambda|j^{\mu 5}(x)|0\rangle \\ &= (2\pi)^4\delta^{(4)}(p+k-q)\epsilon^*_\nu(p)\epsilon^*_\lambda(k)\mathcal{M}^{\mu\nu\lambda}(p,k) \quad . \end{aligned}\tag{2.4.4}$$

The four-dimensional delta distribution ensures four-momentum conservation.
$\epsilon^*_\nu(p)$ is the polarization vector of an outgoing photon A_ν with momentum p.
$\mathcal{M}^{\mu\nu\lambda}(p,k)$ is the abbreviation for the rest of a process involving the expression $\gamma^\mu\gamma^5$ from the axial vector current interaction and two external photons with momenta p and k. The leading order contribution to $\mathcal{M}^{\mu\nu\lambda}(p,k)$ is shown in the triangle diagram of figure 2.2.
Computing $\partial_\mu\tilde{j}^{\mu 5}$ on the left-hand side of (2.4.4) corresponds to multiplying the right-hand side of (2.4.4) by $(-\mathrm{i}q_\mu)$:

$$\begin{aligned}\langle p,\nu;k,\lambda|\partial_\mu\tilde{j}^{\mu 5}|0\rangle &= \int d^4x\,(-\mathrm{i}q_\mu)e^{-\mathrm{i}qx}\langle p,\nu;k,\lambda|j^{\mu 5}(x)|0\rangle \\ &= (2\pi)^4\delta^{(4)}(p+k-q)\epsilon^*_\nu(p)\epsilon^*_\lambda(k)(-\mathrm{i}q_\mu)\mathcal{M}^{\mu\nu\lambda}(p,k). \end{aligned}\tag{2.4.5}$$

Evaluating the expression $q_\mu\mathcal{M}^{\mu\nu\lambda}$, the term $q_\mu\gamma^\mu\gamma^5$ emerges in a loop integral over the unfixed momentum l, which we write as

$$q_\mu\gamma^\mu\gamma^5 = (\not{l}+\not{k}+\not{p}-\not{l})\gamma^5 \quad . \tag{2.4.6}$$

If one perfoms the loop integral in d dimensions (see appendix D), a generic momentum p can be written as $p_d = p_4 + p_{d-4}$, where p_4 has components in four dimensional spacetime and p_{d-4} has components in the $(d-4)$ extra dimensions. γ^5 anticommutes with γ^μ in four dimensional space time and commutes with γ^μ in the $(d-4)$ extra

dimensions. The unfixed momentum l lives in d dimensions, the external momenta q, p and k in four dimensions. Equation (2.4.6) is then modified to

$$\begin{aligned} q_\mu\gamma^\mu\gamma^5 &= (\not{l}_4+\not{l}_{d-4}+\not{k}_4+\not{p}_4-\not{l}_4-\not{l}_{d-4})\gamma^5 \\ &= (\not{l}_4+\not{k}_4)\gamma^5+\gamma^5(\not{l}_4-\not{p}_4) \\ &= (\not{l}_d+\not{k}_4)\gamma^5-\not{l}_{d-4}\gamma^5+\gamma^5(\not{l}_d-\not{p}_4)-\gamma^5\not{l}_{d-4} \\ &= (\not{l}_d+\not{k}_4)\gamma^5+\gamma^5(\not{l}_d-\not{p}_4)-2\gamma^5\not{l}_{d-4} \quad . \end{aligned} \tag{2.4.7}$$

There exists an additional diagram which is obtained from figure 2.2 after crossing (p,ν) and (k,λ). However, equation (2.4.7) is antisymmetric under crossing (p,ν) and (k,λ). Hence only the term $(-2\gamma^5\not{l}_{d-4})$ is left in the loop integral. In [32], it is shown that this term gives

$$\mathrm{i}q_\mu\cdot\mathcal{M}^{\mu\nu\lambda}(p,k)\propto\epsilon^{\alpha\lambda\beta\nu}k_\alpha p_\beta \quad . \tag{2.4.8}$$

Inserting (2.4.8) into (2.4.4), we obtain the anomalous nonconservation of the axial vector current:

$$\langle p,\nu;k,\lambda|\partial_\mu\tilde{j}^{\mu5}|0\rangle=\text{const.}\cdot\langle p,\nu;k,\lambda|\epsilon^{\alpha\nu\beta\lambda}F_{\alpha\nu}F_{\beta\lambda}|0\rangle \quad . \tag{2.4.9}$$

In the derivation of (2.4.9) we used the antisymmetry of $\epsilon^{\alpha\lambda\beta\nu}$ under interchange of indices which allows us to rewrite

$$\epsilon^{\alpha\nu\beta\lambda}\partial_\alpha A_\nu=\frac{1}{2}\cdot 2\,\epsilon^{\alpha\nu\beta\lambda}\partial_\alpha A_\nu=\frac{1}{2}\left(\epsilon^{\alpha\nu\beta\lambda}\partial_\alpha A_\nu+\epsilon^{\nu\alpha\beta\lambda}\partial_\nu A_\alpha\right)=\frac{1}{2}\epsilon^{\alpha\nu\beta\lambda}(\partial_\alpha A_\nu-\partial_\nu A_\alpha) \quad .$$

which is equal to $\frac{1}{2}\epsilon^{\alpha\nu\beta\lambda}F_{\alpha\nu}$ in an abelian gauge theory.
In the case of a non-abelian gauge symmetry, the non-conservation of the axial vector current

$$j^{\mu a}(x)=\overline{\Psi(x)}\gamma^\mu\left(\frac{1-\gamma^5}{2}\right)t^a\Psi(x)$$

reads:

$$\langle p,\nu,b;k,\lambda,c|\partial_\mu\tilde{j}^{\mu a}|0\rangle=\text{const. }\epsilon^{\alpha\nu\beta\lambda}\,p_\alpha k_\beta\cdot\mathcal{A}^{abc} \quad . \tag{2.4.10}$$

$j^{\mu a}(x)$ is a chiral axial vector current; comparing with expression (B.1.10), we see that $j^{\mu a}(x)$ projects on left handed fermions.
The variable $\mathcal{A}^{abc}$ is given by $\mathcal{A}^{abc}=\text{tr}\,[t^a\{t^b,t^c\}]$, where t^a are the generators of the gauge group in a specific representation and the trace is taken over all fermion species that can run in the loop of the triangle diagram with an extra minus sign for left-handed fermions.
To ensure that the classically conserved axial vector current is also conserved in a non-abelian gauge theory, $\mathcal{A}^{abc}$ has to be zero.
The Standard Model with the non-abelian gauge group $G^{(SM)}=SU(3)_C\times SU(2)_L\times U(1)_Y$ is anomaly-free: $\mathcal{A}^{abc}$ equals zero for every possible triangle diagram if one sums over all the Standard Model fermions. For every extension of $G^{(SM)}$ one has to satisfy the anomaly condition $\mathcal{A}^{abc}\stackrel{!}{=}0$.

2.5 The Right-Handed Majorana Neutrino

Within the current experimental limits, all Standard Model interactions seem to preserve lepton number L and baryon number B. In the Standard Model, the combination $(B-L)$ is therefore conserved, too.
The global $U(1)_{B-L}$ symmetry need not to be an exact symmetry. It can be regarded as an additional gauge symmetry which is spontaneously broken during a phase transition by a complex scalar singlet φ receiving its vacuum expectation value.
The scale at which φ obtains its vacuum expectation value then defines the scale of new physics. Processes in which $(B-L)$ is violated are suppressed by the symmetry breaking scale.
The Standard Model gauge group $G^{(SM)}$ is then extended to $G^{(SM)} \times U(1)_{B-L}$.
The covariant derivative (2.1.5) becomes:

$$\mathcal{D}_\mu = \mathcal{D}_\mu^{(SM)} - \mathrm{i}\, g_{B-L} Z'_\mu \ , \tag{2.5.1}$$

with $U(1)_{B-L}$ gauge field $Z'_\mu(x)$ and coupling constant g_{B-L}.
We want to remark that the ratio of the mass $M_{Z'}$ of the Z' boson to its coupling constant g_{B-L} is bounded from below by electroweak precision observables which can be expressed in terms of the S, T and U parameters [44]. Given the measured value of the electroweak precision observables, one can fit the S, T and U parameters to lie in certain intervals. In Z' models, S, T and U depend on the ratio $\frac{M_{Z'}}{g_{B-L}}$. From the fitted range for S, T and U, one then obtains the following bound [45]:

$$\frac{M_{Z'}}{g_{B-L}} > 6 \text{ TeV} \ . \tag{2.5.2}$$

The Z' boson has the gauge kinetic term

$$\mathcal{L}^{Z'}_{gauge} = -\frac{1}{4} F_{3,\mu\nu}(x) F_3^{\mu\nu}(x) \tag{2.5.3}$$

with $U(1)_{B-L}$ field strength tensor

$$F_{3,\mu\nu}(x) = \partial_\mu Z'_\nu(x) - \partial_\nu Z'_\mu(x) \ .$$

We assume no gauge kinetic mixing between $U(1)_Y$ and $U(1)_{B-L}$. If we further assume a flavor-independent q_{B-L} charge assignment for the Standard Model fermions, then the coupling of the Z' boson is unaffected by the fermion mixings expressed in the matrices (2.1.1) and (2.3.2). So there are no flavor changing neutral currents induced by the Z' couplings. From the $[SU(2)_L]^2 U(1)_{B-L}$ anomaly cancellation (compare figure 2.3) we conclude [32]:

$$\begin{aligned} 0 \stackrel{!}{=} \sum_{\Psi_L} q_{B-L}(\Psi_L) &= -q_{B-L}(\Psi_L) - 3 q_{B-L}(\Psi_{L,q}) \\ &\Leftrightarrow \quad q_{B-L}(\Psi_L) = -3 q_{B-L}(\Psi_{L,q}) \ . \end{aligned} \tag{2.5.4}$$

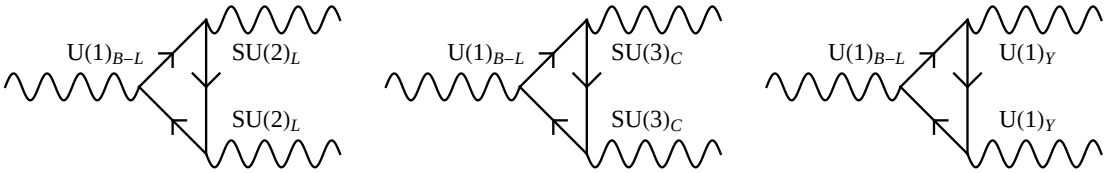

Figure 2.3: $[SU(2)_L]^2U(1)_{B-L}$, $[SU(3)_C]^2U(1)_{B-L}$ and $[U(1)_Y]^2U(1)_{B-L}$ anomaly

The $[SU(3)_C]^2U(1)_{B-L}$ anomaly cancellation condition (compare figure 2.3) gives [32]:

$$\begin{aligned} 0 \overset{!}{=} \sum_{\Psi_q} q_{B-L}(\Psi_q) &= -2q_{B-L}(\Psi_{L,q}) + q_{B-L}(\Psi_{R,u}) + q_{B-L}(\Psi_{R,d}) \\ &\Leftrightarrow \quad q_{B-L}(\Psi_{R,d}) = 2q_{B-L}(\Psi_{L,q}) - q_{B-L}(\Psi_{R,u}) \ . \end{aligned} \tag{2.5.5}$$

The $[U(1)_Y]^2U(1)_{B-L}$ anomaly cancellation condition (compare figure 2.3) implies [32]:

$$\begin{aligned} 0 \quad &\overset{!}{=} \quad \sum_{L,R} q_Y^2(\Psi_{L,R}) q_{B-L}(\Psi_{L,R}) \\ &= \quad -2q_Y^2(\Psi_L) q_{B-L}(\Psi_L) + q_Y^2(\Psi_R) q_{B-L}(\Psi_R) \\ &\quad\ +3\left(-2q_Y^2(\Psi_{L,q}) q_{B-L}(\Psi_{L,q})\right. \\ &\quad\ \left. +\ q_Y^2(\Psi_{R,u}) q_{B-L}(\Psi_{R,u}) + q_Y^2(\Psi_{R,d}) q_{B-L}(\Psi_{R,d})\right) \\ &= \quad -2\left(-\frac{1}{2}\right)^2 q_{B-L}(\Psi_L) + (-1)^2 q_{B-L}(\Psi_R) \\ &\quad\ +3\left(-2\left(\frac{1}{6}\right)^2 q_{B-L}(\Psi_{L,q})\right. \\ &\quad\ \left. +\left(\frac{2}{3}\right)^2 q_{B-L}(\Psi_{R,u}) + \left(-\frac{1}{3}\right)^2 q_{B-L}(\Psi_{R,d})\right) \\ &\overset{(2.5.4),(2.5.5)}{=} \quad 2q_{B-L}(\Psi_{L,q}) + q_{B-L}(\Psi_R) + q_{B-L}(\Psi_{R,u}) \\ \Leftrightarrow q_{B-L}(\Psi_R) \quad &= \quad -2q_{B-L}(\Psi_{L,q}) - q_{B-L}(\Psi_{R,u}) \ . \end{aligned} \tag{2.5.6}$$

The conditions (2.5.4), (2.5.5) and (2.5.6) hold for any $U(1)$ gauge extension of $G^{(SM)}$ [46]. For the special case of $U(1)_{B-L}$ we have the restriction $q_{B-L}(\Psi_{R,u}) = q_{B-L}(\Psi_{L,q})$. Then the q_{B-L} charges of the Standard Model fermions are those included in table 2.1. Other $U(1)_{Z'}$ extensions and their charge assignments arising from anomaly cancellation can be found in [47].
The triangle anomaly of the Standard Model fermion currents coupled to the $U(1)_{B-L}$ (see figure 2.4) sums up to

$$\sum_{L,R} q_{B-L}^3(\Psi_{L,R}) = -2(-1)^3 + (-1)^3 + 3\left[-2\left(\frac{1}{3}\right)^3 + \left(\frac{1}{3}\right)^3 + \left(\frac{1}{3}\right)^3\right] = 1.$$

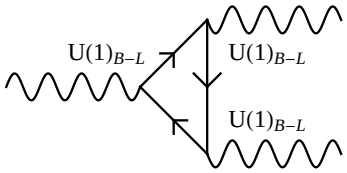

Figure 2.4: $[U(1)_{B-L}]^3$ anomaly

Anomaly cancellation then compels to introduce a Standard Model fermion singlet N_R with $U(1)_{B-L}$ charge $q_{B-L} = -1$. The only particle to which N_R can couple is the scalar φ:

$$\mathcal{L}_{N_R} = -\frac{1}{2}\lambda_c \varphi \overline{N_R^C} N_R + \text{ h.c. } . \tag{2.5.7}$$

Invariance under $U(1)_{B-L}$ assigns to φ the $U(1)_{B-L}$ charge $q_{B-L} = 2$. λ_c is a dimensionless coupling constant. Thus N_R has to be a right-handed Majorana neutrino. In its covariant derivative term

$$L_{cov}^{N_R} = \mathrm{i}\overline{N}_R \not{D} N_R \ , \tag{2.5.8}$$

only the $U(1)_{B-L}$ part acts.
Being a Standard Model fermion singlet with hypercharge $q_Y = 0$, N_R cannot contribute to one-loop corrections of the vacuum polarization amplitudes of $W^\pm$ and Z. This means that there are no constraints for N_R arising from elctroweak precision parameters (compare to end of section 4.2.1).
The covariant derivative term for the singlet φ becomes the mass term of the Z' boson after spontaneous symmetry breaking of $U(1)_{B-L}$. Let w' be the vacuum expectation value of φ (see equation (4.2.2)) and recall that $q_{B-L}(\varphi) = 2$. Then it follows:

$$\begin{aligned} (\mathcal{D}_\mu \varphi)^* (\mathcal{D}^\mu \varphi) &= \frac{1}{2} \cdot 4 g_{B-L}^2 w'^2 Z'_\mu Z'^\mu \\ \Rightarrow M_{Z'}^2 &= 4 g_{B-L}^2 w'^2 \ . \end{aligned}$$

From the bound (2.5.2), we then infer that the singlet vacuum expectation value w' must satisfy

$$w' > 3 \text{ TeV} \ .$$

Chapter 3

Dark Matter Candidates: A Three-Point Test

Particle dark matter is the interface of particle physics and astrophysics. This chapter starts with an introduction into astrophysics by deriving the Friedmann equations in section 3.1. In section 3.2, based on observational results, we point out that the lion's share of the matter content of the universe is dark matter. To match all observations, a possible particle candidate for dark matter has to fulfill necessary conditions of which we will study three, assembled in a three point test: Does the particle candidate match the correct relic density?, Is it cold? and Can it be probed experimentally?. The thermal relic density of a particle is deduced from the Boltzmann equation in section 3.3. In section 3.4, we argue that a bottum-up approach for structure formation in the universe favors cold dark matter. The strategies for detecting dark matter are studied in section 3.5: the principle of direct detection experiments with the examples of the CDMS II and the DAMA/LIBRA experiment in section 3.5.1, indirect detection experiments with the example of the Fermi-LAT experiment in section 3.5.2 and collider production with the example of the LHC in section 3.5.3. A critical discussion of these strategies follows in section 3.5.4.

3.1 Cosmological Equations

The basic equations of the Standard Model of Cosmology [30], the ΛCDM model , rely on Einstein's equations of General Relativity, i.e., dynamical equations for a metric tensor $g^{\mu\nu}$ which characterizes the geometry of space time. These can be derived from the principle of least action.
The geometry of four-dimensional space time is encoded in the Riemann curvature tensor $\mathcal{R}_{\mu\nu\rho\sigma}$ which is a unique expression derived from combinations of the metric tensor $g^{\mu\nu}$. Since an action S is given by integrating a scalar, we have to construct a scalar from the Riemann curvature tensor to obtain an action for gravity. This is done by first contracting the indices of the Riemann curvature tensor with the metric tensor $g^{\mu\nu}$ yielding the Ricci tensor $\mathcal{R}_{\mu\rho} \equiv \mathcal{R}_{\mu\nu\rho\sigma} \cdot g^{\nu\sigma} = \mathcal{R}_{\mu\nu\rho}{}^{\nu}$. In a second step we calculate the trace of the Ricci tensor resulting in the curvature scalar $\mathcal{R} = \mathcal{R}_{\mu\nu} \cdot g^{\mu\nu} = \mathcal{R}_{\mu}{}^{\mu}$.
The action S for General Relativity has to lead to the same physics after transforming the coordinates through a diffeomorphism. The rule for integration by substitution as-

signs the following diffeomorphism-invariant integral for any integrable function $f(x)$:

$$\int d^4x \sqrt{-g}\, f(x) \quad ,$$

with $g \equiv$ det $(g^{\mu\nu})$.
The minus sign arises because locally $g^{\mu\nu}$ can be equal to the Minkowski metric $g^{\mu\nu} =$ diag $(-,+,+,+)$, for which $g = -1$.
S then follows to

$$S = \int d^4x \sqrt{-g} \left(\frac{1}{2\sqrt{8\pi}G_N} \cdot \mathcal{R} + \mathcal{L}_{matter} \right),$$

with $\mathcal{L}_{matter}$ containing the energy momentum tensor $T_{\mu\nu}$ and the cosmological constant Λ.
Applying the principle of least action [48], the outcome are Einstein's equations of General Relativity :

$$\mathcal{R}_{\mu\nu} - \frac{1}{2} g_{\mu\nu} \mathcal{R} = 8\pi G_N T_{\mu\nu} + \Lambda g_{\mu\nu}. \tag{3.1.1}$$

On scales larger than 10^8 pc, cosmological observations suggest that the universe is homogeneous and isotropic (compare [49]). The metric satisfying homogeneity and isotropy is the Robertson-Walker metric

$$ds^2 = x^\mu x^\nu g_{\mu\nu} = dt^2 - R^2(t) \left[\frac{dr^2}{1 - kr^2} + r^2(d\theta^2 + \sin^2\theta \phi^2) \right], \tag{3.1.2}$$

with comoving radial coordinate r, the scale factor $R(t)$ expressing the physical distance $x(t)$ as $x(t) = R(t) \cdot r$ and the curvature constant $k \in \{+1, -1, 0\}$ corresponding to closed $(k = +1)$, open $(k = -1)$ or spatially flat $(k = 0)$ geometries.
The energy momentum tensor $T_{\mu\nu}$ has to be diagonal in a homogeneous universe and its spatial components have to be equal due to isotropy. If we assume that the matter content of the universe behaves like a perfect fluid with energy density ρ and pressure p, then

$$T_{\mu\nu} = \text{diag } (\rho, p, p, p). \tag{3.1.3}$$

With (3.1.2) and (3.1.3), the (00) component of (3.1.1) is evaluated to

$$H(t)^2 \equiv \left(\frac{\dot{R}(t)}{R(t)} \right)^2 = \frac{8\pi G_N \rho(t)}{3} - \frac{k}{R(t)^2} + \frac{\Lambda}{3} \quad . \tag{3.1.4}$$

Dividing by the present day Hubble expansion rate $H_0^2 = H(t = t_0)^2$ and introducing the critical density

$$\rho_c \equiv \frac{3H_0^2}{8\pi G_N} \quad ,$$

equation (3.1.4) is equivalent to

$$\frac{\rho(t)}{\rho_c} - \frac{k}{H_0^2 R(t)^2} + \frac{\Lambda}{8\pi G_N \rho_c} = \frac{H(t)^2}{H_0^2} \quad . \tag{3.1.5}$$

The (ii) components of (3.1.1) are

$$\left(\frac{\ddot{R}(t)}{R(t)}\right) = \frac{\Lambda}{3} - \frac{4\pi G_N}{3}\left(\rho(t) + 3p(t)\right). \tag{3.1.6}$$

Setting $\Lambda = 0$, equation (3.1.6) shows that the universe is either expanding or contracting.
Equations (3.1.4) and (3.1.6) are the Friedmann equations .
Performing the operation

$$\frac{\partial}{\partial t}\left(R(t)^2 \cdot (3.1.4)\right) - 2\dot{R}(t)R(t) \cdot (3.1.6) \quad ,$$

we find

$$\begin{aligned} 2\dot{R}(t)\ddot{R}(t) &= \frac{8\pi G_N \rho(t)}{3} 2R(t)\dot{R}(t) + \frac{8\pi G_N R(t)^2}{3}\dot{\rho}(t) + \frac{\Lambda}{3}2R(t)\dot{R}(t) \\ -2\dot{R}(t)\ddot{R}(t) &= -\frac{\Lambda}{3}2R(t)\dot{R}(t) + \frac{8\pi G_N \rho(t)}{3}R(t)\dot{R}(t) + 8\pi G_N p(t)R(t)\dot{R}(t) \\ \Rightarrow \dot{\rho}(t) &= -3H(t)(\rho(t) + p(t)) \quad . \end{aligned} \tag{3.1.7}$$

To solve equation (3.1.7), we use the general equation of state

$$p = \omega\rho \quad . \tag{3.1.8}$$

For this case, (3.1.7) is integrated to

$$\rho(t) \propto R(t)^{-3(1+\omega)} \quad .$$

The solutions are classified according to their equation of state parameter:

- For a photon gas $\omega = \frac{1}{3}$ and $\rho(t)_\gamma \propto R(t)^{-4}$.
- For a pressureless gas, i.e., cold and therefore non-relativistic matter, $\omega = 0$ and $\rho(t)_m \propto R(t)^{-3}$.
- For the cosmological constant we demand $\omega = -1$ and thus $\rho(t)_\Lambda = \rho_\Lambda = \text{const.} = \frac{\Lambda}{8\pi G_N} = -p$ leading to an accelerated expansion of the universe as observed in Type Ia supernovae (SNe) surveys.

We introduce the cosmological density parameter

$$\Omega_{tot} = \Omega_\gamma + \Omega_m + \Omega_\Lambda = \frac{\rho_{tot}}{\rho_c} \tag{3.1.9}$$

with the total energy density $\rho_{tot} = ((\rho_0)_\gamma + (\rho_0)_m) + \rho_\Lambda = \rho + \rho_\Lambda$. Ω_m contains baryonic (b) and dark matter (DM):

$$\Omega_m = \Omega_b + \Omega_{DM} \quad .$$

Equation (3.1.9) allows to rewrite equation (3.1.5) at present day $t = t_0$ as

$$\frac{k}{R_0^2} = H_0^2(\Omega_{tot} - 1) \quad . \tag{3.1.10}$$

Equation (3.1.10) reveals that ρ_c is the critical density for a spatially flat universe: $\rho_c = \rho_{tot} \Rightarrow \Omega_{tot} = 1 \Rightarrow k = 0$.
Identifying $\Omega_k = -\frac{k}{H_0^2 R_0^2}$ as curvature density parameter and using the classified solutions for the specific energy densities, equation (3.1.5) reads:

$$\sqrt{\Omega_\gamma \left(\frac{R_0}{R(t)}\right)^4 + \Omega_m \left(\frac{R_0}{R(t)}\right)^3 + \Omega_k \left(\frac{R_0}{R(t)}\right)^2 + \Omega_\Lambda} = \frac{H(t)}{H_0} \quad . \tag{3.1.11}$$

With the substitution $y \equiv \frac{R(t)}{R_0}$ it follows that $H(t) = \frac{\dot{y}}{y}$. From equation (3.1.11) the expansion age of the universe results to:

$$dt = \frac{dy}{yH_0\sqrt{\Omega_\gamma y^{-4} + \Omega_m y^{-3} + \Omega_k y^{-2} + \Omega_\Lambda}} \quad . \tag{3.1.12}$$

An important qualifier has to be made concerning the integration of equation (3.1.12): (3.1.12) cannot be integrated from $t = 0$ to $t = t'$ because general relativity, which was the starting point in deriving the Friedmann equations, is not valid at the exact beginning of the universe. We have to split the integration interval into two parts: part one from $t = 0$ to $t = \delta t'$ is the scope in which a more fundamental theory than classical general relativity has to be applied, i.e., a quantum field theory of gravity; and part two from $t = \delta t'$ to $t = t'$ is the validity period of classical general relativity. However, we assume that $\delta t' \ll 1$ and neglect quantum gravity effects for the expansion age of the universe.

3.2 The Amount of Dark Matter

From the fit of the ΛCDM parameters to the WMAP 7-year data of the Cosmic Microwave Background (CMB) [41] combined with the Baryon Acoustic Oscillations (BAO) (see section 3.4 and [50]) and the supernovae Type Ia (SNe) data [51], the following density parameters are found (`http://lambda.gsfc.nasa.gov./`):

- $\Omega_m = 0.278 \pm 0.015$
  - $\Omega_b = 0.0461 \pm 0.0015$
  - $\Omega_{DM} = 0.232 \pm 0.013$
- $\Omega_\Lambda = 0.722 \pm 0.015$.

All baryonic matter including luminous baryonic matter and non-luminous baryonic dark matter, e.g., non-luminous baryonic gas, massive astrophysical compact halo

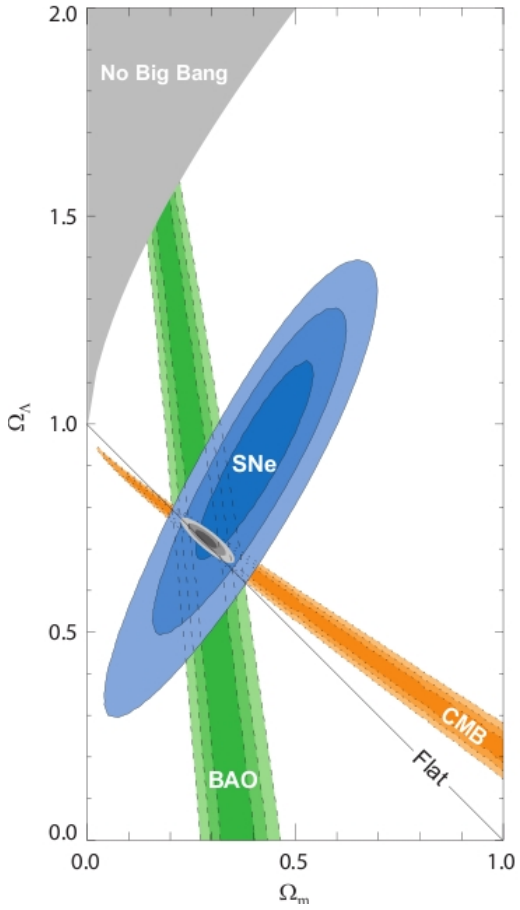

Figure 3.1: 68.3 %, 95.4 % and 99.7% confidence level contours on Ω_Λ and Ω_m obtained from CMB, BAO and the Union Supernova set, as well as their combination (assuming $w = -1$). Figure from [2].

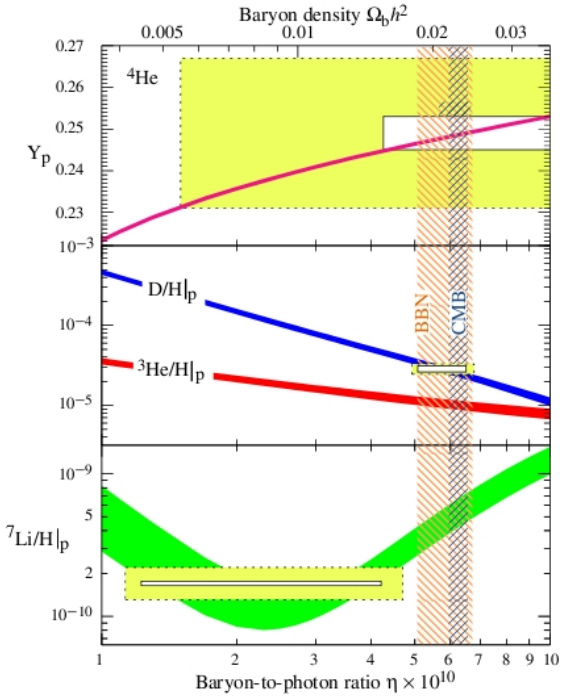

Figure 3.2: The abundances of ^{4}He, D, ^{3}He, and ^{7}Li as predicted by the standard model of Big Bang nucleosynthesis [3]. The bands show the 95 % CL range. Boxes indicate the observed light element abundances (smaller boxes: $\pm 2\sigma$ statistical errors; larger boxes: $\pm 2\sigma$ statistical and systematic errors). The narrow vertical band indicates the CMB measurement of the cosmic baryon density, while the wider band indicates the BBN concordance range (both at 95 % CL). Figure from [4].

objects, etc. contributes with only about 17 % to the total matter density Ω_m.
Figure 3.1 illustrates the combination of WMAP, BAO and SNe data.
The predictions of Big-Bang nucleosynthesis (BBN) are shown in figure 3.2, where h is the present day normalized Hubble expansion rate (cf.section 3.3) and Y_p is the primordial mass fraction of ^{4}He:

$$Y_p = \frac{2\frac{n}{p}}{1+\frac{n}{p}} \quad . \tag{3.2.1}$$

n and p denote neutron and proton number densities, respectively. Applied to the matter content of the universe, the combined data sets of figure 3.1 and figure 3.2 highlight that most of the matter consists of non-baryonic dark matter.
One could argue that neutrinos contribute a large amount to Ω_m. But as pointed out in section 2.3.1, the sum Σ of neutrino masses is limited by $\sum m_i \leq 1.3$ eV for three

light neutrinos. This limit corresponds to a neutrino matter density $\Omega_\nu < 0.05$, which is too small to account for the missing matter density. In principle, Ω_ν could be larger if there were more than three light neutrinos. However, more light neutrinos would induce more relativistic degrees of freedom. From equation (3.3.5) it then follows that the expansion rate would grow. Consequently, the freeze out temperature for $\frac{n}{p}$ would increase (compare section 3.3), i.e., the ratio $\frac{n}{p}$ would decouple earlier leading to a larger value for Y_p (see equation (3.2.1)) because there were more free neutrons. With a lower estimate for the nucleon density, only one new neutrino flavor with Standard Model weak interaction strength could be accommodated [52]. Thus we can argue that the lion's share of the matter content of the universe is indeed a yet undiscovered non-baryonic new matter component, the dark matter with a density parameter $\Omega_{DM} = 0.232$.
The Standard Model describes very well baryonic matter but it fails to describe a particle-like dark matter. Therefore, any theory of a particle dark matter goes beyond the Standard Model of particle physics. The search for a particle dark matter candidate thus merges physics beyond the Standard model with cosmology.
However, possible particle candidates for dark matter have to fulfill necessary conditions to match all observations. We list three points [53] to each of which a good dark matter candidate must give a positive answer and discuss them in dedicated sections:

A Does it match the correct relic density?

B Is it cold?

C Can it be probed experimentally?

3.3 The Dark Matter Relic Density

In the very earliest epoch of its history, the universe was composed of a gas of radiation, i.e., hot and therefore relativistic particles. Solving equation (3.1.7) for a gas of photons one obtains the following proportionality: $\rho_\gamma \propto R^{-4}$.
We want to reproduce this result from thermodynamics and then use the relations obtained to determine the theoretically expected amount of dark matter.
Given the approximation that the universe was near thermal equilibrium during its earliest epoch, the total energy density of all present particle species i is expressed in terms of the photon temperature T_γ [30]:

$$\rho_{rad} = T_\gamma^4 \sum_i \left(\frac{T_i}{T_\gamma}\right)^4 \frac{g_i}{2\pi^2} \int_{x_i}^{\infty} du \, \frac{1}{e^{u-y_i} \pm 1} \sqrt{u^2 - x_i^2}\, u^2 \quad , \tag{3.3.1}$$

where we have introduced the dimensionless quantity $u \equiv \frac{E}{T_\gamma}$. The temperature T_i is the temperature of the particle species i, g_i is the number of degrees of freedom, $x_i = \frac{m_i}{T_\gamma}$ and μ_i are the chemical potentials entering into $y_i = \frac{\mu_i}{T_\gamma}$. According to the

first law of thermodynamics, a change in energy E of a system is caused by a change in entropy S, a change in volume V and a change in particle number N:

$$dE = TdS - pdV + \mu dN \quad . \tag{3.3.2}$$

We want to emphasize that the chemical potential μ expresses the change in energy E due to a change in particle number N.
We have used that any energy density $\rho(t)$ is the integral over phase space of all possible energy values E weighted with the phase space distribution function $f(\mathbf{p}, t)$

$$\rho(t) = \frac{g}{(2\pi)^3} \int d^3p \, E(\mathbf{p}) f(\mathbf{p}, t) \quad , \tag{3.3.3}$$

where $E = \sqrt{\mathbf{p}^2 + m^2}$.
In thermal equilibrium, $f(\mathbf{p}, t)$ is time-independent; for particles with half-integer spin it is the Fermi-Dirac distribution $(+)$ and for particles with integer spin it is the Bose-Einstein distribution $(-)$:

$$f(E, t) = f(E) = \left(e^{\frac{E-\mu}{T}} \pm 1 \right)^{-1} \quad .$$

Assuming that all present particle species i are relativistic, i.e., $m_i \ll T_\gamma$, equation (3.3.1) simplifies to

$$\rho_{rad} = \frac{\pi^2}{30} g_* \, T_\gamma^4 \tag{3.3.4}$$

with

$$g_* = \sum_{Bosons} g_i \left(\frac{T_i}{T_\gamma} \right)^4 + \frac{7}{8} \sum_{Fermions} g_i \left(\frac{T_i}{T_\gamma} \right)^4 \quad ,$$

where the sums run over all species [30].
The content of the early universe is dominated by radiation. If we assume that $\rho_{rad} = \rho_c$ in this epoch, then $k = 0$ according to equation (3.1.10). In this epoch, the cosmological constant Λ is zero, too. Equation (3.1.4) then reads

$$H_{rad} = \sqrt{\frac{8\pi G_N \rho_{rad}}{3}} \overset{(3.3.4)}{=} \sqrt{\frac{8\pi^3}{90}} \sqrt{g_*} \, \frac{T_\gamma^2}{m_{pl}} \quad , \tag{3.3.5}$$

with the Planck mass $m_{pl} = \sqrt{\frac{1}{G_N}}$.
Integrating (3.1.12) in a radiation dominated universe the outcome for the expansion age t of the universe is [30]:

$$t \approx \frac{1}{2} \frac{1}{H_{rad}} \overset{(3.3.5)}{=} \sqrt{\frac{45}{16\pi^3}} \sqrt{\frac{1}{g_*}} \frac{m_{pl}}{T_\gamma^2} = \sqrt{\frac{45}{16\pi^3}} \sqrt{\frac{1}{g_*}} \frac{m_{pl}}{m^2} \, x^2 \quad , \tag{3.3.6}$$

where we have made the approximation $\Omega_{tot} \approx 1$.
If we further assume that the expansion of the universe is isentropic, then the entropy

S is constant in a comoving volume $R(t)^3$. S equals the product of $R(t)^3$ and the entropy density s. In a radiation dominated universe, s is written as [30]

$$\begin{aligned} s &= \sum_i \frac{\rho_{rad,\,i} + p_{rad,\,i}}{T_i} \\ &= \sum_i \frac{1}{T_i}\left(\rho_{rad,\,i} + \frac{1}{3}\rho_{rad,\,i}\right) \quad \text{| equation of state parameter } \omega = \frac{1}{3} \\ &= \sum_i \frac{1}{T_i}\frac{4\pi^2}{90} g_*\, T_\gamma^4 \\ &= \frac{2\pi^2}{45} g_{*\,S}\, T_\gamma^3 \end{aligned} \tag{3.3.7}$$

with

$$g_{*\,S} = \sum_{Bosons} g_i \left(\frac{T_i}{T_\gamma}\right)^3 + \frac{7}{8}\sum_{Fermions} g_i \left(\frac{T_i}{T_\gamma}\right)^3 \quad .$$

The constancy of the entropy S implies

$$T_\gamma(t) \propto {g_{*\,S}}^{-\frac{1}{3}}\, R^{-1}(t) \quad . \tag{3.3.8}$$

Comparing with equation (3.3.1) we obtain $\rho_{rad} \propto R^{-4}$.
Equation (3.3.8) displays the decrease in the temperature T_γ due to the expansion of the universe. This means that any particle with mass m which had been relativistic becomes non-relativistic when $m > T_\gamma(t)$. If these massive non-relativistic particles are in thermal equilibrium with other present massive particles, the Fermi-Dirac and the Bose-Einstein distribution, respectively, are approximated by the Maxwell-Boltzmann distribution. In this case, the energy density $\rho(t)$ is given by $\rho(t) = m\, n(t)$ with number density

$$n(t) = g\left(\frac{m T_\gamma(t)}{2\pi}\right)^{\frac{3}{2}} e^{-\frac{m-\mu}{T_\gamma(t)}} \quad . \tag{3.3.9}$$

Consequently, any massive non-relativistic species, which would stay in thermal equilibrium, would be nearly absent today due to the exponential decrease of its number density and could therefore not contribute to the matter content of the universe. But as it is pointed out in section 3.2, experiments suggest that today the dark matter contributes about 80 % to the matter content.
If we suppose that the dark matter is made up of stable, weakly interacting massive particles (WIMPs), it must decouple from thermal equilibrium distribution at some early time during the evolution of the universe in order to get rid of the exponential suppression factor. The details of this decoupling process are governed by Boltzmann equations which describe the evolution of the phase space distribution functions $f_i(E,t)$ for each species i. $f_i(E,t)$ do not depend on spatial coordinates, since in the Robertson-Walker metric (3.1.2), the phase space distributions are spatially homogeneous and isotropic. A single Boltzmann equation can be written as [54]

$$\mathbf{L}\,[f](E,t) = \mathbf{C}\,[f](E,t) \quad , \tag{3.3.10}$$

where **L** is the Liouville operator giving the net rate of change in time of the particle phase space distribution function and **C** is the collision operator expressing the number of particles per phase space volume that are lost or gained per unit time due to collisions with other particles. We consider the case of annihilations of a particle-antiparticle pair (1 and 2) into a particle-antiparticle pair (3 and 4).
In the Robertson-Walker metric (3.1.2) the Liouville operator becomes

$$\mathbf{L}\left[f(E,t)\right] = \left(\frac{\partial}{\partial t} - H\,\frac{|\mathbf{p}|^2}{E}\,\frac{\partial}{\partial E}\right) f(E,t) = \left(\frac{\partial}{\partial t} - H\,\frac{E^2-m^2}{E}\,\frac{\partial}{\partial E}\right) f(E,t) \quad .$$

As in equation (3.3.3), the actual number density $n(t)$ takes the form

$$\begin{aligned} n(t) &= \int dn(t) \\ &= \frac{g}{(2\pi)^3}\int d^3p\, f(\mathbf{p},t) \\ &= \frac{g}{(2\pi)^3}\,4\pi\int dp\, p^2\, f(\mathbf{p},t) \\ &= \frac{g}{2\pi^2}\int dE\,\frac{1}{2\sqrt{E^2-m^2}}\,2E(E^2-m^2)\,f(E,t) \\ &= \frac{g}{2\pi^2}\int dE\,E\sqrt{E^2-m^2}\,f(E,t) \quad . \end{aligned}$$

Applying the Liouville operator **L** to the number density $n_1(t)$ of particle 1, the term becomes

$$\begin{aligned} & \frac{g_1}{2\pi^2}\int dE_1\,E_1\sqrt{E_1^2-m^2}\left(\frac{\partial}{\partial t} - H\frac{E_1^2-m^2}{E_1}\,\frac{\partial}{\partial E_1}\right) f_1(E_1,t) \\ = \;& \frac{\partial}{\partial t}\left(\frac{g_1}{2\pi^2}\int dE_1\,E_1\sqrt{E_1^2-m^2}\,f_1(E_1,t)\right) \\ & - H\,\frac{g_1}{2\pi^2}\int dE_1\,(E_1^2-m^2)^{\frac{3}{2}}\,\frac{\partial}{\partial E_1}\,f_1(E_1,t) \\ = \;& \dot{n}_1(t) + H\,\frac{g_1}{2\pi^2}\int dE_1\,\frac{\partial}{\partial E_1}\,(E_1^2-m^2)^{\frac{3}{2}}\,f_1(E_1,t) \\ = \;& \dot{n}_1(t) + 3H\,\frac{g_1}{2\pi^2}\int dE_1\,E_1\sqrt{E_1^2-m^2}\,f_1(E_1,t) \\ = \;& \dot{n}_1(t) + 3Hn_1(t) \quad . \end{aligned}$$

It is useful to express the integrated Liouville term $\dot{n}_1(t) + 3Hn_1(t)$ in terms of a quantity which scales as $R(t)^{-3}$. Thus one follows the number of particles per comoving volume and one has scaled out the expansion of the universe. The entropy density s calculated in equation (3.3.7) scales as $R(t)^{-3}$. The conservation of entropy S yields:

$$0 \stackrel{!}{=} \frac{d}{dt}\left(sR(t)^3\right) \Rightarrow \dot{s} = -3Hs \quad .$$

Defining the abundance Y as the number density divided by the entropy density, $Y \equiv \frac{n_1}{s}$, s times the time derivative of Y equals the integrated Liouville term:

$$s \cdot \dot{Y} = s \cdot \left(\frac{\dot{n}_1}{s} - \frac{n_1 \dot{s}}{s^2} \right) = \dot{n}_1 - Y\dot{s} = \dot{n}_1 + 3Hn_1 \quad .$$

Equation (3.3.6) allows to write the time derivative in terms of a derivative with respect to x:

$$\begin{aligned} \frac{dx}{dt} &= \frac{1}{2} \frac{1}{x} \frac{m^2}{m_{pl}} \sqrt{\frac{16\pi^3}{45}} \sqrt{g_*} \\ \frac{d}{dx} &= \frac{x}{H_m} \frac{d}{dt} \end{aligned}$$

with $H_m = 2\,\frac{m^2}{m_{pl}} \sqrt{g_*} \sqrt{\frac{\pi^3}{45}}$. It follows:

$$\frac{dY}{dx} = \frac{x}{H_m} \frac{dY}{dt} \quad . \tag{3.3.11}$$

For the process $1 + 2 \leftrightarrow 3 + 4$, the integrated collision term reads [54]

$$\begin{aligned} & \frac{g_1}{(2\pi)^3} \int d^3p_1 \, \mathbf{C}\left[f_1\right] \\ = & -\sum_{spins} \int \frac{d^3p_1}{(2\pi)^3\, 2E_1} \frac{d^3p_2}{(2\pi)^3\, 2E_2} \frac{d^3p_3}{(2\pi)^3\, 2E_3} \frac{d^3p_4}{(2\pi)^3\, 2E_4} \\ & \cdot (2\pi)^4\, \delta^{(4)}\left(p_1 + p_2 - p_3 - p_4\right) \\ & \cdot \left(f_1 f_2 (1 \pm f_3)(1 \pm f_4) |\mathcal{M}_{1+2\to 3+4}|^2 \right. \\ & \left. - f_3 f_4 (1 \pm f_1)(1 \pm f_2) |\mathcal{M}_{3+4\to 1+2}|^2 \right) \quad . \end{aligned} \tag{3.3.12}$$

Here we sum over the initial and final spins and integrate over all particle momenta. The delta distribution ensures energy-momentum conservation. The signs in the Pauli blocking $(-)$ and enhancing $(+)$ factors $1 \pm f_i$ arise from Fermi-Dirac and Bose-Einstein distribution, respectively. The squared amplitudes $|\mathcal{M}|^2$ are specific for the process $1 + 2 \leftrightarrow 3 + 4$.
Under CP invariance we have $\sum_{spins} |\mathcal{M}_{1+2\to 3+4}|^2 = \sum_{spins} |\mathcal{M}_{3+4\to 1+2}|^2 \equiv |\mathcal{M}|^2$. For non-relativistic particles i in thermal equilibrium, the chemical potentials μ_i are zero because in thermal equilibrium, the particle numbers N_i adjust to their equilibrium value and hence there is no net change in N_i (compare (3.3.2)). The Maxwell-Boltzmann distribution becomes accurate and all particle species have the phase space distribution function $f_i^{eq}(E_i) \propto e^{-\frac{E_i}{T_\gamma}}$. In addition, the error we make in the computation of the phase space integral in equation (3.3.12) by approximating the Pauli blocking and enhancing factors $1 \pm f_i$ with 1 will be small. These assumptions sim-

plify the collision term to

$$\begin{aligned} & \frac{g_1}{(2\pi)^3}\int d^3p_1\,\mathbf{C}\left[f_1\right] \\ = & -\int \frac{d^3p_1}{(2\pi)^3\,2E_1}\,\frac{d^3p_2}{(2\pi)^3\,2E_2}\,\frac{d^3p_3}{(2\pi)^3\,2E_3}\,\frac{d^3p_4}{(2\pi)^3\,2E_4}\cdot(2\pi)^4\,\delta^{(4)}\left(p_1+p_2-p_3-p_4\right) \\ & \cdot\left(f_1f_2-f_3f_4\right)|\mathcal{M}|^2 \quad . \end{aligned}$$

If the final particles 3 and 4 approach thermal equilibrium, their distribution functions f_3 and f_4 become f_3^{eq} and f_4^{eq}. The delta distribution in the collision term then enforces $f_3^{eq}f_4^{eq}=f_1^{eq}f_2^{eq}$.
For the process $1+2\leftrightarrow 3+4$, we introduce the annihilation cross section $\sigma_{1+2\leftrightarrow3+4}$ as follows [54]:

$$\int \frac{d^3p_3}{(2\pi)^3\,2E_3}\,\frac{d^3p_4}{(2\pi)^3\,2E_4}\,|\mathcal{M}|^2\,(2\pi)^4\,\delta^{(4)}\left(p_1+p_2-p_3-p_4\right)\equiv 4Fg_1g_2\,\sigma_{1+2\leftrightarrow3+4} \quad ,$$

where the Lorentz invariant flux factor F is defined as

$$\begin{aligned} F &= \sqrt{(p_1\cdot p_2)^2-m_1^2\,m_2^2} \quad |m_1^2=m_2^2\equiv m^2 \\ &= \sqrt{(p_1\cdot p_2)^2-m^4} \quad |p_1\cdot p_2=\frac{s-2m^2}{2} \\ &= \frac{1}{2}\sqrt{s\,(s-4m^2)} \end{aligned} \tag{3.3.13}$$

and the g_i result from spin summation.
The collision term can then be written as

$$\begin{aligned} \frac{g_1}{(2\pi)^3}\int d^3p_1\,\mathbf{C}\left[f_1\right] &= -\int \frac{d^3p_1}{(2\pi)^3\,2E_1}\,\frac{d^3p_2}{(2\pi)^3\,2E_2}\,4Fg_1g_2\,\sigma_{1+2\leftrightarrow3+4}\,\left(f_1f_2-f_1^{eq}f_2^{eq}\right) \\ &= -\int \frac{d^3p_1\,g_1}{(2\pi)^3}\,\frac{d^3p_2\,g_2}{(2\pi)^3}\,\frac{F}{E_1E_2}\,\sigma_{1+2\leftrightarrow3+4}\,\left(f_1f_2-f_1^{eq}f_2^{eq}\right) \\ &= -\int \left(dn_1dn_2-dn_1^{eq}dn_2^{eq}\right)\sigma_{1+2\leftrightarrow3+4}\,v_r \quad , \end{aligned}$$

with the relative velocity $v_r=\frac{F}{E_1E_2}$. According to (C.2.9), in the center of mass frame the product $E_{1cm}E_{2cm}$ is equal to

$$E_{1cm}E_{2cm}=\frac{s}{4}$$

and the relative velocity becomes

$$v_r=\frac{F}{E_{1cm}E_{2cm}}=\frac{4F}{s}\overset{(3.3.13)}{=}2\sqrt{1-\frac{4m^2}{s}} \quad . \tag{3.3.14}$$

Solving (3.3.14) for s, we obtain

$$s = \frac{4m^2}{1 - \frac{v_r^2}{4}} \quad . \tag{3.3.15}$$

We assume that for the thermal average of the annihilation cross section $\sigma_{1+2\leftrightarrow 3+4}$ times the relative velocity v_r,

$$\langle \sigma_{1+2\leftrightarrow 3+4}\, v_r \rangle = \frac{\int \sigma_{1+2\leftrightarrow 3+4}\, v_r\, dn_1^{eq} dn_2^{eq}}{\int dn_1^{eq} dn_2^{eq}} \quad ,$$

the following relation holds

$$\int (dn_1 dn_2 - dn_1^{eq} dn_2^{eq})\, \sigma_{1+2\leftrightarrow 3+4}\, v_r = (n_1 n_2 - n_1^{eq} n_2^{eq}) \cdot \langle \sigma_{1+2\leftrightarrow 3+4}\, v_r \rangle \quad ,$$

and so the collision term finally results to

$$\frac{g_1}{(2\pi)^3} \int d^3 p_1\, \mathbf{C}\,[f_1] = -\langle \sigma_{1+2\leftrightarrow 3+4}\, v_r \rangle\, (n_1 n_2 - n_1^{eq} n_2^{eq}) \quad .$$

Putting the Liouville term and the collision term together, the rate equation for the particle number density $n_1(t)$ follows:

$$\dot{n}_1(t) = -3Hn_1(t) - \langle \sigma_{1+2\leftrightarrow 3+4}\, v_r \rangle \left((n_1(t))^2 - (n_1^{eq}(t))^2 \right), \tag{3.3.16}$$

with $n_1 = n_2$ for particle-antiparticle pairs, or equivalently

$$\frac{dY}{dx} = -\frac{x\, \langle \sigma_{1+2\leftrightarrow 3+4}\, v_r \rangle\, s}{H_m} \left(Y(x)^2 - Y_{eq}(x)^2 \right), \tag{3.3.17}$$

using equation (3.3.11). Equation (3.3.16) is the Lee-Weinberg approximation [55] of the Boltzmann equation (3.3.10).
The rate of change in time of the particle's actual number density $n_1(t)$ originates from a decrease of $n_1(t)$ caused by the expansion of the universe and from interactions with other particles in which the particle under consideration is lost or gained.
During the radiation-dominated epoch, i.e., $x \ll 1$, the equilibrium number density n_1^{eq} is proportional to T_γ^3. Since the entropy density s is also proportional to T_γ^3, the equilibrium abundance $Y_{eq} = \frac{n_1^{eq}}{s}$ is constant and there is no change in the amount of particles per comoving volume. Putting it in another way, in the radiation-dominated epoch, $Y = Y_{eq}$ such that $\frac{dY}{dx} = 0$.
But when $x \gg 1$, the particle creation process $3 + 4 \rightarrow 1 + 2$ essentially stops and $n_1^{eq}(t)$ begins to decrease like $e^{-\frac{m}{T_\gamma(t)}}$ according to equation (3.3.9). Although the number density $n_1(t)$ decreases and the universe keeps expanding, the annihilation process $1 + 2 \rightarrow 3 + 4$ is still somewhat important, causing a slight reduction in Y compared to its value at $x = x_f$ [56]. The freeze-out value x_f is defined by the condition $Y(x_f) - Y_{eq}(x_f) \equiv \Delta(x_f) = cY_{eq}(x_f)$, where c is a constant of order unity [30]. Notice

that $Y^2 - Y_{eq}^2 = \Delta(2Y_{eq} + \Delta)$.
In the non-relativistic regime $x > 1$, which is the regime of interest here, the following relation holds: $\langle \sigma_{1+2\leftrightarrow 3+4}\, v_r \rangle \propto (v_r)^{2l}$, where l denotes the order of the partial wave contributing to the annihilation cross section. Since $v_r \propto x^{-\frac{1}{2}}$, the thermal average of the cross section times relative velocity can be parametrized as $\langle \sigma_{1+2\leftrightarrow 3+4}\, v_r \rangle \equiv \sigma_0 x^{-l}$, where $l = 0$ for s-wave, $l = 1$ for p-wave annihilation, and so on. Then with use of equation (3.3.7) and the definition of H_m, the fraction on the right hand side of equation (3.3.17) multiplied by $\frac{x^2}{x^2}$ equals

$$\frac{x \langle \sigma_{1+2\leftrightarrow 3+4}\, v_r \rangle\, s}{H_m} \frac{x^2}{x^2} = \frac{2\pi^2}{45} \sqrt{\frac{90}{8\pi^3}} \frac{g_{*S}}{\sqrt{g_*}}\, m_{pl}\, m\, \sigma_0\, x^{-l-2} \quad .$$

Equation (3.3.17) can then be written in terms of Δ:

$$\frac{d\Delta}{dx} = -\frac{dY_{eq}}{dx} - \lambda x^{-l-2}\, \Delta(2Y_{eq} + \Delta) \quad , \tag{3.3.18}$$

with $\lambda = \frac{2\pi^2}{45} \sqrt{\frac{90}{8\pi^3}} \frac{g_{*S}}{\sqrt{g_*}}\, m_{pl}\, m\, \sigma_0$.
For $x \gg x_f$, $Y_{eq}(x) \ll Y(x)$ such that $\Delta(x) \approx Y(x)$. Then the term $-2\lambda x^{-l-2} \Delta Y_{eq}$ as well as the term $-\frac{dY_{eq}}{dx}$ are negligible [56] and equation (3.3.18) simplifies to

$$\begin{aligned} & \frac{d\Delta}{dx} \equiv \Delta' = -\lambda x^{-l-2} \Delta^2 \\ \Leftrightarrow \quad & \frac{\Delta'}{\Delta^2} = -\lambda x^{-(l+2)} \quad . \end{aligned}$$

Integration from $x = x_f$ to $x = \infty$ yields:

$$\begin{aligned} & \int_{x_f}^{\infty} dx\, \frac{\Delta'}{\Delta^2} = \int_{x_f}^{\infty} dx\, (-\lambda) x^{-(l+2)} \\ \Leftrightarrow \quad & \left[-\frac{1}{\Delta} \right]_{x_f}^{\infty} = \left[\frac{\lambda}{l+1} x^{-(l+1)} \right]_{x_f}^{\infty} \\ \Leftrightarrow \quad & \frac{-\Delta(x_f) + \Delta(\infty)}{\Delta(x_f) \cdot \Delta(\infty)} = -\frac{\lambda}{l+1} x_f^{-(l+1)} \quad | \, \Delta(x_f) \gg \Delta(\infty) \\ \Rightarrow \quad & -\frac{\Delta(x_f)}{\Delta(x_f) \cdot \Delta(\infty)} = -\frac{\lambda}{l+1} x_f^{-(l+1)} \\ \Leftrightarrow \quad & -\frac{1}{\Delta(\infty)} = -\frac{\lambda}{l+1} x_f^{-(l+1)} \quad . \end{aligned}$$

The outcome for the final dark matter abundance $Y_\infty \equiv \Delta(\infty)$ is

$$Y_\infty = \frac{l+1}{\lambda}\, x_f^{l+1} = \frac{45}{2\pi^2} \sqrt{\frac{8\pi^3}{90}} \frac{\sqrt{g_*}}{g_{*S}} \frac{(l+1) x_f^{l+1}}{m_{pl}\, m\, \sigma_0} \quad .$$

The definition of Y allows us to express today's number density n_0^{DM} of dark matter particles: $n_0 = s_0 Y_\infty$.
Since $\rho_0^{DM} = m_{DM}\, n_0^{DM}$, the density parameter $\Omega_{DM} = \frac{\rho_0^{DM}}{\rho_c}$ of dark matter is computed to

$$\Omega_{DM} = \frac{45}{2\pi^2}\sqrt{\frac{8\pi^3}{90}}\, 8\pi G_N\, \frac{s_0}{3H_0^2}\frac{\sqrt{g_*}}{g_{*\,S}}\frac{(l+1)x_f^{l+1}}{m_{pl}\sigma_0} \quad .$$

Inserting the numerical values and assuming that all particle species i have the common temperature $T_i = T_\gamma$ in the early universe such that $g_* = g_{*\,S}$, the outcome is the dark matter relic density

$$\Omega_{DM}h^2 = 1.04 \times 10^9\, \frac{(l+1)x_f^{l+1}}{\sqrt{g_*}m_{pl}\sigma_0}\ \mathrm{GeV}^{-1} \quad , \tag{3.3.19}$$

with the present day normalized Hubble expansion rate h and the present day entropy density $s_0 = 7.04\, n_\gamma$ [30]. Note that in (3.3.19), g_* is the number of relativistic degrees of freedom which are not decoupled at the time of freeze-out.
In the approximation of s-wave annihilation, equation (3.3.19) simplifies to [57, 58]

$$\Omega_{DM}h^2 \approx \frac{3\cdot 10^{-27}\ \mathrm{cm}^3\ \mathrm{s}^{-1}}{\langle \sigma_{1+2\leftrightarrow 3+4}\, v_r\rangle} \quad . \tag{3.3.20}$$

To obtain the measured dark matter relic density $\Omega_{DM}h^2 \approx 0.1$, the order of magnitude of $\langle \sigma_{1+2\leftrightarrow 3+4}\, v_r\rangle$ has to be

$$\langle \sigma_{1+2\leftrightarrow 3+4}\, v_r\rangle = 3\cdot 10^{-26}\ \mathrm{cm}^3\ \mathrm{s}^{-1} = 1\ \mathrm{pb} \tag{3.3.21}$$

according to equation (3.3.20). The strength of weak scale interactions is [58]

$$\langle \sigma_{1+2\leftrightarrow 3+4}\, v_r\rangle^{\mathrm{weak}} = 1\ \mathrm{pb} \quad .$$

This coincidence is called the WIMP-miracle, meaning that a stable particle associated with new physics at the electroweak scale can contribute the necessary dark matter relic density.

3.4 Does Dark Matter Have to Be Cold?

In the computation of the relic density in section 3.3, we assumed that at the time of freeze-out the dark matter is non-relativistic, i.e., cold. The discussion of equation (3.3.17) reveals that for relativistic, i.e., hot dark matter, the calculation of the relic density simplifies because Y_{eq} remains constant.
Prototypes for hot dark matter are neutrinos. The bound on Y_p and its implications (see section 3.2) suggest that new neutrinos with Standard Model weak interactions are disfavored as candidates for hot dark matter. However, Standard Model sterile neutrinos which decouple earlier than Standard Model neutrinos are allowed [52].

Cold and hot dark matter have different impacts on the structure formation of the universe. The energy in radiation during the radiation-dominated epoch provided the gravitation according to equation (3.1.1). Due to equation (3.1.8) a gas of radiation has pressure which counteracts the gravitational contraction of small scale clumps. The radiation fluid interacts with the fluid of protons and electrons through Thomson scattering. Protons and electrons interact through Coulomb scattering and therefore they effectively form one fluid, the baryon fluid. Thus there remains the photon-baryon fluid with a net pressure arising from the radiation fluid. Apart from the photon-baryon fluid there is the dark matter fluid and the neutrino fluid. All the different fluids interact via gravity. The interplay between contraction and expansion of the photon-baryon fluid is called the baryon acoustic oscillations (BAO) . On large scales, clumps collapse under gravity since the radiation pressure is relatively small [59]. In the matter dominated epoch, the difference between cold and hot dark matter becomes important. From equation (3.1.8) it follows that cold dark matter is pressureless. Without pressure, the BAO stop. Small and large scales clump together and the structures we observe today begin to form in a bottom-up formation.
The first scales to collapse in a hot dark matter universe would correspond to superclusters. Galaxies would form by fragmentation of superclusters [60] in a top-down formation. However, we know from observations that galaxies are older than superclusters [61]. Therefore, the observed structures disfavor hot dark matter. The standard theory of structure formation thus requires that dark matter is cold [53]. Between cold and hot there are warm dark matter models which do not contradict structure formation [62]. We will stick to cold dark matter.

3.5 Strategies for Detection of Dark Matter

Figure 3.3 demonstrates strategies to learn about the nature of dark matter [63]. These are direct detection and indirect detection experiments and dark matter production at colliders.

3.5.1 Direct Detection

By crossing symmetry (see figure 3.3), the amplitude for dark matter s-channel annihilation into quarks q is related to the amplitude for t-channel elastic scattering of dark matter off quarks. Thus a non-zero coupling of dark matter to nuclei is expected [58]. Direct detection experiments aim to measure the recoil energy of a nucleus after the scattering process. These energies are of order $\mathcal{O}(10)$ keV which is far below typical nuclear excitation energies which are of order $\mathcal{O}(10)$ MeV. That means that a dark matter particle effectively interacts coherently with the entire nucleus.
The detection rate is proportional to the detector mass, the dark matter flux expected on Earth, and to the dark-matter-nucleus-scattering cross section (see e.g. [57]).
The matrix element for the dark-matter-nucleus-scattering cross section involves the expectation values $\langle N|\overline{q}\Gamma q|N\rangle$ of quark bilinear operators inside the nucleon N with

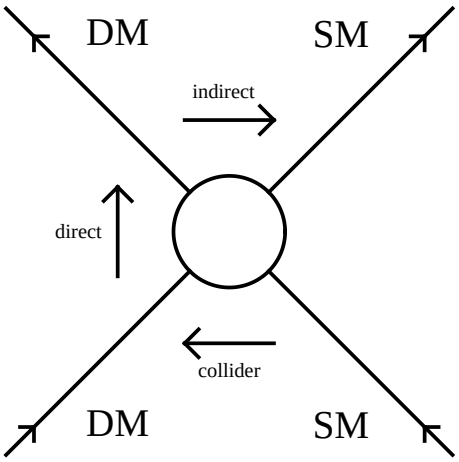

Figure 3.3: Elucidating dark matter: Direct detection experiments observe the t-channel scattering of dark matter off Standard Model nuclei, indirect detection experiments probe final Standard Model products through dark matter s-channel annihilation. At colliders, dark matter could be produced through s-channel annihilation of Standard Model particles.

Γ (see appendix B) representing the Dirac bilinears [64]. In the non-relativistic limit the vector current $\overline{q}\gamma^\mu q$ and the tensor current $\overline{q}\sigma^{\mu\nu}q$ have the same form as the scalar $\overline{q}q$ and axial vector current $\overline{q}\gamma^\mu\gamma^5 q$ (see (B.2.5) and (B.2.6)), respectively. Thus the relevant interactions are scalar $\overline{q}q$ and axial-vector $\overline{q}\gamma^\mu\gamma^5 q$ interactions for dark matter velocities v smaller than the speed c of light.
In scalar couplings, which are spin-independent (SI), the t-channel-mediated scalar particle interacts through Yukawa interactions coherently with all the nucleons in the nucleus. Hence the cross section is enhanced by the squared mass number A^2 of the nucleus and thus the detection rate is larger for heavier nuclei.
Axial-vector couplings lead to spin-dependent (SD) interactions, in which the spins of the nucleons cancel in pairs.
For SI interactions, the dark matter-nucleus-scattering cross section is larger than for SD interactions [64]. Therefore we concentrate on SI elastic scattering processes.
Given that the mean density ρ_0 of elementary particles trapped in the galactic gravitational field at the position of the Sun is $\rho_0 \approx 0.3\ \mathrm{GeV\,cm^{-3}}$ [65], the number density n_0 of an elementary dark matter particle equals

$$n_0 = \frac{1}{m_{DM}}\rho_0 \approx 10^{-3}\ \mathrm{cm}^{-3}\left(\frac{100\ \mathrm{GeV}}{m_{DM}}\right) \quad .$$

We take the velocity v of dark matter particles at the position of the Sun to be the circular velocity $v_\odot$ of the Sun on its path around the galactic center:

$$v = v_\odot = 220\,\frac{\mathrm{km}}{\mathrm{s}} \quad .$$

parameter	neutron n	proton p
f_{Tu}	0.018	0.023
f_{Td}	0.042	0.033
f_{Ts}	0.26	0.26

Table 3.1: Nucleon parameters

v is then approximately three orders of magnitude smaller than c, so the non-relativistic limit applies.
The dark matter flux J_0 expected at the Earth is

$$J_0 = n_0\, v \approx 10^5 \text{ cm}^{-2} \text{ s}^{-1} \left(\frac{100 \text{ GeV}}{m_{DM}}\right) \quad . \tag{3.5.1}$$

The antagonist of the large dark matter flux is the weakness of the interaction strength, which makes it hard to distinguish a dark matter signal from background signals.
The calculation of the dark-matter-nucleus-scattering cross section proceeds in two steps [58]: in a first step, the matrix element of the quark operators in a nucleon has to be evaluated. In a second step, the effective interaction of dark matter particles with nuclei has to be determined by computing the matrix elements of nucleon operators in a nuclear state.
Starting with step one, we define the nucleon parameters $f_{Tq}^{(N)}$ by the matrix elements of the light quarks $q = u\,, d\,, s$ inside a nucleon N with mass m_N:

$$\langle N|m_q \overline{q} q|N\rangle = m_N f_{Tq}^{(N)} \quad .$$

The nucleon parameters $f_{Tq}^{(N)}$ are associated with hadronic uncertainties in the computation of the σ-term from πN scattering $\sigma_{\pi N} = \frac{1}{2}(m_u + m_d)\langle N|\overline{u}u + \overline{d}d|N\rangle$. In table 3.1, we give the values presented in [66].
For the matrix elements of the heavy quarks $Q = c,\, b,\, t\,$, the heavy-quark expansion is used, resulting in [58]:

$$\langle N|m_Q \overline{Q} Q|N\rangle = \frac{2}{27} m_N \left(1 - \sum_{q=u,\,d,\,s} \left(1 - f_{Tq}^{(N)}\right)\right) \quad .$$

Since we concentrate on SI elastic scattering, the effective coupling of the t-channel mediated scalar particle to a nucleon N is a Yukawa coupling. Writing the quark mass terms in the form $m_q = y_q \cdot w$, the outcome for the effective coupling is

$$f_N = \frac{m_N}{w} \left(\sum_{q=u,d,s} f_{Tq}^{(N)} + \frac{2}{27}\left(1 - \sum_{q=u,d,s} f_{Tq}^{(N)}\right)\right) \quad . \tag{3.5.2}$$

Note that, owing to different valence quark densities for proton and neutron, $f_p \neq f_n$.

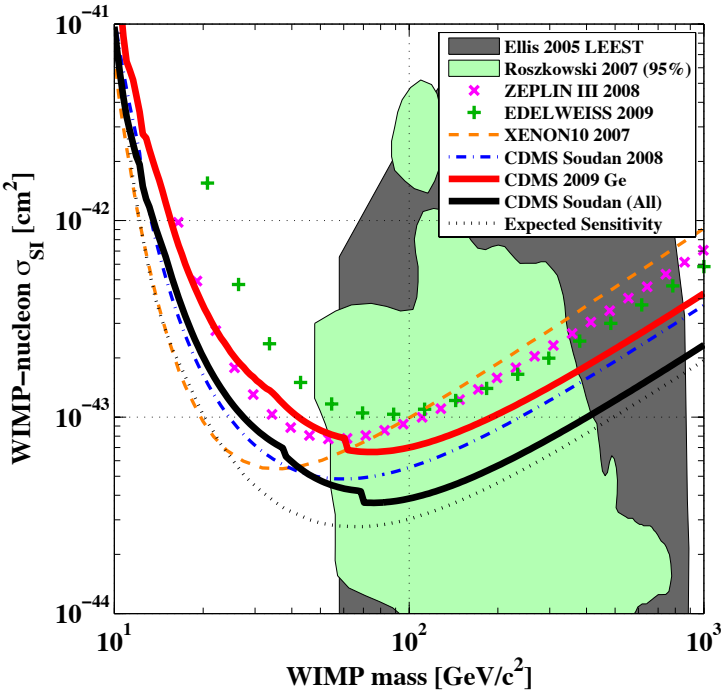

Figure 3.4: 90% C.L. upper limits on the WIMP-nucleon spin-independent cross section as a function of WIMP mass. The red (upper) solid line shows the limit obtained from the exposure analyzed in [5]. The solid black line shows the combined limit for the full data set recorded at Soudan. The dotted line indicates the expected sensitivity for this exposure based on the background in [5] combined with the observed sensitivity of past Soudan data. Prior results from CDMS [6], EDELWEISS II [7], XENON10 [8], and ZEPLIN III [9] are shown for comparison. The shaded regions indicate allowed parameter space calculated from certain Minimal Supersymmetric Models [10, 11]. Figure borrowed from [5].

Step two simplifies for SI elastic scattering because the interaction of a dark matter particle with a nucleus is just the sum of the effective interactions with the nucleons inside the nucleus. With the proton number Z, the dark-matter-nucleus-scattering cross section then turns out to be

$$\sigma_{SI} \simeq \frac{4}{\pi}\left(\frac{m_p m_n}{m_p + m_n}\right)^2 \frac{1}{m_t^4}\left(Z f_p + (A - Z) f_n\right)^2 \quad . \tag{3.5.3}$$

Here, m_t refers to the mass of the t-channel mediated mass eigenstate. The exact expression for σ_{SI} depends on the model-specific mass eigenstates.
With a given detector mass, the dark matter flux expected on earth (equation (3.5.1)) and the measured detection rate, the dark-matter-nucleus-scattering cross section (equation (3.5.3)) can be constrained.
In the CDMS II experiment , two events in the signal region were observed with a total exposure of 612 kg-days. Taking this observation as statistically significant and combining it with all previous CDMS II data, the dark matter-nucleus-scattering cross section is limited from above by $3.8 \cdot 10^{-8}$ pb [5] for a WIMP mass 70 GeV (compare figure 3.4). However, one expects 0.8 events as background, and the probability to detect at least two events is 23 %, which is too low to make any conclusion.
We concentrate on elastic scattering processes in which the final particles are in the same state as the corresponding initial particles. It is possible that for a particle dark matter candidate, there exists an excited state with a mass splitting δ to the ground state, which would allow inelastic scattering processes.
A non-zero δ increases the minimum WIMP speed required to produce a given nuclear recoil energy [13, 67]. It follows that the detection rate for inelastic dark matter scattering is more sensitive to the dark matter velocity than for elastic scattering [68]. However, the minimum dark matter velocity changes in the rest frame of the detector due the combined motion of the Sun in the galactic rest frame and of the earth around the Sun. Thus, inelastic scattering detection experiments should detect an annual modulation of their recorded signals. In fact, the DAMA/LIBRA experiment located at the Gran Sasso National Laboratory has registered an annual modulation in the signal. This signal could be explained in the context of inelastic dark matter with a mass splitting of order $\delta \sim \mathcal{O}(100)$ keV [12], which is compatible with the CDMS data for a narrow region of the parameter space (figure 3.5). But the question remains whether the annual modulation could be traced back to other cyclic changes, e.g., the composition of the Earth's atmosphere, the water level at Gran Sasso, etc.

3.5.2 Indirect Detection

Indirect detection experiments search for the dark matter annihilation products (compare figure 3.3). The most promising channel to learn about the nature of dark matter is the annihilation into photons. Due to their vanishing electric charge, photons do not experience any deflection in magnetic fields and can provide local information about the dark matter annihilation and thus about the dark matter distribution.

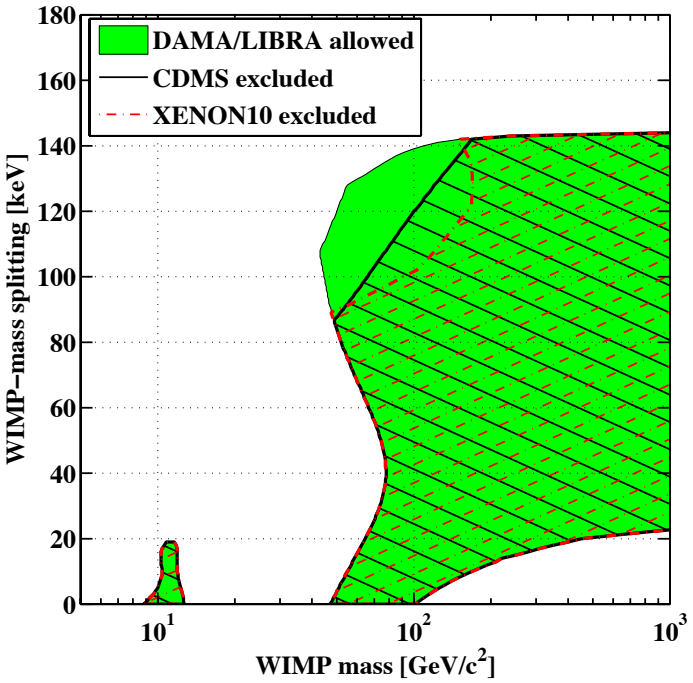

Figure 3.5: The shaded green region represents WIMP masses and mass splittings for which there exists a cross section compatible at 90% C. L. with the modulation spectrum of DAMA/LIBRA [12] under the inelastic dark matter interpretation [13]. Excluded regions for CDMS II (solid-black hatched) and XENON10 [14] (red-dashed hatched) were calculated in [5] using the Optimum Interval Method. Figure borrowed from [5].

In most models, the spectrum of photons produced in dark matter annihilation depends on the details of the dark matter particle [63]. In our proposed model, the dark matter particle is a right-handed Majorana neutrino. For any dark matter model of this type, a similar spectrum is expected without dependence on further parameters [69].
The expected gamma ray flux J_γ arriving from the galactic center is proportional to the number of dark matter annihilation events per time per volume. Dimensional analysis yields:

$$J_\gamma \propto \sigma_a v_r n^2 = \sigma_a v_f \frac{\rho^2(r)}{m_{DM}^2} \quad . \tag{3.5.4}$$

In equation (3.5.4), σ_a is the annihilation cross section, v_r is the relative velocity of the dark matter particles at freeze-out, n is the dark matter number density and $\rho(r)$ is the dark matter energy density. In the standard halo model, the dark matter distribution is spherically symmetric. Therefore, the dark matter energy density only depends on the distance r to the galactic center. Compared to equation (3.5.1), we see that (3.5.4) is more sensitive to the dark matter distribution $\rho(r)$.
The gamma ray spectrum is given by [63]

$$\Phi_\gamma\left(E_\gamma, \Omega_\gamma\right) = \frac{1}{8\pi}\langle\sigma_a v_r\rangle \frac{dN_\gamma}{dE_\gamma} \int_{\Delta\Omega} d\Omega \int_{\text{l.o.s.}} ds\, \frac{\rho^2(r)}{m_{DM}^2} \quad , \tag{3.5.5}$$

where $\langle\sigma_a v_r\rangle$ is the thermal average of the dark matter annihilation cross section times relative velocity, $\frac{dN_\gamma}{dE_\gamma}$ is the gamma ray energy spectrum generated per dark matter annihilation, Ω is the observation angle relative to the direction of the galactic center and l.o.s. stands for line-of-sight.
Equation (3.5.5) once again illustrates the merging of particle physics with cosmology: the thermal average of the annihilation cross section times relative velocity $\langle\sigma_a v_r\rangle$ involves all possible annihilation channels of dark matter particles and belongs to the realm of particle physics. The dark matter energy density profile $\rho(r)$ belongs to the realm of cosmology and is highly unknown near to the galactic center.
N-body simulations results indicate [70]

$$\rho(r) = \frac{\rho_s}{(\frac{r}{r_s})^\gamma [1 + (\frac{r}{r_s})^\alpha]^{\frac{\beta-\alpha}{\alpha}}} \quad ,$$

with scale density ρ_s and scale radius r_s. The Navarro-Frenk-White (NFW) profile has the parameters $\alpha = 1$, $\beta = 3$ and $\gamma = 1$ [71], the Moore profile has the set $\alpha = 1.5$, $\beta = 3$ and $\gamma = 1.5$ [72] and the isothermal profile is given by $\alpha = \beta = 2$, $\gamma = 0$. The NFW profile seems to underestimate the dark matter density for small r while the Moore profile overestimates it [70]; in contrast, the Einasto profile [73], being an exponential function, seems to estimate the dark matter density correctly for small radii r. The isothermal profile is nearly constant for radii $r \ll r_s$. These dark matter density profiles, shown in figure 3.6, produce the constant galaxy rotation curves for distances r approximately between 8 kpc and 20 kpc. For larger distances, the dark

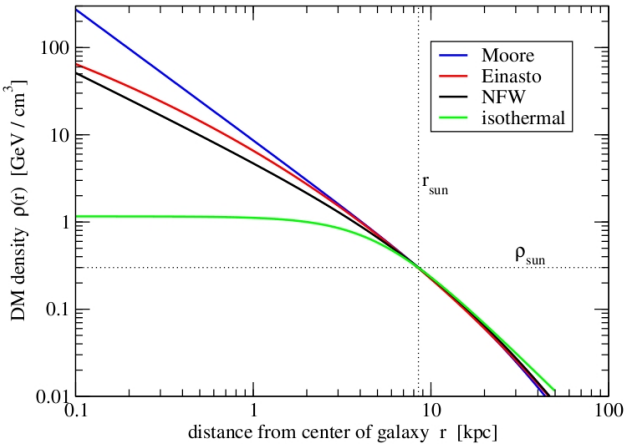

Figure 3.6: Dark matter density profiles with $\rho_s = \rho_{sun}$ and $r_s = r_{sun}$. Figure borrowed from [15].

matter density profiles decrease faster than r^{-2}. As a consequence, the galaxy rotation curves decline for large distances, opposed to the constant circular velocity profiles at large distances predicted by MOND theories (compare to section 1). Indeed, MOND is in conflict with the determined motion of satellite galaxies around normal galaxies at distances between 50 kpc and 500 kpc [74], which in turn is in perfect agreement with the ΛCDM model.
The Fermi-LAT experiment [16] can measure the gamma ray energy spectrum. Knowing the gamma ray background and choosing a specific dark matter density profile, the dark matter annihilation cross section can be constrained by equation (3.5.5). The results from [16] are presented in figure 3.7. In [16], the properties of dark matter are deduced from the quantity $\Lambda^2(z)$ which describes the enhancement of the annihilation signal arising due to the clustering of dark matter into halos and subhalos [75]. In order to derive $\Lambda^2(z)$, [16] uses four procedures:

(i) In MS II-Res, only the contributions to the dark matter annihilation signal from halos and subhalos resolved in the Millenium II simulation [76] are considered.

(ii) In MS II-Sub1, the contribution from structures and substructures down to 10^{-6} solar masses are extrapolated in a very conservative way (compare [16]).

(iii) In MS II-Sub2, subhalos and halos down to 10^{-6} solar masses are involved.

(iv) BulSub is a semi-analytical procedure to calculate $\Lambda^2(z)$; the contribution from halos of all masses is integrated based on the Bullock model [77].

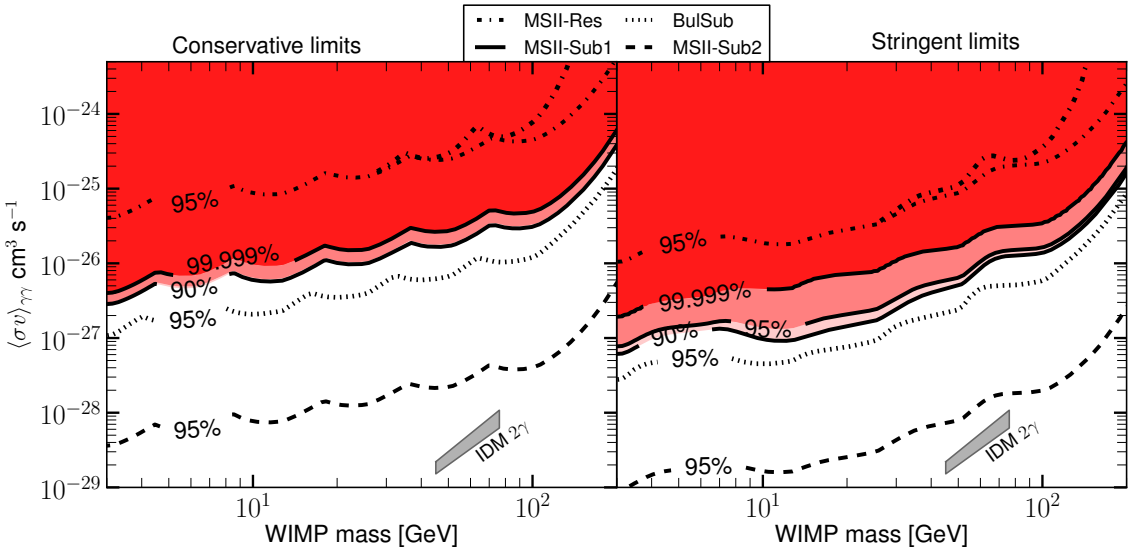

Figure 3.7: Cross section $\langle\sigma v\rangle$ limits on dark matter annihilation into two photons. The red regions mark the (90, 95, 99.999)% exclusion regions in the MSII-Sub1 $\Delta^2(z)$ dark matter structure scenario (and for the other structure scenarios only 95% upper limit lines). Figure from [16].

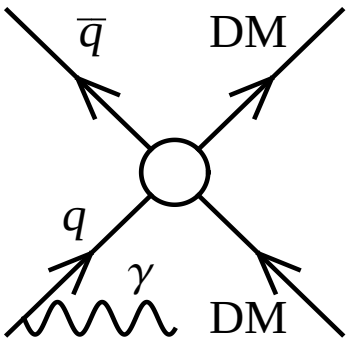

Figure 3.8: Production of dark matter at colliders with initial state radiated photon.

3.5.3 Collider Production

A key quantity at colliders is the luminosity $\mathfrak{L}$. Integrated over the time interval in which data are taken, the integrated luminosity $\int dt\, \mathfrak{L}$ times the production cross section for a specific particle yields the number of events in which the particle under consideration is observed.
At colliders, dark matter particles can be produced in s-channel annihilations of Standard Model particles. The production cross section depends on the mass of the dark matter particle and the available center of mass energy. The general behavior is a decreasing production cross section with an increasing dark matter mass by a fixed center of mass energy. Therefore, to produce dark matter at the LHC , which is a proton-proton collider, the mass of the dark matter has to be small relative to the center of mass energy.
Since dark matter is neutral under the Standard Model gauge interactions, it can only be detected through missing transverse energy $\not{E}_T$. The collider signature $\gamma + \not{E}_T$ of a mono-photon γ plus large missing transverse energy $\not{E}_T$ (see figure 3.8) is most suited to measure $\not{E}_T$: the energy of the initial state radiated photon γ is detected in the electromagnetic calorimeters. Given the center of mass energy, the missing energy $\not{E}_T$ is determined. The mass of the dark matter particle follows.

3.5.4 Critical Remarks

The strategies for the detection of dark matter presented above have to be taken with a pinch of salt. The detection rate in direct detection experiments depends on the dark matter flux J_0 expected on Earth, which in turn depends on the local dark matter density ρ_0. The conclusion of [78] is that the astronomical constraints are consistent with a local dark matter density between $\rho_0 = 0.2\ \mathrm{GeV\,cm^{-3}}$ and $\rho_0 = 0.4\ \mathrm{GeV\,cm^{-3}}$. J_0 further depends on the Sun's circular velocity $v_\odot$. Different methods obtain different results: with the angular velocity of the Sun about the galactic center, which is the ratio between the total velocity $v_\odot$ of the Sun about the galactic center and the distance of the Sun from the galactic center [79], and the fitted distance of the Sun from the galactic center [80], $v_\odot$ results to $v_\odot = 242 \pm 12\ \mathrm{kms^{-1}}$. In [81], $v_\odot = 221 \pm 18\ \mathrm{kms^{-1}}$ is used.
However, spin independent elastic scatterings are resistant against these uncertainties for a dark matter particle with mass higher than 50 GeV [82].
Apart from the highly unknown dark matter density profile, indirect detection experiments rely on the gamma ray background. The astrophysical sources for gamma ray emission are not known in detail, so it is hard to distinguish between an astrophysical signal in the gamma ray spectrum and a signal produced by dark matter annihilations. Anisotropies in the gamma ray background may help to distinguish between astrophysical sources and dark matter sources: if one assumes that astrophysical gamma ray sources have the same distribution as the matter distribution ρ_m, then the corresponding gamma ray signal depends linearly on ρ_m. Equation (3.5.5) shows that the gamma ray signal expected from dark matter annihilations depends

quadratically on ρ_m. That means that dark matter annihilations could generate larger anisotropies in the gamma ray signal than expected from astrophysical sources [83]. The Fermi-LAT experiment may resolve such anisotropies.
The search for dark matter at colliders relies on missing transverse energy, which could have several sources. Only the combined data analysis of direct and indirect detection and collider production reveals whether the source for a detected missing transverse energy is indeed annihilation of Standard Model particles into dark matter: if the mass of dark matter produced at colliders fits with the mass of dark matter gained from recoil energy spectra in direct detection experiments and with the mass of dark matter obtained from gamma ray spectra in indirect detection experiments, then the missing transverse energy would be due to the creation of dark matter particles [84].

Chapter 4

Zee-Babu in the Dark

To solve the two issues of astroparticle physics, namely the neutrino mass and the dark matter of the universe, we build a model which generates masses for two Standard Model neutrinos at the two loop level and which has a right-handed Majorana neutrino N_R as a candidate for particle dark matter. The input is the Zee-Babu model reviewed in section 4.1. In section 4.2, we consider two possible extensions of it, having both N_R as a particle dark matter: in a first scenario, a local $U(1)_{B-L}$ forces the introduction of N_R in order to cancel the $U(1)_{B-L}$ triangle anomaly as discussed in chapter 2, and in a second scenario, $U(1)_{B-L}$ is global and N_R is put in *ad hoc*. In both scenarios, $U(1)_{B-L}$ is spontaneously broken when N_R becomes massive, so, in the second scenario, there enters a Majoron into the theory. In section 4.3, we demonstrate that N_R passes the three point test set up in chapter 3. In addition, we discuss the verification of our model at the LHC in section 4.4.

4.1 The Zee-Babu Model

As outlined in section 2.3.2, neutrino masses can be produced radiatively. Loop suppression factors entering into radiative mass generation mechanism lead to light masses for additional particles running in the loops. We focus on the Zee-Babu Model [27] as an example for radiative neutrino masses and build extensions to describe dark matter.

While still unobserved, the Standard Model relies on one complex scalar Higgs doublet ϕ which directs electroweak symmetry breaking in the common lore. Additional scalars are theoretically motivated.

In addition to the Standard Model Higgs doublet, the scalar sector of the Zee-Babu Model [27] contains two complex scalar singlets: a singly charged scalar singlet h^+ and a doubly charged scalar singlet k^{++} (see table 2.1). Since the vacuum state is electrically neutral, the new scalars do not receive a vacuum expectation value, i.e., $\langle 0|h^+(x)|0\rangle = \langle 0|k^{++}(x)|0\rangle = 0$.

The gauge group is the Standard Model gauge group $G^{(SM)}$. Since no right-handed neutrinos are added, there are no Dirac masses m_D for neutrinos.

h^+ couples to left-handed leptons

$$f_{ij}\left(\Psi^{i,T}_{L,a}\mathbf{C}\,\Psi^{j}_{L,b}\right)\epsilon_{ab}\,h^+ \tag{4.1.1}$$

and k^{++} couples to right-handed leptons

$$h'_{ij}\left(\Psi^T_{R,i}\mathbf{C}\,\Psi_{R,j}\right)\,k^{++}\quad . \tag{4.1.2}$$

Yukawa couplings of h^+ and k^{++} to Standard Model quarks have no vanishing hypercharge q_Y and are thus not gauge invariant (compare table 2.1).
$i\,,j$ are flavor indices and a,b are $SU(2)_L$ gauge indices. f_{ij} and h'_{ij} are generic complex matrices. The antisymmetric $SU(2)_L$ invariant ϵ_{ab} tensor together with relation (B.3.4) forces f_{ij} in (4.1.1) to be antisymmetric, i.e., $f_{ij}=-f_{ji}$.
For the three Standard Model flavor generations, (4.1.1) and (4.1.2) contribute the following interaction Lagrangian

$$\begin{aligned}\mathcal{L}^{int}_{Babu} &= 2\Big[f_{e\mu}\left(\overline{\nu_e^C}\mu_{\rm L}-\overline{\nu_\mu^C}e_{\rm L}\right)+f_{e\tau}\left(\overline{\nu_e^C}\tau_{\rm L}-\overline{\nu_\tau^C}e_{\rm L}\right)\\ &\quad+\ f_{\mu\tau}\left(\overline{\nu_\mu^C}\tau_{\rm L}-\overline{\nu_\tau^C}\mu_{\rm L}\right)\Big]\,h^+\\ &\quad+\Big[h_{ee}\overline{e^C}e_{\rm R}+h_{\mu\mu}\overline{\mu^C}\mu_{\rm R}+h_{\tau\tau}\overline{\tau^C}\tau_{\rm R}\\ &\quad+m\,h_{e\mu}\overline{e^C}\mu_{\rm R}+h_{e\tau}\overline{e^C}\tau_{\rm R}+h_{\mu\tau}\overline{\mu^C}\tau_{\rm R}\Big]\,k^{++}\quad .\end{aligned} \tag{4.1.3}$$

In (4.1.3) we have defined $h_{ii}=h'_{ii}$ and $h_{ij}=2h'_{ij}$ for $i\neq j$ because h'_{ij} is symmetric due to (B.3.4), i.e., $h'_{ij}=h'_{ji}$.
The interaction terms in equation (4.1.3) are invariant under $U(1)_{B-L}$ in the given charge assignment of table 2.1. Owing to the $U(1)_{B-L}$ invariance, Majorana mass terms are not allowed at tree level, so neutrinos are massless in the Zee-Babu model at tree level.
The scalars h^+ and k^{++} together with the Standard Model Higgs doublet ϕ give the following scalar potential:

$$\begin{aligned}V(\phi) &= \mu_2^2\phi^\dagger\phi+\mu_3^2k^{++}k^{--}+\mu_4^2h^+h^-\\ &\quad+\lambda_2(\phi^\dagger\phi)^2+\lambda_3(k^{++}k^{--})^2+\lambda_4(h^+h^-)^2\\ &\quad+\lambda_8(\phi^\dagger\phi)(k^{++}k^{--})+\lambda_9(\phi^\dagger\phi)(h^+h^-)+\lambda_{10}(k^{++}k^{--})(h^+h^-)\\ &\quad+\mu\left(k^{++}h^-h^-+k^{--}h^+h^+\right)\quad .\end{aligned} \tag{4.1.4}$$

The μ term in (4.1.4) softly breaks the $U(1)_{B-L}$ symmetry. In the Zee-Babu model, this term has to be introduced by hand in order to generate Majorana neutrino masses at two-loop level. The induced lepton number violation is then suppressed by $\frac{1}{(16\pi^2)^2}$.
The effective Majorana neutrino mass term is

$$\mathcal{L}_\nu=-\frac{1}{2}\overline{\varkappa_i}\,(\mathcal{M}_\nu)_{ij}\,\varkappa_j\quad , \tag{4.1.5}$$

where

$$\varkappa_i=\nu_i+\nu_i^C$$

and $(\mathcal{M}_\nu)_{ij}$ is the neutrino mass matrix.
In the example of figure 4.1, we calculate the mass matrix element $(\mathcal{M}_\nu)_{ee}$:

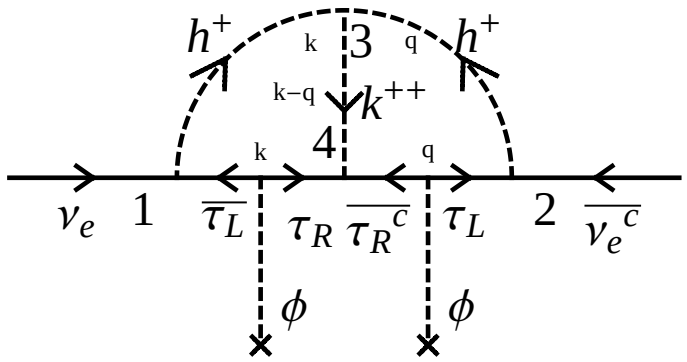

Figure 4.1: Example for two-loop neutrino mass generation

- At vertex 1, we have the interaction $2\left(f_{e\tau}\overline{\nu_e^C}\tau_{\rm L}h^+\right)^\dagger = 2(f_{e\tau}^\dagger)\overline{\tau}_{\rm L}\nu_e h^-$ with Majorana condition $\nu_e^C = \nu_e$.
- Similarly, at vertex 2 the interaction is $2\left(f_{e\tau}\overline{\nu_e^C}\tau_{\rm L}h^+\right)$.
- At vertex 3, we have the lepton number violating interaction $\mu\, k^{++}h^-h^-$.
- At vertex 4, the interaction is $h_{\tau\tau}\overline{\tau^C}\tau_{\rm R}$.
- The vertices with Standard Model Higgs insertion $\langle\phi\rangle$ lead to mass terms m_τ.
- One has to integrate over the unfixed momenta k and q. The two-loop integral is

$$I_{\tau\tau} = \int \frac{d^4k}{(2\pi)^4}\int \frac{d^4q}{(2\pi)^4}\,\frac{1}{k^2-m_\tau^2}\,\frac{1}{k^2-m_h^2}\,\frac{1}{q^2-m_\tau^2}\,\frac{1}{q^2-m_h^2}\,\frac{1}{(k-q)^2-m_k^2}\quad . \tag{4.1.6}$$

The mass matrix element $(\mathcal{M}_\nu)_{ee}$ then results to

$$\begin{aligned}(\mathcal{M}_\nu)_{ee} &= 2\cdot 4\,\mu f_{e\tau}h_{\tau\tau}m_\tau^2 I_{\tau\tau}(f_{e\tau})^\dagger \\ &= 8\,\mu f_{e\tau}h_{\tau\tau}m_\tau^2 I_{\tau\tau}(f_{e\tau})^\dagger\quad .\end{aligned} \tag{4.1.7}$$

The additional factor 2 in (4.1.7) arises because $(\mathcal{M}_\nu)_{ee}$ is not the mass matrix for ν_e, but for the self conjugated field $\varkappa_e = \nu_e + \nu_e^C$.
From this example, we conclude that a general mass matrix element $(\mathcal{M}_\nu)_{ij}$ has the form

$$(\mathcal{M}_\nu)_{ij} = 8\,\mu f_{is}h_{st}m_s m_t I_{st}(f_{tj})^\dagger\,. \tag{4.1.8}$$

(4.1.8) has a special texture. If we define

$$K_{st} \equiv 8\,\mu h_{st}m_s m_t I_{st}\quad ,$$

we can write (4.1.8) as

$$(\mathcal{M}_\nu)_{ij} = (fKf^\dagger)_{ij}\quad . \tag{4.1.9}$$

The determinant of (4.1.8) is:

$$\begin{aligned} \det \mathcal{M}_\nu &= \det f \cdot \det K \cdot \det f^\dagger \\ &= \det f \cdot \det f^* \cdot \det K \\ &= |\det f|^2 \cdot \det K \,. \end{aligned} \tag{4.1.10}$$

For an odd number of flavor generations, the determinant of f is zero because f is antisymmetric. From (4.1.10) it then follows that for three generations the determinant of the neutrino mass matrix (4.1.8) vanishes, i.e., $\det \mathcal{M}_\nu = 0$.
The eigenvalue problem for (4.1.8), namely

$$\det \; (\mathcal{M}_\nu - \lambda \mathbf{1}) \stackrel{!}{=} 0 \;\; ,$$

reveals that one eigenvalue of (4.1.8) is zero. Thus we find that in the Zee-Babu model, one neutrino is massless. From section 2.3.1, we then infer that the heaviest neutrino mass m_ν is given by the atmospheric mass difference Δm^2_{atm}:

$$m_\nu \approx 0.05 \text{ eV} \;\; .$$

To learn more about neutrino masses in the Zee-Babu model, it is essential to further analyse the integral (4.1.6). If we assume that the masses of the scalars h^+ and k^{++} are at the TeV scale (see below), we can, in a first approximation, neglect the fermion masses m_i and m_j in I_{ij} and (4.1.6) becomes

$$\int \frac{d^4k}{(2\pi)^4} \int \frac{d^4q}{(2\pi)^4} \frac{1}{k^2} \frac{1}{k^2 - m_h^2} \frac{1}{q^2} \frac{1}{q^2 - m_h^2} \frac{1}{(k-q)^2 - m_k^2} \;\; . \tag{4.1.11}$$

Concentrating on the k integration and using Feynman parameters x_1, x_2, x_3, we arrive at the equality (see (D.1.1))

$$\begin{aligned} & \frac{1}{k^2} \frac{1}{k^2 - m_h^2} \frac{1}{(k-q)^2 - m_k^2} \\ = & \int_0^1 dx_1\, dx_2\, dx_3\, \delta(x_1 + x_2 + x_3 - 1) \frac{2!}{(x_1 k^2 + x_2(k^2 - m_h^2) + x_3((k-q)^2 - m_k^2))^3} \\ = & \int_0^1 dx_1\, dx_2 \frac{2!}{(x_1 k^2 + x_2(k^2 - m_h^2) + (1 - x_1 - x_2)((k-q)^2 - m_k^2))^3} \;\; . \end{aligned} \tag{4.1.12}$$

We shift the integration variable k to

$$k \to l_1 \equiv k - (1 - x_1 - x_2) q$$

and introduce

$$\Delta_1 = x_2 m_h^2 + (1 - x_1 - x_2)^2 q^2 - (1 - x_1 - x_2)(q^2 - m_k^2) \;\; .$$

Observe that Δ_1 is independent of k.
In dimensional regularization (see appendix D), (4.1.12) takes the form

$$\begin{aligned}&\int \frac{d^4k}{(2\pi)^4}\,\frac{1}{k^2}\,\frac{1}{k^2-m_h^2}\,\frac{1}{(k-q)^2-m_k^2}\\ =\;& 2!\int_0^1 dx_1\int_0^{x_1} dx_2\,\lim_{d\to 4}\int \frac{d^dl_1}{(2\pi)^d}\,\frac{1}{(l_1^2-\Delta_1)^3}\quad .\end{aligned}$$

The d dimensional integral over l_1 is evaluated to (see (D.2.1))

$$\begin{aligned}\lim_{d\to 4}\int \frac{d^dl_1}{(2\pi)^d}\,\frac{1}{(l_1^2-\Delta_1)^3} &= \lim_{d\to 4}\frac{-\mathrm{i}}{(4\pi)^{\frac{d}{2}}}\frac{\Gamma(3-\frac{d}{2})}{\Gamma(3)}\left(\frac{1}{\Delta_1}\right)^{3-\frac{d}{2}}\\ &= \frac{-\mathrm{i}}{16\pi^2}\frac{1}{2}\left(\frac{1}{\Delta_1}\right)\end{aligned}\tag{4.1.13}$$

The q integration contributes another factor $\frac{1}{16\pi^2}$, such that (4.1.6) is suppressed by $\frac{1}{(16\pi^2)^2}$.
Treating scalar integrals as in [85], the two-loop integral (4.1.6) is evaluated in [86]:
For the case $m_k \gg m_h$, the dominant behavior of (4.1.6) is

$$I_{ij} \simeq \frac{1}{(16\pi^2)^2}\,\frac{1}{m_k^2}\left(\log^2\frac{m_h^2}{m_k^2}+\frac{\pi^2}{3}-1\right)+\mathcal{O}\left(\frac{1}{m_k^4}\right)$$

and thus to leading order

$$I_{ij} \approx \frac{1}{(16\pi^2)^2}\,\frac{1}{m_k^2}\log^2\left(\frac{m_h^2}{m_k^2}\right)\quad .\tag{4.1.14}$$

For the case $m_h \gg m_k$, the leading term of (4.1.6) is

$$I_{ij} \approx \frac{1}{(16\pi^2)^2}\,\frac{1}{m_h^2}\,\frac{\pi^2}{3}\quad .\tag{4.1.15}$$

Defining $M \equiv \max(m_h, m_k)$ and using the leading terms (4.1.14) and (4.1.15), respectively, we can approximate (4.1.7) by [87]

$$\mathcal{M}_\nu \approx \frac{f^2h}{(16\pi^2)^2}\,\frac{m_\tau^2}{\Lambda}\quad ,\tag{4.1.16}$$

where $\Lambda = \frac{M^2}{\mu}$ is the scale of physics beyond the Standard Model.
From (4.1.16), we see that for $\mathcal{M}_\nu \sim \mathcal{O}(0.1)$ eV, the scale Λ of new physics has to be of order $\Lambda \sim \mathcal{O}(1)$ TeV if we demand that $f \sim h \sim \mathcal{O}(0.1)$ and use $m_\tau \approx 1.7$ GeV. As already mentioned in section 2.3.2, this scale Λ for generating neutrino masses is much below the scale of seesaw models because of the two-loop suppression factor $\frac{1}{(16\pi^2)^2}$ which is of order $\mathcal{O}(10^4)$.
Hence, Λ is within the range of the LHC and may thus be probed soon.

4.2 Extensions of the Zee-Babu Model

4.2.1 Scenario 1: $G^{(SM)} \times$ local $U(1)_{B-L} \times \mathbb{Z}_2$

To make neutrinos massive in the Zee-Babu model, one has to add the $U(1)_{B-L}$ breaking term $\mu\, k^{++}h^-h^-$ to the potential 4.1.4.
An alternative to explicitly introducing a symmetry breaking term by hand is to generate it dynamically by spontaneous symmetry breaking of an additional gauge symmetry. In section 2.5, we have seen that the local $U(1)_{B-L}$ symmetry is broken by a complex scalar singlet φ charged under $U(1)_{B-L}$. Recall that we assume no gauge kinetic mixing between $U(1)_Y$ and $U(1)_{B-L}$.
If one extends the Zee-Babu model with a $U(1)_{B-L}$ gauge symmetry and adds φ to the particle content, the term

$$\lambda_\mu\, \varphi\, k^{++}h^-h^-$$

is gauge invariant. In particular, it does not violate $U(1)_{B-L}$.
If $U(1)_{B-L}$ is spontaneously broken, the μ term in the potential 4.1.4 arises through the replacement $\mu \to \lambda_\mu \langle\varphi\rangle$. Since the scale $\Lambda = \frac{M^2}{\mu}$ for generating neutrino masses at two-loop level has to be $\mathcal{O}(1)$ TeV and given the bounds on the masses of the charged scalars [88], the breaking scale of $U(1)_{B-L}$ is in the TeV range, i.e., $\langle\varphi\rangle \sim \mathcal{O}(1)$ TeV for the coupling constant $\lambda_\mu \sim \mathcal{O}(1)$.
The scalar interactions of φ have to be included into the scalar potential 4.1.4, yielding the $U(1)_{B-L}$ invariant potential:

$$\begin{aligned} V(\varphi,\, \phi) \;=\; & \mu_1^2\varphi^*\varphi + \mu_2^2\phi^\dagger\phi + \mu_3^2 k^{++}k^{--} + \mu_4^2 h^+h^- \\ & + \lambda_1(\varphi^*\varphi)^2 + \lambda_2(\phi^\dagger\phi)^2 + \lambda_3(k^{++}k^{--})^2 + \lambda_4(h^+h^-)^2 \\ & + \lambda_5(\varphi^*\varphi)(\phi^\dagger\phi) + \lambda_6(\varphi^*\varphi)(k^{++}k^{--}) + \lambda_7(\varphi^*\varphi)(h^+h^-) \\ & + \lambda_8(\phi^\dagger\phi)(k^{++}k^{--}) + \lambda_9(\phi^\dagger\phi)(h^+h^-) + \lambda_{10}(k^{++}k^{--})(h^+h^-) \\ & + \lambda_\mu\,(\varphi k^{++}h^-h^- + \varphi^* k^{--}h^+h^+) \quad . \end{aligned} \tag{4.2.1}$$

Notice that the new electrically neutral complex scalar φ is a singlet under the Standard Model gauge group and thus the Glashow-Weinberg criteria [89] for the natural absence of neutral current flavor violation are fulfilled.
To obtain the propagating neutral mass eigenstates, we parametrize the Higgs fields $\phi(x)$ and $\varphi(x)$ around their vacuum expectation values w and w' (compare to equation (2.1.2)). Here, we work in the t'Hooft-Feynman gauge to separate the physical and gauge degrees of freedom. $\phi(x)$ and $\varphi(x)$ are then given by:

$$\varphi(x) \;=\; \frac{1}{\sqrt{2}}\left(w' + (R_1(x) + \mathrm{i}I_1(x))\right) \tag{4.2.2}$$

$$\phi(x) \;=\; \frac{1}{\sqrt{2}}\begin{pmatrix} R_3(x) + \mathrm{i}I_3(x) \\ w + (R_2(x) + \mathrm{i}I_2(x)) \end{pmatrix} \quad . \tag{4.2.3}$$

The vacuum expectation values w and w' have to fulfill the minimization conditions of the potential (4.2.1):

$$0 \stackrel{!}{=} \frac{\partial}{\partial w'} \langle 0|V(\varphi,\, \phi)|0\rangle = \mu_1^2 w' + \lambda_1 w'^3 + \frac{1}{2}\lambda_5 w^2 w' \tag{4.2.4}$$

and

$$0 \stackrel{!}{=} \frac{\partial}{\partial w} \langle 0|V(\varphi,\, \phi)|0\rangle = \mu_2^2 w + \lambda_2 w^3 + \frac{1}{2}\lambda_5 w'^2 w. \tag{4.2.5}$$

To determine the masses m_{R_1}, m_{R_2}, m_{R_3}, m_{I_1}, m_{I_2} and m_{I_3}, we have to find, in (4.2.1), the terms quadratic in the fields and proportional to the corresponding vacuum expectation values squared (compare section 2.2.2). These are

$$\left(\frac{1}{2}\mu_1^2 + \frac{3}{2}\lambda_1 w'^2 + \frac{1}{4}\lambda_5 w^2\right) R_1^2 \tag{4.2.6}$$

and

$$\left(\frac{1}{2}\mu_2^2 + \frac{3}{2}\lambda_2 w^2 + \frac{1}{4}\lambda_5 w'^2\right) R_2^2 \quad . \tag{4.2.7}$$

Inserting (4.2.4) and (4.2.5) into (4.2.6) and (4.2.7), respectively, we find $m_{R_1}^2 = 2\lambda_1 w'^2$ and $m_{R_2}^2 = 2\lambda_2 w^2$, where we have used the convention of an explicit factor $\frac{1}{2}$ in the mass term.
The terms quadratic in R_3, I_1, I_2 and I_3 are zero due the minimization conditions.
$R_3(x)$, $I_3(x)$ and $I_2(x)$ are the Standard Model massless Goldstone bosons . It can be shown that Feynman diagrams with s-channel exchange of these Goldstone bosons cancel with Feynman diagrams in which timelike polarization states of gauge bosons are exchanged in the s-channel [32]. This means that $R_3(x) + iI_3(x)$ is eaten by the Standard Model gauge bosons $W^{\pm}$, and $I_2(x)$ is eaten by the Z boson. In this way, the Standard Model gauge bosons have two transversal and one longitudinal polarization state.
The mass terms of the states R_1 and R_2 can be written as

$$\frac{1}{2} \cdot \begin{pmatrix} R_1 & R_2 \end{pmatrix} \cdot \mathbf{M^2} \cdot \begin{pmatrix} R_1 \\ R_2 \end{pmatrix},$$

with

$$\mathbf{M^2} = \begin{pmatrix} 2\lambda_1 w'^2 & \lambda_5 w' w \\ \lambda_5 w' w & 2\lambda_2 w^2 \end{pmatrix} \quad . \tag{4.2.8}$$

Defining the orthogonal matrix (compare to section 2.2.2)

$$\mathbf{O} = \begin{pmatrix} \cos\beta & \sin\beta \\ -\sin\beta & \cos\beta \end{pmatrix} \quad ,$$

equation (4.2.8) reads

$$\mathbf{M}^2 = \mathbf{O}^T \cdot \begin{pmatrix} m_{H_1}^2 & 0 \\ 0 & m_{H_2}^2 \end{pmatrix} \mathbf{O} \quad . \tag{4.2.9}$$

From equation (4.2.8) combined with equation (4.2.9), it follows:

$$\begin{aligned} 2\lambda_1 w'^2 &= \cos^2\beta\, m_{H_1}^2 + \sin^2\beta\, m_{H_2}^2 && (4.2.10)\\ 2\lambda_5 w' w &= \sin 2\beta\,(m_{H_1}^2 - m_{H_2}^2) && (4.2.11)\\ 2\lambda_2 w^2 &= \sin^2\beta\, m_{H_1}^2 + \cos^2\beta\, m_{H_2}^2 \ ; \end{aligned}$$

so

$$2\lambda_1 w'^2 - 2\lambda_2 w^2 = \cos 2\beta\,(m_{H_1}^2 - m_{H_2}^2) \ ,$$

and the mixing angle β must satisfy

$$\tan 2\beta = \frac{\lambda_5 w' w}{\lambda_1 w'^2 - \lambda_2 w^2} \ .$$

The mass eigenstates are

$$\begin{pmatrix} H_1 \\ H_2 \end{pmatrix} = \begin{pmatrix} \cos\beta & \sin\beta \\ -\sin\beta & \cos\beta \end{pmatrix} \cdot \begin{pmatrix} R_1 \\ R_2 \end{pmatrix} \qquad (4.2.12)$$

with mass eigenvalues

$$\begin{aligned} m_{H_1}^2 &= \frac{1}{2}\left(2\lambda_1 w'^2 + 2\lambda_2 w^2\right) + \frac{1}{2}\sqrt{\left(2\lambda_1 w'^2 - 2\lambda_2 w^2\right)^2 + 4\lambda_5^2 w'^2 w^2}\\ m_{H_2}^2 &= \frac{1}{2}\left(2\lambda_1 w'^2 + 2\lambda_2 w^2\right) - \frac{1}{2}\sqrt{\left(2\lambda_1 w'^2 - 2\lambda_2 w^2\right)^2 + 4\lambda_5^2 w'^2 w^2} \ . \end{aligned}$$

Inverting (4.2.12), one obtains:

$$\begin{pmatrix} R_1 \\ R_2 \end{pmatrix} = \begin{pmatrix} \cos\beta & -\sin\beta \\ \sin\beta & \cos\beta \end{pmatrix} \cdot \begin{pmatrix} H_1 \\ H_2 \end{pmatrix} \ . \qquad (4.2.13)$$

The potential (4.2.1) written in terms of the Higgs mass eigenstates H_1 and H_2 is given in appendix E.

To fulfill the gauge anomaly conditions, one has to introduce a right-handed Majorana neutrino N_R with $(B-L)$ charge $q_{B-L} = -1$, as shown in section 2.5. To be the candidate for dark matter, N_R has to be stable. But so far, the following $G^{(SM)} \times U(1)_{B-L}$ invariant coupling leads to decays of N_R:

$$\overline{\Psi}_L \tilde{\phi} N_R \ .$$

We forbid this interaction by introducing an abelian discrete stabilization $\mathbb{Z}_2$ symmetry under which N_R is odd and all other particles are even (compare table 2.1). Then N_R is a Standard Model neutral stable particle and can therefore serve as a particle dark matter candidate (see section 3). Its mass follows from the term (2.5.7) after sponteaneous symmetry breaking: $m_{N_R} = \frac{\lambda_c w'}{\sqrt{2}}$, using the convention $\frac{1}{2} m \overline{N_R} N_R$ for the dark matter mass terms. So the dark matter mass is naturally in the TeV range where the $U(1)_{B-L}$ is spontaneously broken. Observe that N_R is not weakly interacting.

Thus, we can merge the two issues of astroparticle physics at one common scale: the

scale for generating neutrino masses and the mass scale of the dark matter particle is naturally the TeV scale.
Note that in the case of a local $U(1)_{B-L}$, $I_1(x)$ is eaten by the Z' gauge boson , so that there are no massless scalar degrees of freedom in the theory after φ obtains a vacuum expectation value. The stabilization symmetry $\mathbb{Z}_2$ is unaffected by the spontaneous breakdown of $U(1)_{B-L}$, so N_R remains a stable particle dark matter candidate.
In [29] it is shown that for hidden dark matter models, i.e., models in which dark matter has no Standard Model charges, there are only two renormalizable communication channels between the hidden sector and the Standard Model. The first possibility is gauge kinetic mixing between a hidden $U(1)_H$ under which dark matter is charged and the Standard Model $U(1)_Y$. Gauge kinetic mixing is discussed for example in [90]. The second possibility is the Higgs portal which relies on mass mixing between hidden Higgs fields and the Standard Model Higgs field.
The same reasoning holds for models with additional $U(1)$ gauge symmetries which are not hidden, i.e., under which Standard Model particles are charged; our $U(1)_{B-L}$ gauge extension of the Zee-Babu model is just an example. The direct communication channel between dark matter and the Standard Model via the exchange of a Z' boson is suppressed due to the bound (2.5.2) and is therefore neglected in the following. Thus the dominant renormalizable communication channel between dark matter and the Standard Model is the mixing between φ and ϕ. The coupling term λ_5 in (4.2.1) opens the door for dark matter to annihilate into Standard Model particles and contributes considerably to the relic abundance. Considering the resulting annihilation channels, our model coincides with the Higgs portal dark matter model published in [18] while our work was in progress.
With (2.1.4), (2.1.6), (2.1.7), (2.5.1), (2.5.3), (2.5.7), (4.1.3) and (4.2.1) the $G^{(SM)} \times U(1)_{B-L}$ Lagrangian reads:

$$\begin{aligned}\mathcal{L}_{Babu} &= \mathcal{L}_{cov} + (\mathcal{D}_\mu\varphi)^*(\mathcal{D}^\mu\varphi) + (\mathcal{D}_\mu k^{++})^*(\mathcal{D}^\mu k^{++}) + (\mathcal{D}_\mu h^+)^*(\mathcal{D}^\mu h^+) \\ &\quad + \mathcal{L}_{gauge} + \mathcal{L}^{Z'}_{gauge} \\ &\quad + \mathcal{L}_{Yukawa} + \mathcal{L}^{int}_{Babu} \\ &\quad + \mathcal{L}_{N_R} \\ &\quad + V(\phi,\varphi) \quad . \end{aligned} \tag{4.2.14}$$

Writing the covariant derivative terms of the additional scalars in (4.2.14) in terms of the physical mass eigenstates, there are couplings of the mass eigenstates to the Standard Model gauge bosons changing their vacuum polarization amplitudes. The vacuum polarization amplitudes of the $W^\pm$ and Z bosons affect the ρ parameter (see equation (2.2.8)). However, precision experiments constrain any contributions beyond the Standard Model to the ρ parameter, which are encoded in oblique correction parameters. One of these parameters, the T parameter, is defined as [44]

$$\begin{aligned}\alpha T &\equiv \frac{4}{w^2}\left(\Pi_{11}(0) - \Pi_{33}(0)\right) \\ \Rightarrow \rho &= 1 + \alpha T \quad ,\end{aligned}$$

with fine-structure constant α. Π_{ii} represent the vacuum polarization amplitudes of the W ($i = 1$) and Z ($i = 3$) boson. The effect of additional scalar particles on the T parameter is studied in [91]. We still have to evaluate the T parameter for our model by generalizing the result of [92], where the contribution to the T parameter arising from just one Higgs singlet is presented.

4.2.2 Scenario 2: $G^{(SM)} \times \mathbb{Z}_4$

Furthermore, we investigate the possibility of a dark matter stabilization $\mathbb{Z}_4$ symmetry. The Standard Model gauge group is then only extended with the abelian discrete $\mathbb{Z}_4$ symmetry instead of a local $U(1)_{B-L}$ and an additional $\mathbb{Z}_2$ as in [18]. With the charge assignments given in table 2.1, the $\mathbb{Z}_4$ symmetry forbids trilinear couplings in the scalar sector such that the potential (4.2.1) is reproduced with the λ_μ term. In addition to that, N_R is stable. Unfortunately, we have to pay the price for the motivation of the dark matter particle: without the local $U(1)_{B-L}$, there is no further gauge anomaly condition to fulfill and therefore no theoretically justified need for the introduction of N_R.
If a potential enjoys only a discrete symmetry, then with the spontaneous breakdown of this discrete symmetry domain walls appear in the vacuum structure of the potential [93]. Unless there is a mechanism that leads to the disappearance of domain walls at a very early stage in the history of the universe, the domain walls dominate the energy density of the universe [30] which is in contradiction to observations (compare section 3.2). In scenario 2, however, $U(1)_{B-L}$ is a global symmetry of the Lagrangian. In particular, all terms in the potential are invariant under global $U(1)$ phase transformations, such that the zeroth order homotopy group of the vacuum manifold is trivial, i.e., no domain walls appear [94].
When φ receives its vacuum expectation value, $\mathbb{Z}_4$ and $U(1)_{B-L}$ are broken to a $\mathbb{Z}_2$ which stabilizes N_R. After spontaneous symmetry breaking of the global $U(1)_{B-L}$, $I_1(x)$ survives as a massless Goldstone boson , i.e., a Majoron enters into the theory [95,96,97]. Since φ transforms as a singlet under the Standard Model gauge group, I_1 does not directly couple to the Z boson opposed to triplet Majoron models [98], which are ruled out by experiment [99] due to their contributions to the invisible Z width.
The couplings of the Majoron I_1 to the Higgs mass eigenstates H_1 and H_2 (compare figure 4.2) are obtained from the λ_1 and λ_5 terms in (4.2.1). These contain:

$$\lambda_1 w' \left(\cos\beta\, H_1 - \sin\beta\, H_2\right) I_1^2 \text{ and } \frac{1}{2}\lambda_5 w' w \left(\sin\beta\, H_1 + \cos\beta\, H_2\right) I_1^2 \quad . \tag{4.2.15}$$

(4.2.10) and (4.2.11) allow to express λ_1 and λ_5 in terms of the vacuum expectation values w and w', the mass eigenvalues m_{H_1} and m_{H_2}, and the mixing angle β:

$$\begin{aligned} \lambda_1 &= \frac{1}{2w'^2}\left(\cos^2\beta\, m_{H_1}^2 + \sin^2\beta\, m_{H_2}^2\right) \\ \lambda_5 &= \frac{1}{2w'w}\sin 2\beta\left(m_{H_1}^2 - m_{H_2}^2\right) \quad . \end{aligned} \tag{4.2.16}$$

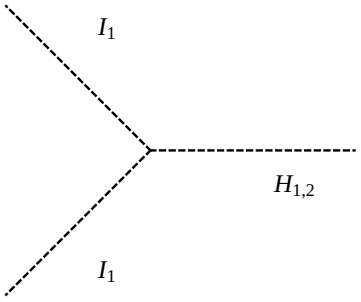

Figure 4.2: Majoron coupling to Higgs mass eigenstates H_1 and H_2

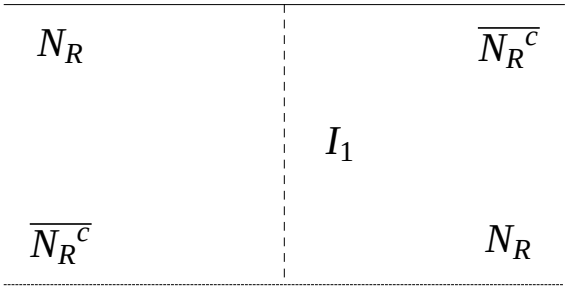

Figure 4.3: t-channel exchange of Majoron leading to attractive force between dark matter particles.

The Majoron couplings (4.2.15) to the Higgs mass eigenstates result to:

$$\begin{aligned} \lambda_1 \text{ term} &: \frac{1}{2w'}\left(\cos^2\beta\, m_{H_1}^2 + \sin^2\beta\, m_{H_2}^2\right)\left(\cos\beta\, H_1 - \sin\beta\, H_2\right) I_1^2 \\ \lambda_5 \text{ term} &: \frac{1}{4}\sin 2\beta\left(m_{H_1}^2 - m_{H_2}^2\right)\left(\sin\beta\, H_1 + \cos\beta\, H_2\right) I_1^2 \quad . \end{aligned} \tag{4.2.17}$$

The λ_1 term opens the dark matter annihilation channel into Majorons.
The λ_5 term lead to a decay of the Standard Model Higgs doublet ϕ into Majorons I_1. This decay mode is an invisible Higgs decay [96]. Its analysis in our model is postponed to a future work.
Apart from the couplings to the Higgs mass eigenstates H_1 and H_2, the Majoron I_1 also couples to the dark matter (see figure 4.3) and mediates a Yukawa type force which is by definition attractive and in our case infinitely long-ranged due to the vanishing mass of I_1. The corresponding potential $V(r)$ is proportional to $-\frac{1}{r}$, e.g., for the Coulomb potential the proportionality factor is the electromagnetic fine-structure constant $\alpha = \frac{e^2}{4\pi}$ [32]. The coupling constant of the Majoron I_1 to the dark matter particle N_R is λ_c, i.e., the Majoron fine structure constant is $\alpha_{Maj} = \frac{\lambda_c^2}{4\pi}$.
So the Majoron induces a self interaction for dark matter. But from the claim that dark matter should be non self-interacting in order to explain objects like Bullet Clusters

(compare to section 1), the Majoron fine structure constant α_{Maj} is limited from above. In [100] it is shown that for a dark matter particle with mass m, the *dark fine-structure constant* $\hat{\alpha}$ which relies on a *dark photon* as gauge boson of an unbroken $U(1)_D$ *dark gauge symmetry* is bounded from above by

$$\hat{\alpha} \lesssim \sqrt{\frac{1}{300}} \left(\frac{m}{\text{TeV}}\right)^{\frac{3}{2}} \quad , \tag{4.2.18}$$

in order to match the observational constraints on the dark matter self interaction. To be clear, the *dark photon* is massless and apart from additional γ matrices and an extra $ig_{\mu\nu}$ for the propagoator, it produces the same matrix element as the Majoron I_1 for the dark matter self interaction diagram shown in figure 4.3. This means that we can apply the bound (4.2.18) to α_{Maj} and, accordingly, constrain the coupling constant λ_c:

$$\lambda_c = \sqrt{4\pi\alpha_{Maj}} \lesssim \sqrt{\frac{2\pi}{5\sqrt{3}}} \left(\frac{m}{\text{TeV}}\right)^{\frac{3}{4}} \quad .$$

4.3 The Three-Point Test for Dark Matter Revisited

Having set up our model in the previous section, we can answer the three questions posed in section 3.2 related to dark matter.

4.3.1 A: Does It Match the Correct Relic Density ?

In scenario 1, due to the bound (2.5.2), the annihilation of dark matter into Standard Model particles through Z' exchange is suppressed compared to annihilation channels through the Higgs portal . For scenario 2, we have checked with micrOMEGAs [66] that the annihilation of dark matter into Majorons has a minor effect on the relic density for our chosen parameters in table 4.1. Therefore, we determine the relic density for the dominant Higgs portal annihilations, which are the same for the two scenarios. We perform a detailed calculation of the cross sections for s-channel annihilation into $b\bar{b}$ quarks and W bosons through Higgs exchange, but we neglect the partial decay widths. However, in a work under progress, we determine the relic density with micrOMEGAs [66] taking all possible annihialation channels into account with partial decay widths.
We start with the annihilation into $b\bar{b}$ quarks through the exchange of the Higgs mass eigenstate H_1 (*left part* of figure 4.4). At vertex 1, the coupling is (2.5.7):

$$2 \cdot \overline{v}_{s'}(p')u_s(p)\frac{1}{2}\lambda_c\frac{1}{\sqrt{2}}\cos\beta\frac{1}{s-m_{H_1}^2} \quad , \tag{4.3.1}$$

where the additional factor 2 takes into account the Majorana nature of N_R (see comments below (B.3.5)).

At vertex 2, we have the Yukawa interaction (2.1.7)

$$\overline{u}_r(k)v_{r'}(k')y_b\frac{1}{\sqrt{2}}\sin\beta \quad .$$

The matrix element $\mathcal{M}_{b\bar{b}}^{H_1}$ for the whole process is the product of the vertex terms:

$$\mathcal{M}_{b\bar{b}}^{H_1} = \frac{1}{2}\lambda_c y_b \cos\beta \sin\beta \overline{v}_{s'}(p')u_s(p)\overline{u}_r(k)v_{r'}(k')\frac{1}{s-m_{H_1}^2} \,. \tag{4.3.2}$$

To get $|\mathcal{M}_{b\bar{b}}^{H_1}|^2$, we have to average over the initial spins s, s' and to sum over the final spins k, k' using (B.2.7) and (B.2.8).
The spin average is

$$\begin{aligned}\frac{1}{2}\sum_{s'=1}^{2}\frac{1}{2}\sum_{s=1}^{2} v_{s'}(p)\overline{v}_{s'}(p')u_s(p)\overline{u}_s(p) &= \frac{1}{4}(\not{p}' - m_{N_R})(\not{p} + m_{N_R}) \\ &= p'\cdot p - m_{N_R}^2 \\ &= \frac{s-4m_{N_R}^2}{2} \quad , \end{aligned} \tag{4.3.3}$$

and the spin summation gives

$$\begin{aligned}\sum_{r'=1}^{2}\sum_{r=1}^{2} u_r(k)\overline{u}_r(k)v_r(k')\overline{v}_{r'}(k') &= (\not{k} + m_b)(\not{k} - m_b) \\ &= 4(k'\cdot k - m_b^2) \\ &= 4\cdot\frac{s-4m_b^2}{2} \quad . \end{aligned} \tag{4.3.4}$$

With (4.3.2), (4.3.3) and (4.3.4), we can evaluate $|\mathcal{M}_{b\bar{b}}^{H_1}|^2$:

$$\begin{aligned}|\mathcal{M}_{b\bar{b}}^{H_1}|^2 &= \frac{1}{4}\lambda_c^2\, y_b^2\, \cos^2\beta \sin^2\beta \frac{1}{2}(s-4m_{N_R}^2)2(s-4m_b^2)\frac{1}{(s-m_{H_1}^2)^2} \\ &= \frac{1}{4}\lambda_c^2\, y_b^2\, \frac{1}{4}\sin^2 2\beta\left(s-4m_{N_R}^2\right)4\left(\frac{s}{4}-m_b^2\right)\frac{1}{(s-m_{H_1}^2)^2} \\ &= \frac{1}{4}\lambda_c^2\, y_b^2\, \sin^2 2\beta \frac{1}{(s-m_{H_1}^2)^2}\left(s-4m_{N_R}^2\right)\left(\frac{s}{4}-m_b^2\right) \quad . \end{aligned} \tag{4.3.5}$$

The evaluation of the annihilation process into $b\,\bar{b}$ quarks through the exchange of the Higgs mass eigenstate H_2 proceeds analogously. The main difference is the minus sign in $\mathcal{M}_{b\bar{b}}^{H_2}$ compared to (4.3.2) which arises from Higgs mixing (see (4.2.12)):

$$\mathcal{M}_{b\bar{b}}^{H_2} = -\frac{1}{2}\lambda_c\, y_b\, \cos\beta \sin\beta\, \overline{v}_{s'}(p')u_s(p)\overline{u}_r(k)v_{r'}(k')\frac{1}{s-m_{H_2}^2} \quad .$$

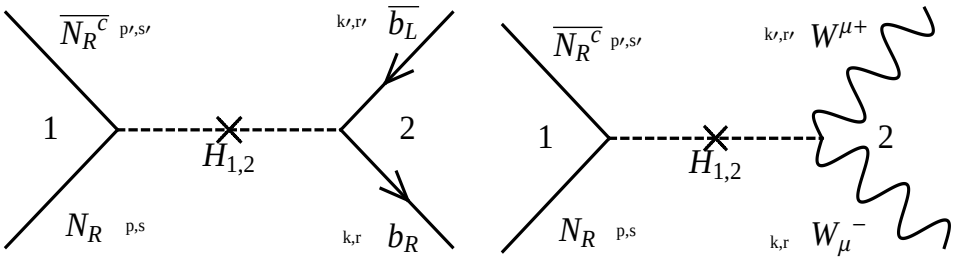

Figure 4.4: Dominant annihilation channels

Since both processes have the same initial and final states they are indistinguishable, and the squared absolute value $|\mathcal{M}_{b\bar{b}}|^2$ of the total matrix element is the coherent sum of $\mathcal{M}_{b\bar{b}}^{H_1}$ and $\mathcal{M}_{b\bar{b}}^{H_2}$:

$$\begin{aligned}
|\mathcal{M}_{b\bar{b}}|^2 &= |\mathcal{M}_{b\bar{b}}^{H_1} + \mathcal{M}_{b\bar{b}}^{H_2}|^2 \\
&= \frac{1}{4}\lambda_c^2\, y_b^2\, \sin^2 2\beta \left(s - 4m_{N_R}^2\right)\left(\frac{s}{4} - m_b^2\right) \\
&\quad \cdot \left(\frac{1}{(s-m_{H_1}^2)^2} - \frac{2}{(s-m_{H_1}^2)(s-m_{H_2}^2)} + \frac{1}{(s-m_{H_2}^2)^2}\right) \\
&= \frac{1}{4}\lambda_c^2\, y_b^2\, \sin^2 2\beta \frac{\left(s - 4m_{N_R}^2\right)\left(\frac{s}{4} - m_b^2\right)}{(s-m_{H_1}^2)^2(s-m_{H_2}^2)^2}\left(m_{H_1}^2 - m_{H_1}^2\right)^2 \quad .
\end{aligned}$$

Using (C.2.8) and (C.2.11), the cross section turns out to be

$$\sigma_{Hb\bar{b}} = \frac{\lambda_c^2\, y_b^2}{64\pi} \cdot \sin^2(2\beta) \cdot \left(m_{H_1}^2 - m_{H_2}^2\right)^2 \cdot \frac{\sqrt{\left(s - 4m_{N_R}^2\right)\left(s - 4m_{b\bar{b}}^2\right)}}{s\left(s - m_{H_1}^2\right)^2\left(s - m_{H_2}^2\right)^2} \cdot \left(\frac{s}{4} - m_b^2\right) \quad . \tag{4.3.6}$$

The relic abundance Ωh^2 (3.3.20) involves the thermal average $\langle\sigma v_r\rangle$ of the total annihilation cross section times relative velocity. To see the contributions from annihilation into $b\,\bar{b}$ quarks and W bosons, we calculate the thermal average separately for both channels.
In the expression (4.3.6), v_r enters through the Mandelstam variable s (see (3.3.15))

$$s = \frac{4m_{N_R}^2}{1 - \frac{v_r^2}{4}} \quad .$$

Given that the relative velocity v_r follows a Maxwell distribution (compare to the argumentation in section 3.3), we approximate the thermal average over v_r by using the root mean square velocity

$$v_r \sim v_{rms} = \sqrt{\frac{3T}{m}} = \sqrt{\frac{3}{x}} \quad .$$

w'	m_{H_1}	m_{H_2}	$m_{Z'}$	$\sin\beta$
3000 GeV	200 GeV	120 GeV	1000 GeV	0.7

Table 4.1: Parameter set (cf. [18])

For WIMPs, $x_f \approx 20$ at freeze-out [58], so that $\langle v_r^2 \rangle \sim 0.15 < 1$ and we can expand $\langle \sigma_{Hb\bar{b}} v_r \rangle$ in v_r. The leading order contribution reads :

$$\langle \sigma_{Hb\bar{b}} v_r \rangle = \frac{\lambda_c^2\, y_b^2}{128\pi} \cdot \sin^2(2\beta) \cdot \frac{\left(m_{H_1}^2 - m_{H_2}^2\right)^2 \cdot (m_{N_R}^2 - m_b^2)}{(m_{H_1}^2 - 4m_{N_R}^2)^2 (4m_{N_R}^2 - m_{H_2}^2)^2} \cdot \sqrt{1 - \frac{m_b^2}{m_{N_R}^2}} \cdot \langle v_r^2 \rangle \quad . \tag{4.3.7}$$

For the calculation of the annihilation process into W bosons (*right part* of figure 4.4), the coupling at vertex 1 is the same as in (4.3.1).
To determine the analytic expression for vertex 2, we have to recall (2.2.2). The relevant term is

$$\frac{1}{4} g^2 W_\mu^- W^{\mu +} 2wH(x) \quad .$$

The polarization vectors $\epsilon_\mu^*(k)$ and $(\epsilon^*)^\mu(k')$ of the final W bosons enter into the vertex expression such that we obtain

$$\frac{1}{2} g^2\, w\, \epsilon_\mu^*(k) (\epsilon^*)^\mu(k') \sin\beta \quad . \tag{4.3.8}$$

The matrix element $\mathcal{M}_W^{H_1}$ turns into

$$\mathcal{M}_W^{H_1} = \frac{1}{4\sqrt{2}} \lambda_c\, g^2\, w \cos\beta \sin\beta\, \overline{v}_{s'}(p') u_s(p) \frac{1}{s - m_{H_1}^2} \epsilon_\mu^*(k) (\epsilon^*)^\mu(k') \quad . \tag{4.3.9}$$

To get $|\mathcal{M}_W^{H_1}|^2$, we have to average over the initial spins s, s' and sum over the final polarization vectors $\epsilon_\mu^*(k)$ and $(\epsilon^*)^\mu(k')$. For a massive gauge boson, there are two transversal and one longitudinal polarization vector.
The result of the spin average is (4.3.3).

The summation over the polarization vectors yields:

$$\begin{aligned}
&\sum_{i=1,2,3}\sum_{j=1,2,3}(\epsilon_i^*)_\mu(k)(\epsilon_i^*)^\mu(k')(\epsilon_j)_\nu(k)(\epsilon_i)^\nu(k') \\
&= \sum_{i=1,2,3}\epsilon_\mu^*(k)\epsilon_\nu(k)\cdot\sum_{j=1,2,3}(\epsilon^*)^\mu(k')\epsilon^\nu(k') \\
&= \left(\frac{k_\mu k_\nu}{m_W^2}-g_{\mu\nu}\right)\cdot\left(\frac{k'^\mu k'^\nu}{m_W^2}-g^{\mu\nu}\right) \\
&= \frac{(k\cdot k')^2}{m_W^4}-\frac{k^2}{m_W^2}-\frac{k'^2}{m_W^2}+4 \quad |k^2=k'^2=m_W^2 \\
&= 2+\frac{(k\cdot k')^2}{m_W^4} \quad |s=(k+k')^2\Rightarrow k\cdot k'=\frac{s-2m_W^2}{2} \\
&= 2\cdot\left(1+\frac{\left(\frac{s}{2}-m_W^2\right)^2}{2m_W^4}\right) \quad . \qquad (4.3.10)
\end{aligned}$$

With (4.3.9), (4.3.3) and (4.3.10) we obtain:

$$\begin{aligned}
|\mathcal{M}_W^{H_1}|^2 &= \frac{1}{8}\lambda_c^2\, g^4\, w^2\cos^2\beta\sin^2\beta\frac{1}{(s-m_{H_1}^2)^2}\left(s-4m_{N_R}^2\right)\left(1+\frac{1}{2m_W^4}\left(\frac{s}{2}-m_W^2\right)^2\right) \\
&= \frac{1}{8}\lambda_c^2\left(\frac{1}{2}g^2w\right)^2\sin^2 2\beta\frac{1}{(s-m_{H_1}^2)^2}\left(s-4m_{N_R}^2\right)\left(1+\frac{1}{2m_W^4}\left(\frac{s}{2}-m_W^2\right)^2\right). \qquad (4.3.11)
\end{aligned}$$

Again, the evaluation of the annihilation process into W bosons through the exchange of the Higgs mass eigenstate H_2 proceeds analogously. The main difference is the minus sign in $\mathcal{M}_W^{H_2}$ compared to (4.3.9), which arises from Higgs mixing (see (4.2.12)):

$$\mathcal{M}_W^{H_2}=-\frac{1}{4\sqrt{2}}\lambda_c g^2 w\cos\beta\sin\beta\overline{v}_{s'}(p')u_s(p)\frac{1}{s-m_{H_2}^2}\epsilon_\mu^*(k)(\epsilon^*)^\mu(k') \quad .$$

The squared absolute value $|\mathcal{M}_W|^2$ of the total matrix element is

$$\begin{aligned}
|\mathcal{M}_W|^2 &= |\mathcal{M}_W^{H_1}+\mathcal{M}_W^{H_2}|^2 \\
&= \frac{1}{8}\lambda_c^2\left(\frac{1}{2}g^2w\right)^2\sin^2 2\beta\frac{(m_{H_1}^2-m_{H_1}^2)^2(s-4m_{N_R}^2)}{(s-m_{H_1}^2)^2(s-m_{H_2}^2)^2} \\
&\quad\cdot\left(1+\frac{1}{2m_W^4}\left(\frac{s}{2}-m_W^2\right)^2\right).
\end{aligned}$$

The corresponding annihilation cross section reads

$$\begin{aligned}
\sigma_{HW} &= \frac{\lambda_c^2}{128\pi}\cdot\left(\frac{1}{2}g^2w\right)^2\cdot\sin^2(2\beta)\cdot\left(m_{H_1}^2-m_{H_2}^2\right)^2\cdot\frac{\sqrt{\left(s-4m_{N_R}^2\right)\left(s-4m_W^2\right)}}{s\left(s-m_{H_1}^2\right)^2\left(s-m_{H_2}^2\right)^2} \\
&\quad\cdot\left(1+\frac{1}{2m_W^4}\left(\frac{s}{2}-m_W^2\right)^2\right) \quad ,
\end{aligned}$$

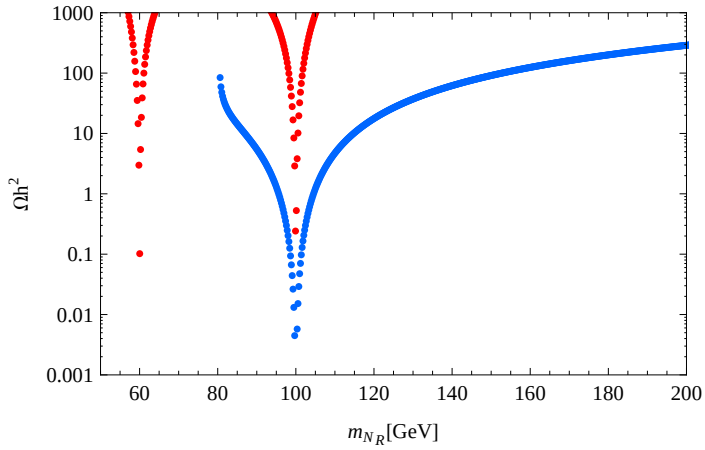

Figure 4.5: Test of relic density : s-channel annihilation into $b\,\bar{b}$ quarks (red) and into W bosons (blue) through Higgs exchange using the parameter set of table 4.1.

and the leading-order contribution to the thermal average is

$$\begin{aligned}\langle \sigma_{HW} v_r \rangle &= \frac{\lambda_c^2}{2048\pi} \cdot \left(\frac{1}{2} g^2 w\right)^2 \cdot \sin^2(2\beta) \cdot \sqrt{1 - \frac{m_W^2}{m_{N_R}^2}} \cdot \langle v_r^2 \rangle \\ &\quad \cdot \frac{\left(m_{H_1}^2 - m_{H_2}^2\right)^2 \cdot (4m_{N_R}^4 - 4m_{N_R}^2 m_W^2 + 3m_W^4)}{(m_{H_1}^2 - 4m_{N_R}^2)^2 (4m_{N_R}^2 - m_{H_2}^2)^2\, m_W^4} \quad . \end{aligned} \tag{4.3.12}$$

The denominators of (4.3.7) and (4.3.12) clearly reveal that for $m_{N_R} = \frac{1}{2} m_{H_{1,2}}$, there are Higgs resonances. In the vicinity of these resonances, we can match the correct dark matter relic abundance (see figure 4.5).
The $\langle v_r^2 \rangle$ dependence of (4.3.7) and (4.3.12) is linked to the Majorana character of the dark matter particle N_R [101]:
Let l and s denote the angular momentum and the spin, respectively. A generic wave function has a spatial part and a spin part. From the expansion of a spatial wave function in terms of spherical harmonics, one can infer that it transforms under a parity operation P like $(-1)^l$. The spin wave function is even under P for triplet states $s = 1$ and odd for singlet states $s = 0$, i.e., it transforms like $(-1)^{s+1}$. A fermion has an additional intrinsic parity of (-1) due to the opposite parity of the Dirac spinors u and v [32], which enter into the plane wave ansatz for the fermion. Thus, a fermion transforms under P like $(-1)^l(-1)^{s+1}(-1) = (-1)^{l+s}$.
Particle-antiparticle exchange transformations C have the same dependence on l and s as P: $C = (-1)^{l+s}$.
Majorana fermions are even under C. That means that l and s must both be either even or odd. In spin-parity notation J^{PC} with total angular momentum J, the dark matter particle must be in the 0^{++} state to obtain the coupling to a scalar in the Higgs portal channels considered above. In spectroscopic notation, ${}^{2S+1}L_J$, this state is a

$^1P_1$ state, which corresponds to $l = 1$.
On general grounds, the l^{th} partial wave contribution to the annihilation cross section times velocity is proportional to v^{2l} (see section 3.3). Thus the leading contribution in $\langle v_r \rangle$ is $\langle v_r^2 \rangle$, which corresponds to p-wave annihilation.
The results (4.3.5) and (4.3.11) are written in a form which allows the direct comparision with the corresponding results in [18].
The results (4.3.7) and (4.3.12) for the leading order contributions to the thermal average of the annihilation cross section times velocity are inserted into (3.3.19), where we use the approximation of s-wave annihilation. We assume $x_f \approx 20$. Since the additional scalars h^+, k^{++}, φ are at the same mass scale as the dark matter particle N_R, they are non-relativistic at the time of freeze-out of N_R and only Standard Model particles contribute to the number g_* of relativistic degrees of freedom, i.e., $g_* = 106.75$. Figure 4.5 finally reveals that for the parameter set in table 4.1, we can match the correct relic abundance (compare (3.3.20) and (3.3.21)) in the vicinity of the Higgs resonances.
In a work under progress, we use the code micrOMEGAs [66] to determine the dark matter relic abundance by numerically solving the Boltzmann equation for N_R in the Lee-Weinberg approximation ((3.3.16)). To implement our model in micrOMEGAs, we generate the needed Feynman rules with LanHEP [102].
Numerically solving the Boltzmann equation involves the thermal average of the annihilation cross section times relative velocity v_r. So far, we have approximated the thermal average over a Maxwell distribution by the root mean square velocity. In an elaborated calculation performed in micrOMEGAs, the thermal average results to [54]:

$$\langle \sigma v_r \rangle = \frac{1}{8 m_{N_R}^4 T K_2^2 \left(\frac{m_{N_R}}{T}\right)} \int\limits_{4m_{N_R}^2}^{\infty} ds\, \sigma \cdot \left(s - 4m_{N_R}^2\right) \cdot \sqrt{s} \cdot K_1\left(\frac{\sqrt{s}}{T}\right) \quad ,$$

where the modified Bessel functions $K_i(z)$ [103] are solutions to the differential equation

$$z^2 \frac{d^2 w}{dz^2} + z \frac{dw}{dz} - \left(z^2 + i^2\right) \cdot w = 0 \quad .$$

The very interesting fact about the thermal average is the contribution of all velocities instead of just the root mean square velocity v_{rms}, especially of velocities larger than v_{rms}. For example, let the dark matter mass m be variable and consider the availabel energy E in the center of mass frame for two annihilating dark matter particles with equal masses $m = m_1$ and a relative velocity $v_1 = v_{rms}$ (see equation (3.3.15)):

$$E = \frac{4m_1^2}{1 - \frac{v_1^2}{4}} \quad .$$

Since the relative velocity is thermally distributed, there are velocities v_2 with $v_2 > v_1$. To provide the same energy E, a dark matter particle with mass $m = m_2$ must obey

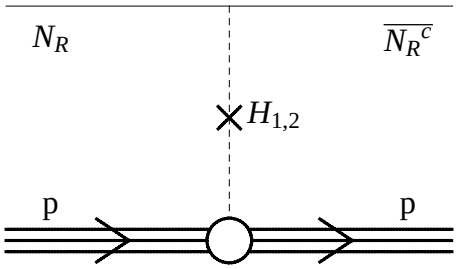

Figure 4.6: Direct detection

the relation:

$$\begin{aligned} \frac{4m_2^2}{1-\frac{v_2^2}{4}} &= \frac{4m_1^2}{1-\frac{v_1^2}{4}} \\ \Leftrightarrow \frac{m_2^2}{m_1^2} &= \frac{1-\frac{v_2^2}{4}}{1-\frac{v_1^2}{4}} \quad | \, v_2 > v_1 \\ \Rightarrow m_2 &< m_1 \ . \end{aligned}$$

This means that when we are scanning the thermal relic density as a function of the dark matter mass m, annihilation channels become possible for a lower m, which would be kinematically forbidden without taken into account the thermal distribution of the relative velocity (compare to [104]). Consequently, the resonance peaks in figure 4.5 are broadened to smaller m below the threshold leading to an asymmetric relic density in the vicinity of the resonance thresholds.

4.3.2 B: Is It Cold?

In scenario 1, the mass scale of the dark matter particle is given by the symmetry breaking scale of the gauged $U(1)_{B-L}$, which is the TeV scale. Clearly, dark matter particles with masses in the TeV range of are non-relativistic, i.e., cold.
In scenario 2, the mass of the dark matter particle is determined by the breaking scale of the global $U(1)_{B-L}$. $(B-L)$ is preserved within the experimental range, i.e., up to $\mathcal{O}$ (100 GeV). $(B-L)$ violating interactions are thus expected above the experimental range and therefore the dark matter is cold in this scenario as well.

4.3.3 C: Can It Be Probed Experimentally?

We have calculated the cross section σ_{proton} for elastic spin independent scattering of dark matter off a proton through t-channel exchange of the mass eigenstates H_1 and H_2 (see figure 4.6). The result reads:

$$\sigma_{proton} = \frac{4m_{red}^2}{\pi} \left(g_{N_R N_R H_1} + g_{N_R N_R H_2}\right)^2 g_{Hp}^2 \ .$$

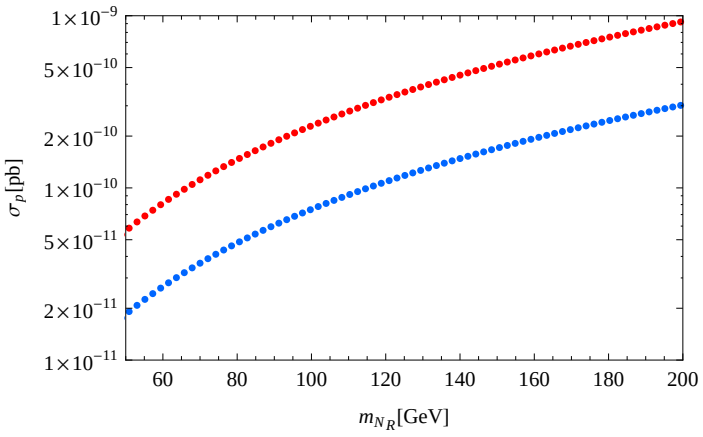

Figure 4.7: The elastic scattering cross section in pb with a proton. All parameters are the same as those listed in table 4.1. Red dots correspond to $\sin\beta = 0.7$, blue dots correspond to $\sin\beta = 0.3$.

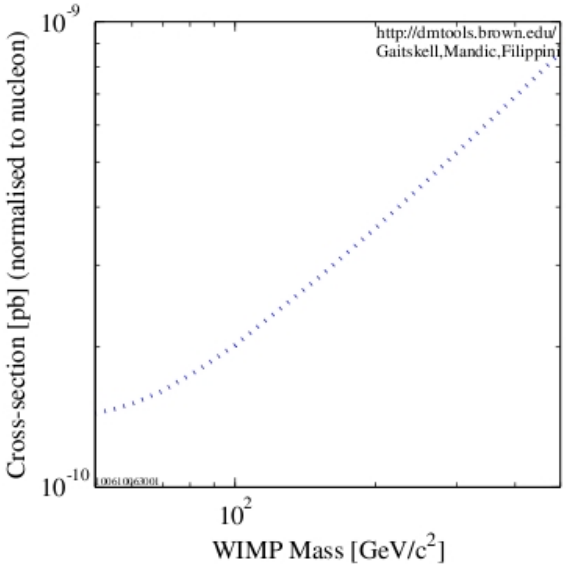

Figure 4.8: XENON100 upgrade projected sensitivity: 60,000 kg-d, 5-30 keV, 45% eff. Figure created with plotter provided in [17].

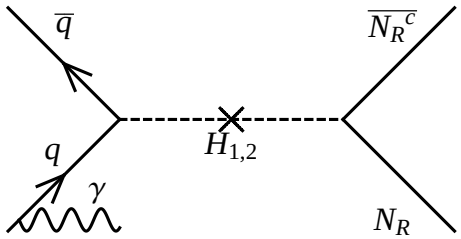

Figure 4.9: Production of dark matter at the LHC with initial state radiated photon.

Here, m_{red} is the reduced mass of the dark-matter-proton system. The terms $g_{N_R N_R H_i}$ are the couplings between dark matter and the Higgs mass eigenstates:

$$\begin{aligned} g_{N_R N_R H_1} &= +\frac{1}{2}\lambda_c \cos\beta \frac{1}{m_{H_1}^2} \sin\beta \\ g_{N_R N_R H_2} &= -\frac{1}{2}\lambda_c \cos\beta \frac{1}{m_{H_2}^2} \sin\beta \quad . \end{aligned}$$

According to (3.5.2), the coupling g_{Hp} between the Standard Model Higgs particle and the proton is:

$$g_{Hp} = \frac{m_p}{w}\left(\sum_{q=u,d,s} f_{Tq}^{(p)} + \frac{2}{27}\left(1 - \sum_{q=u,d,s} f_{Tq}^{(p)}\right)\right) \quad ,$$

with the Yukawa couplings y_q satisfying $m_q = w \cdot y_q$. Figure 4.7 shows the elastic scattering cross section depending on the mass of the dark matter particle. Comparing figure 4.7 with figure 3.4, one sees that our model is below the current experimental sensitivity, but still within the reach of upcoming experiments (see figure 4.8).
Note that, due to the Higgs portal , the considered annihilation channels and the scattering of N_R off protons are governed by one common coupling constant, namely λ_c.
Under T transformation, the Feynman diagrams in figure 4.4 result in possible dark matter search channels at colliders. In our model, figure 3.8 is dominantly realized through the Higgs portal as depicted in figure 4.9.

4.4 Verification of the Model at the LHC

The most-studied processes to produce new particles at the LHC are Drell-Yan processes as shown in figure 4.10: at the collison of two protons p_1 and p_2, a quark q of proton p_1 annihilates with an antiquark $\overline{q}$ of proton p_2 and a Z boson is created, which then decays either into a Standard Model lepton pair, which we call background signals, or into new particles.

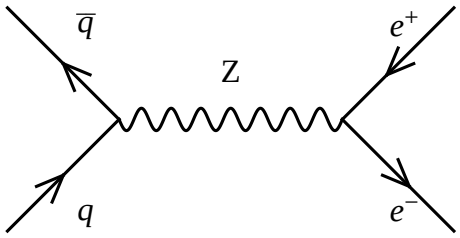

Figure 4.10: Drell-Yan process for Standard Model background

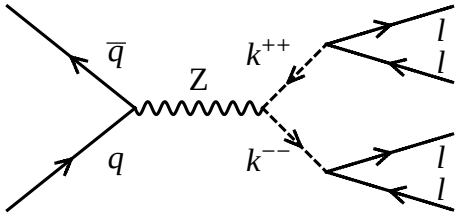

Figure 4.11: Detection channel for the pair-produced doubly charged scalar k^{++}

4.4.1 Scalars h^+ and k^{++}

The scalars h^+ and k^{++} can be pair produced at the LHC via Drell-Yan processes. The corresponding cross section is proportional to the squared charges of the scalars, so that the cross section for production of the doubly charged pair (k^{++}, k^{--}) is four times as large as the cross section for production of the singly charged pair (h^+, h^-) [105]. Since the scalars must satisfy the LEP lower bound for charged scalar masses, which is approximately 100 GeV, we can assume that they will decay inside the detectors. Recall from (4.1.3) that the LHC is more sensitive to the decay channels of k^{++} because all leptonic decays of h^+ involve a neutrino. The best-suited channel to detect a (k^{++}, k^{--}) pair is the decay channel which contains four leptons in the final state (see figure 4.11) [105]. A signature of four leptons would be a clear hint for the scalar k^{++}.

4.4.2 Z' Gauge Boson

In section 4.2.1, we studied the extension of the Zee-Babu model with a minimal gauged $U(1)_{B-L}$.
The Z' gauge boson, being much heavier than the Standard Model Z boson (compare bound from electroweak precision observables in (2.5.2)), could be identified through a resonance in the (e^+, e^-) invariant mass spectrum above the Standard Model Drell-Yan background (compare figure 4.10). The position of the resonance in the invariant mass spectrum directly gives the mass $M_{Z'}$ of the Z' gauge boson. Fitting the resonance with a Breit-Wigner resonance curve permits the determination of the decay width $\Gamma_{Z'}$. The production cross section for a Z' decreases exponentially with increas-

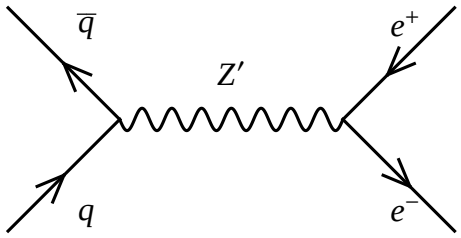

Figure 4.12: Z' gauge boson in dielectron event

ing $M_{Z'}$ [106].
The CDF Collaboration reported the following result on Z' searches at Tevatron: in proton-antiproton collisions at a center of mass energy of $\sqrt{s} = 1.96$ TeV, using a dataset corresponding to an integrated luminosity of 0.45 fb^{-1}, no evidence of a Z' boson is found in the dielectron invariant mass spectrum [107].
The CMS experiment at the LHC will probe the Z' mass range 1 TeV $\leqq m_{Z'} \leqq 2$ TeV at a center of mass energy $\sqrt{s} = 10$ TeV with a dataset corresponding to an integrated luminosity of 300 pb^{-1} [4]. Currently, the LHC runs at a center of mass energy of $\sqrt{s} = 7$ TeV and a luminosity below 100 pb^{-1}. That means that already with the next upgrade in energy, the interesting mass range for our model of the Z' will be probed.

Chapter 5

Conclusion

Neutrinos have mass and the Universe has dark matter.

(Ernest Ma)

Motivated by the two main problems of astroparticle physics, a common framework for radiative neutrino mass generation and dark matter has been presented.
The input was the Zee-Babu model [27] which has in addition to the Standard Model two complex scalar singlets h^+ and k^{++} coupling to left- and right-handed leptons, respectively. Light neutrino masses are generated at the two-loop level. The advantage of loop-induced neutrino masses is the relative low scale at which new physics enters. Compared to tree-level mass models, e.g., the seesaw mechanism, the radiatively produced neutrino masses are suppressed by a factor of $\frac{1}{16\pi^2}$ for each loop. So neutrino flavor oscillation experiments can be explained at the TeV scale which is in current experimental reach.
While the Zee-Babu model has special signatures for experimental verification [87,88, 105], of which only one has been discussed, it does not contain a dark matter particle. Therefore, a right-handed Majorana neutrino N_R has been suggested to be the cold dark matter candidate in the Zee-Babu model.
To realize this idea together with light neutrino mass generation, a $U(1)_{B-L}$ symmetry was imposed. The trilinear scalar coupling μ of the Zee-Babu potential needed to give light neutrino masses was realized in a $(B-L)$ invariant way by a complex scalar singlet φ with $(B-L)$ charge $q_{B-L}(\varphi) = 2$. With spontaneous symmetry breaking driven by φ, the $U(1)_{B-L}$ breaking μ term of the Zee-Babu model arises dynamically as well as the Majorana mass of N_R. Thus light neutrino masses and the mass of the particle dark matter candidate are generated at one common energy scale, which is the $U(1)_{B-L}$ breaking scale.
Two scenarios have been analyzed to bring forward the $(B-L)$ symmetry in the Zee-Babu model. In a first scenario, the $U(1)_{B-L}$ has been gauged. N_R is then a must to prevent $[U(1)_{B-L}]^3$ gauge anomalies. Stabilized by a $\mathbb{Z}_2$ symmetry, it is the candidate for a particle dark matter. In a second scenario, the gauge group has been enlarged with a $\mathbb{Z}_4$ symmetry, i.e., $U(1)_{B-L}$ is global. Although it is a more economic extension compared to $U(1)_{B-L} \times \mathbb{Z}_2$ in scenario 1, this scenario does not theoretically justify the introduction of a dark matter particle, instead, N_R has to be introduced by hand rather than based on gauge anomaly conditions. With the spontaneous symmetry breaking of the global $U(1)_{B-L}$, a Majoron enters into the theory. The calculated

couplings of the Majoron to the Higgs mass eigenstates could lead to interesting Higgs phenomenology at the LHC, e.g., invisible Higgs decays. These signatures have not yet been studied in detail for the given model and are postponed to a future work. For the Majoron scenario, the dark matter couples to the Majoron through the λ_c term. To forbid large dark matter self interactions, λ_c is limited from above.
As it was pointed out, particle candidates for dark matter have to fulfill necessary conditions. Three of them have been introduced and applied to the underlying model, namely the observed relic density, bounds from structure formation and possible signals in detection experiments.
Concerning the thermal relic density, annihilations of N_R into Z', the gauge boson of $U(1)_{B-L}$, do occur in the first scenario, however, are suppressed by the bound $\frac{M_{Z'}}{g_{B-L}} \simeq 6.7$ TeV. The dominant annihilation channels in both scenarios proceed via the Higgs portal opened by the λ_5 coupling, which mixes the Standard Model Higgs doublet ϕ with the Higgs singlet φ. It has been approximately shown that annihilations into $b\bar{b}$ quarks and W bosons could produce the correct dark matter relic abundance. The approximation is based on the use of the root mean square velocity instead of performing the average over a Maxwell distribution in the computation of the thermal average of the annihilation cross section times relative velocity.
It has also been shown that the Higgs portal opens the door for direct detection.
In addition, it has been outlined how the LHC may verify the proposed model by detection of the charged Zee-Babu scalars.
The phenomenology of the Zee-Babu model and its possible verification are extensively discussed in the literature. The suggested extension to a $(B - L)$ invariant Zee-Babu model in the scenario of a gauged $U(1)_{B-L}$ is thus a very promising and verifiable model to solve both the neutrino mass probelm and the dark matter of the universe.

Appendix A

Units, Constants and Parameters

In this work, we use natural units:

$$\hbar = c = k = 1 \ .$$

The fundamental dimension is energy:

$$[\text{Energy}]=[\text{Mass}]=[\text{Temperature}]=[\text{Length}]^{-1}=[\text{Time}]^{-1} \ .$$

Constants and parameters used in this work are adopted from [4]:

Quantity	Symbol	Value
speed of light	c	$299\,792\,458\ \mathrm{m\,s^{-1}}$
Planck constant, reduced	$\hbar$	$6.582\,118\,99(16)\times10^{-22}\ \mathrm{MeV\,s}$
conversion constant	$(\hbar c)^2$	$0.389\,379\,304(19)\ \mathrm{GeV^2\,mb}$
Planck mass	m_{pl}	$1.220\,89(6)\times10^{19}\ \mathrm{GeV/c^2}$
Newtonian gravitational constant	G_N	$6.708\,81(67)\times10^{-39}\ \hbar c(\mathrm{GeV/c^2})^{-2}$
Boltzmann constant	k	$8.617\,343(15)\times10^{-5}\ \mathrm{eV\,K^{-1}}$
fine-structure constant at $Q^2=0$	α	$1/137.035\,999\,679(94)$
Fermi coupling constant	$G_F/(\hbar c)^3$	$1.166\,37(1)\times10^{-5}\ \mathrm{GeV^{-2}}$
weak mixing angle at m_Z in $\overline{MS}$	$\sin^2\Theta_W$	$0.231\,19(14)$
$\mathrm{W^{\pm}}$ bosons mass	m_W	$80.398(25)\ \mathrm{GeV/c^2}$
light year	ly	$0.946\,053...\times10^{16}\ \mathrm{m}$
parsec	pc	$3.085\,677\,6\times10^{16}\ \mathrm{m}$
number density of CMB photons	n_γ	$410.5(\mathrm{T}/2.725)^3\ \mathrm{cm^{-3}}$
present day normalized Hubble expansion rate	h	$0.73(3)$
present day Hubble expansion rate	H_0	$2.1332\,h\ \times10^{-42}\ \mathrm{GeV}$
critical density	ρ_c	$1.878\,35(19)\times10^{-29}\ h^2\,\mathrm{g\,cm^{-3}}$

Table A.1: Constants and parameters

Appendix B

Fermions in Four Dimensional Spacetime

B.1 Dirac and Weyl Spinors

Group theory classifies all particles as members of irreducible representations of an underlying symmetry group, i.e., particles are classified according to their transformation behavior under a symmetry group [108]. The Lorentz group $SO(3,1)$, which is a Lie group, is the symmetry group of rotations and boosts in four dimensional spacetime. Fermions live in the spinor representation of $SO(3,1)$, which we review in this appendix.
Assume a set of $n \times n$ matrices γ^μ, $\mu = 0,1,2,3$, satisfying the Clifford algebra

$$\{\gamma^\mu\ , \gamma^\nu\} = 2\, g^{\mu\nu}\, \mathbf{1}_{n\times n} \tag{B.1.1}$$

with metric tensor $g^{\mu\nu}$.
Define

$$J^{\mu\nu} \equiv \frac{\mathrm{i}}{4}[\gamma^\mu, \gamma^\nu] \quad . \tag{B.1.2}$$

Then the $J^{\mu\nu}$ fulfill the Lie algebra of $SO(3,1)$:

$$[J^{\mu\nu}, J^{\rho\sigma}] = \mathrm{i}(g^{\nu\rho} J^{\mu\sigma} - g^{\mu\rho} J^{\nu\sigma} - g^{\nu\sigma} J^{\mu\nu} + g^{\mu\sigma} J^{\nu\rho}) \tag{B.1.3}$$

and are thus generators of a special representation of the Lorentz group.
A generic element Λ of the Lie group $SO(3,1)$ can always be written as $\Lambda = e^{-\frac{\mathrm{i}}{2}\omega_{\mu\nu}M^{\mu\nu}}$ with $M^{\mu\nu}$ being the generators of the corresponding Lie algebra. $S(\Lambda) = e^{-\frac{\mathrm{i}}{2}\omega_{\mu\nu}J^{\mu\nu}}$ is a special representation of Λ, the spinor representation, for which the generators are $J^{\mu\nu}$. Notice that Lorentz boosts along the $i = 1,2,3$ directions are generated by

$$J^{0i} \overset{\text{B.1.2}}{=} -\frac{\mathrm{i}}{2}\begin{pmatrix} \sigma^i & 0 \\ 0 & -\sigma^i \end{pmatrix} \tag{B.1.4}$$

with Pauli matrices σ^i.
A Dirac spinor $(\Psi_D)_a(x^\mu)\,, a = 1,2,3,4$, is defined as a complex four-component field which has the following transformation law under a Lorentz transformation Λ:

$$(\Psi_D)_a(x^\mu) \xrightarrow{\Lambda} S(\Lambda)_{ab}(\Psi_D)_b((\Lambda^{-1})_\mu{}^\nu\, x^\nu)\ . \tag{B.1.5}$$

In the four dimensional Dirac representation of the Clifford algebra, the γ^μ are represented by the Pauli matrices

$$\sigma^0 = \begin{pmatrix} 1 & 0 \\ 0 & 1 \end{pmatrix}, \sigma^1 = \begin{pmatrix} 0 & 1 \\ 1 & 0 \end{pmatrix}, \sigma^2 = \begin{pmatrix} 0 & -i \\ i & 0 \end{pmatrix}, \sigma^3 = \begin{pmatrix} 1 & 0 \\ 0 & -1 \end{pmatrix}$$

in the following way:

$$\gamma^\mu = \begin{pmatrix} 0 & \sigma^\mu \\ \overline{\sigma}^\mu & 0 \end{pmatrix} \quad , \tag{B.1.6}$$

where $\sigma^\mu = (1, \sigma^i)$ and $\overline{\sigma}^\mu = (1, -\sigma^i)$ with $i = 1, 2, 3$.
In this representation of the Clifford algebra, the generators $J^{\mu\nu}$ of the Lorentz group are diagonal and thus the Dirac spinor representation is reducible. In fact, in a space of even dimension there exists a chirality operator under which reducible representations factorize into irreducible representations. In four dimensions, we define the chirality operator $\gamma^5 \equiv \mathrm{i}\gamma^0\gamma^1\gamma^2\gamma^3$. With the anticommutation relation in (B.1.1), the following properties of γ^5 are obvious:

$$(\gamma^5)^\dagger = \gamma^5 \tag{B.1.7}$$
$$(\gamma^5)^2 = \mathbf{1}_{4\times4} \tag{B.1.8}$$
$$\{\gamma^5, \gamma^\mu\} = 0 \ . \tag{B.1.9}$$

With γ^5, we build the left- and right-handed projection operators $\mathbf{P_R}$ and $\mathbf{P_R}$:

$$\mathbf{P_L} = \frac{1-\gamma^5}{2}, \mathbf{P_R} = \frac{1+\gamma^5}{2} \quad . \tag{B.1.10}$$

It is easy to check that $\mathbf{P_L}$ and $\mathbf{P_R}$ fulfill the defining properties of orthogonal projection operators: $\mathbf{P_L}+\mathbf{P_R} = \mathbf{1}_{4\times4}$, $\mathbf{P_L}\cdot\mathbf{P_R} = \mathbf{P_R}\cdot\mathbf{P_L} = 0$ and $(\mathbf{P_L})^2 = \mathbf{P_L}$, $(\mathbf{P_R})^2 = \mathbf{P_R}$. The last two equalities directly follow from (B.1.8). A Dirac fermion $(\Psi_D)_a$ can then be written as

$$(\Psi_D)_a = \begin{pmatrix} \mathbf{P_L}\,(\Psi_D)_a \\ \mathbf{P_R}\,(\Psi_D)_a \end{pmatrix} \equiv \begin{pmatrix} \Psi_\alpha \\ \overline{\chi}^{\,\dot\alpha} \end{pmatrix} \quad . \tag{B.1.11}$$

The left-handed Weyl-spinor Ψ_α with $\alpha = 1, 2$ lies in the $(\frac{1}{2}, 0)$ representation of the Lorentz group and transforms under Lorentz transformations as $\Psi_\alpha \to \Psi'_\alpha = M_\alpha{}^\beta \ \Psi_\beta$. The right-handed Weyl-spinor $\overline{\chi}^{\,\dot\alpha}$ with $\dot\alpha = 1, 2$ lies in the $(0, \frac{1}{2})$ representation of the Lorentz group and transforms under Lorentz transformations as
$\overline{\chi}^{\,\dot\alpha} \to \overline{\chi'}^{\,\dot\alpha} = (M^{*-1})_{\dot\beta}{}^{\dot\alpha} \ \overline{\chi}^{\,\dot\beta}$.
Here, $\mathbf{M} \in SL(2, \mathbb{C})$. $SL(2, \mathbb{C})$ is the universal double covering group of $SO(3, 1)$.
In this work, we use the formalism of Dirac spinors, i.e., Ψ is a Dirac fermion.

B.2 Solutions to the Dirac Equation

The lagrangian for a free fermion Ψ with mass m is the Dirac Lagrangian:

$$\mathcal{L}_{Dirac} = \overline{\Psi}\,(\mathrm{i}\partial\!\!\!/ - m)\,\Psi \quad , \tag{B.2.1}$$

with $\overline{\Psi} = \Psi^\dagger \gamma_0$ and $\not{\partial} \equiv \gamma^\mu \partial_\mu$.
The classical Euler-Lagrange equations applied to (B.2.1) yield the Dirac equations of motion for Ψ and $\overline{\Psi}$:

$$\begin{aligned} -\gamma^\mu \partial_\mu \Psi &= \mathrm{i} m \Psi && \text{(B.2.2)} \\ \partial_\mu \overline{\Psi} \gamma^\mu &= \mathrm{i} m \overline{\Psi} \ . && \text{(B.2.3)} \end{aligned}$$

Multiplying (B.2.2) with $(-\mathrm{i}\not{\partial} - m)$, we see that if Ψ fulfills the Dirac equation, it automatically satisfies the Klein-Gordon equation:

$$\begin{aligned} 0 &= (-\mathrm{i}\not{\partial} - m) \cdot (\mathrm{i}\not{\partial} - m)\Psi \\ &= (\gamma^\mu \partial_\mu \gamma^\nu \partial_\nu + m^2)\Psi \\ &= \left(\frac{1}{2} \left(\gamma^\mu \gamma^\nu + \gamma^\nu \gamma^\mu \right) \partial_\mu \partial_\nu + m^2 \right) \Psi \\ &\overset{\text{(B.1.1)}}{=} (\partial_\mu \partial^\mu + m^2)\Psi \ . \end{aligned}$$

Solutions to the Klein-Gordon equation $(\partial_\mu \partial^\mu + m^2)\Psi = 0$ are plane waves $e^{-\mathrm{i}px}$, such that a solution to the Dirac equation can be written as

$$\Psi(x) = u(p) e^{-\mathrm{i}px}$$

with Dirac spinor $u(p)$.
For plane wave solutions $e^{\mathrm{i}px}$, we make the ansatz $\Psi(x) = v(p) e^{\mathrm{i}px}$.
In the rest frame of a particle with four momentum $p_0 = (m, \mathbf{0})$, there are two linearly independent solutions of (B.2.2) proportional to

$$u_s(p_0) = \sqrt{m} \begin{pmatrix} \xi_s \\ \xi_s \end{pmatrix} \quad ; \quad s = 1, 2$$

with $\xi_1 = \begin{pmatrix} 1 \\ 0 \end{pmatrix}$ and $\xi_2 = \begin{pmatrix} 0 \\ 1 \end{pmatrix}$.
In a general frame, a Dirac spinor $u(p)$ is obtained from the expression in the rest frame by applying a boost. For example, boosting p_0 along the 3 direction one obtains $E = m \cosh \eta$ and $p_3 = m \sinh \eta$ with rapidity η [32], so that $\sqrt{E + p_3} = \sqrt{m} \cdot e^{\frac{\eta}{2}}$ $(\star)$.
A spinor transforms in the spinor representation of the Lorentz group. Using (B.1.4),

we then obtain:

$$
\begin{aligned}
u(p) &= S(\Lambda_{03})u(p_0) \\
&= \exp\left[-\frac{i}{2}\omega_{03}\left(-\frac{i}{2}\begin{pmatrix}\sigma^3 & 0\\ 0 & -\sigma^3\end{pmatrix}\right)\right]\sqrt{m}\begin{pmatrix}\xi_s\\ \xi_s\end{pmatrix} \quad |\eta \equiv \frac{1}{2}\omega_{03} \\
&= \exp\left[-\frac{\eta}{2}\begin{pmatrix}\sigma^3 & 0\\ 0 & -\sigma^3\end{pmatrix}\right]\sqrt{m}\begin{pmatrix}\xi_s\\ \xi_s\end{pmatrix} \\
&= \exp\left[\begin{pmatrix}-\frac{\eta}{2} & 0 & 0 & 0\\ 0 & \frac{\eta}{2} & 0 & 0\\ 0 & 0 & \frac{\eta}{2} & 0\\ 0 & 0 & 0 & -\frac{\eta}{2}\end{pmatrix}\right]\sqrt{m}\begin{pmatrix}\xi_s\\ \xi_s\end{pmatrix} \quad |\exp(\mathbf{A}) = \sum_{k=0}^{\infty}\frac{\mathbf{A}^k}{k!} \\
&= \begin{pmatrix}\cosh\frac{\eta}{2}-\sinh\frac{\eta}{2} & 0 & 0 & 0\\ 0 & \cosh\frac{\eta}{2}+\sinh\frac{\eta}{2} & 0 & 0\\ 0 & 0 & \cosh\frac{\eta}{2}+\sinh\frac{\eta}{2} & 0\\ 0 & 0 & 0 & \cosh\frac{\eta}{2}-\sinh\frac{\eta}{2}\end{pmatrix} \\
&\quad \cdot\sqrt{m}\begin{pmatrix}\xi_s\\ \xi_s\end{pmatrix} \\
&= \begin{pmatrix}e^{-\frac{\eta}{2}} & 0 & 0 & 0\\ 0 & e^{\frac{\eta}{2}} & 0 & 0\\ 0 & 0 & e^{\frac{\eta}{2}} & 0\\ 0 & 0 & 0 & e^{-\frac{\eta}{2}}\end{pmatrix}\sqrt{m}\begin{pmatrix}\xi_s\\ \xi_s\end{pmatrix} \\
&= \begin{pmatrix}e^{\frac{\eta}{2}}\cdot\left(\frac{1-\sigma^3}{2}\right)+e^{-\frac{\eta}{2}}\cdot\left(\frac{1+\sigma^3}{2}\right) & 0\\ 0 & e^{\frac{\eta}{2}}\cdot\left(\frac{1+\sigma^3}{2}\right)+e^{-\frac{\eta}{2}}\cdot\left(\frac{1-\sigma^3}{2}\right)\end{pmatrix}\sqrt{m}\begin{pmatrix}\xi_s\\ \xi_s\end{pmatrix} \\
&\overset{(\star)}{=} \begin{pmatrix}\left(\sqrt{E+p_3}\left(\frac{1-\sigma^3}{2}\right)+\sqrt{E-p_3}\left(\frac{1+\sigma^3}{2}\right)\right)\xi_s\\ \left(\sqrt{E+p_3}\left(\frac{1+\sigma^3}{2}\right)+\sqrt{E-p_3}\left(\frac{1-\sigma^3}{2}\right)\right)\xi_s\end{pmatrix} \\
&= \begin{pmatrix}\sqrt{p\cdot\sigma}\xi_s\\ \sqrt{p\cdot\overline{\sigma}}\xi_s\end{pmatrix} \quad . \qquad \text{(B.2.4)}
\end{aligned}
$$

From (B.2.4) and the fact that $(p\cdot\sigma)(p\cdot\overline{\sigma}) = \begin{pmatrix}m^2 & 0\\ 0 & m^2\end{pmatrix}$, the field bilinears $\overline{u}(p')\Gamma u(p)$ of table B.1 follow:

$$
\begin{aligned}
\overline{u}(p)\mathbf{1}u(p) &= 2m\xi^\dagger\xi \qquad \text{(B.2.5)} \\
\overline{u}(p)\gamma_5 u(p) &= 0 \\
\overline{u}(p)\gamma_\mu u(p) &= \begin{pmatrix}2p^0 & (\xi^\dagger\xi)\\ 2p^i\sigma_i & (\xi^\dagger\sigma_i\xi)\end{pmatrix} \\
\overline{u}(p)\gamma_\mu\gamma_5 u(p) &= \begin{pmatrix}2p^i\,\sigma_i & (\xi^\dagger\sigma_i\xi)\\ 2p^0 & (\xi^\dagger\sigma_i\xi)\end{pmatrix} \quad . \qquad \text{(B.2.6)}
\end{aligned}
$$

The computation of the tensor is similar to the computation of the vector and the axial vector.

In the non-relativistic limit $v^i \ll 1$, the vector can be absorbed into the scalar,

$$\overline{u}(p)\gamma_\mu u(p) \to \begin{pmatrix} 2p^0 \ (\xi^\dagger \xi) \\ \mathcal{O}(v^i) \end{pmatrix} \ ,$$

and similary, the tensor can be absorbed into the axial vector.
The axial vector becomes

$$\overline{u}(p)\gamma_\mu\gamma_5 u(p) \to \begin{pmatrix} \mathcal{O}(v^i) \\ 2p^0 \ (\xi^\dagger \sigma_i \xi) \end{pmatrix} \ ,$$

where $\xi^\dagger \sigma_i \xi$ is a spin operator.
Thus, we see that in the non relativistic limit, the scalar and the axial vector are the relevant interactions.
The spinors $u(p)$ and $v(p)$ of a particle with mass m satisfy the spin summation rules:

$$\sum_{s=1}^{2} u_s(p)\overline{u}_s(p) = \not{p} + m \tag{B.2.7}$$

$$\sum_{s=1}^{2} v_s(p)\overline{v}_s(p) = \not{p} - m \ . \tag{B.2.8}$$

B.3 Charge Conjugation

For any fermion field $\Psi(x^\mu)$, there exists the charge conjugated field

$$\Psi^C(x^\mu) \equiv \mathbf{C}\overline{\Psi}^T(x^\mu) \ .$$

To get the transformation law of a spinor for $\Psi^C(x^\mu)$ under space-time rotations, the charge conjugation matrix $\mathbf{C}$ has to fulfill:

$$\mathbf{C}^{-1}\gamma_\mu\mathbf{C} = -\gamma_\mu^T \tag{B.3.1}$$

$$\mathbf{C}^\dagger = \mathbf{C}^{-1} \tag{B.3.2}$$

$$\mathbf{C}^T = -\mathbf{C} \ . \tag{B.3.3}$$

From (B.3.1),(B.3.2) and (B.3.3), it follows that $\overline{\Psi^C} = \Psi^T\mathbf{C}$.
Another useful relation concerns scalars involving the charge conjugation matrix $\mathbf{C}$. A scalar s fulfills $s^T = s$. The term $\overline{\Psi_1^C}\Psi_2$ is a scalar. It follows:

$$\overline{\Psi_1^C}\Psi_2 = (\overline{\Psi_1^C}\Psi_2)^T = (\Psi_1^T\mathbf{C}\Psi_2)^T = -\Psi_2^T\mathbf{C}^T\Psi_1 = \Psi_2^T\mathbf{C}\Psi_1 = \overline{\Psi_2^C}\Psi_1 \ . \tag{B.3.4}$$

The minus sign in the third step of (B.3.4) arises due to the anticommutation of Ψ_1 and Ψ_2. In the fourth step, we have used (B.3.3).
It can be shown that for any representation of the Lorentz group, the matrix $\mathbf{C}$ with the properties given above exists. In the special case of the four dimensional spinor

$\mathbf{\Gamma}$	Lorentz transformation	$\mathbf{C}$
1	scalar	+1
γ_5	pseudo-scalar	+1
γ_μ	vector	–1
$\gamma_\mu\gamma_5$	axial-vector	+1
$\frac{i}{2}[\gamma_\mu, \gamma_\nu]$	tensor	–1

Table B.1: Field bilinears

representation, $\mathbf{C} = i\gamma_2\gamma_0$.
A Majorana fermion field $\Psi_M(x^\mu)$ has the property that the charge conjugated field equals the original field: $(\Psi_M)^C(x^\mu) = \Psi_M(x^\mu)$.
If we express the Majorana fermion field $\Psi_M(x)$ in terms of creation and annihilation operators $\mathbf{b}^\dagger$ and $\mathbf{b}$,

$$\Psi_M(x) = \int \frac{d^3p}{(2\pi)^3\sqrt{2E_{\mathbf{p}}}} \sum_{s=1}^{2} \left(\mathbf{b}_s(\mathbf{p})u_s(\mathbf{p})\, e^{-\mathrm{i}px} + \mathbf{b}_s^\dagger(\mathbf{p})v_s(\mathbf{p})\, e^{\mathrm{i}px}\right) \quad . \tag{B.3.5}$$

Using that the charge conjugation matrix $\mathbf{C}$ relates the u and v spinors through

$$u_s(p) = \mathbf{C}\overline{v}_s^T(p) \tag{B.3.6}$$
$$v_s(p) = \mathbf{C}\overline{u}_s^T(p) \ , \tag{B.3.7}$$

and evaluate the transition amplitude $\Psi + \overline{\Psi^C} \to \varphi$ with B.3.1, B.3.2, B.3.6 and B.3.7, we find that the factor $\frac{1}{2}$ in the term (2.5.7) cancels [109].

B.4 Field Bilinears

Consider now a fermion Ψ. Let $\mathbf{\Gamma}$ be any 4×4 constant matrix. The term $\overline{\Psi}\,\mathbf{\Gamma}\,\Psi$ [32] has a definite transformation behaviour under the Lorentz group and under charge conjugation $\mathbf{C}$ for a specific choice of $\mathbf{\Gamma}$, see table B.1. Since a Majorana fermion Ψ_M satisfies $(\Psi_M)^C(x^\mu) = \Psi_M(x^\mu)$, those terms $\overline{\Psi}\,\mathbf{\Gamma}\,\Psi$ which transform non-trivially under charge conjugation $\mathbf{C}$ are forbidden for Ψ_M. In particular, there are no vector currents for Majorana fermions.

Appendix C

Two-Body Reactions

C.1 Mandelstam Variables

Two-body reactions (see figure C.1) are described with the Lorentz-invariant Mandelstam variables s, t, u defined by

$$s = (p_1 + p_2)^2 = (p_3 + p_4)^2 \quad \text{(C.1.1)}$$
$$t = (p_1 - p_3)^2 = (p_2 - p_4)^2 \quad \text{(C.1.2)}$$
$$u = (p_1 - p_4)^2 = (p_2 + -_3)^2 \quad \text{(C.1.3)}$$

and satisfying $s + t + u = m_1^2 + m_2^2 + m_3^2 + m_4^2$.

C.2 Cross Section

The reaction is characterized by the interactions involved in the process. These are accounted for in the calculation of $|\mathcal{M}|^2$, where the Lorentz invariant matrix element $\mathcal{M}$ is determined by use of the Feynman rules. $|\mathcal{M}|^2$ yields the observable cross section σ.
If fermions are involved in the interactions, then $\mathcal{M}$ contains γ matrices defined in Appendix B. In the calculation of $|\mathcal{M}|^2$ one then has to evaluate traces of γ matrices, which obey the following rules:

$$\text{tr}\,(\mathbf{1}_{4\times4}) = 4 \quad \text{(C.2.1)}$$
$$\text{tr (any odd \# of } \gamma\text{'s)} = 0 \quad \text{(C.2.2)}$$
$$\text{tr}\,(\gamma^\mu\gamma^\nu) = 4g^{\mu\nu} \quad \text{(C.2.3)}$$
$$\text{tr}\,(\gamma^\mu\gamma^\nu\gamma^\rho\gamma^\sigma) = 4\left(g^{\mu\nu}g^{\rho\sigma} - g^{\mu\rho}g^{\nu\sigma} + g^{\mu\sigma}g^{\nu\rho}\right) \quad \text{(C.2.4)}$$
$$\text{tr}\,(\gamma^5) = 0 \quad \text{(C.2.5)}$$
$$\text{tr}\,(\gamma^\mu\gamma^\nu\gamma^5) = 0 \quad \text{(C.2.6)}$$
$$\text{tr}\,(\gamma^\mu\gamma^\nu\gamma^\rho\gamma^\sigma\gamma^5) = -4i\epsilon^{\mu\nu\rho\sigma} \ . \quad \text{(C.2.7)}$$

Since most of the reactions we consider are s-channel-mediated annihilation reactions and are thus independently of the Mandelstam variable t, we find it convenient to calculate σ by integration of the differential cross section with respect to t:

$$\frac{d\sigma}{dt} = \frac{1}{64\pi s}\,\frac{1}{|\mathbf{p}_{1cm}|^2}|\mathcal{M}|^2 \ . \quad \text{(C.2.8)}$$

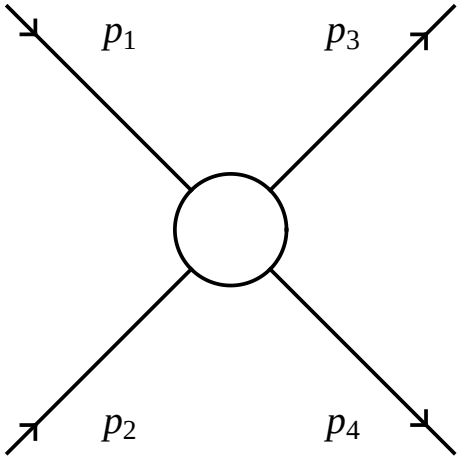

Figure C.1: Two-body reaction

The incoming momentum $\mathbf{p}_{1cm}$ in the center-of-mass system is given by $p_{1cm} = \sqrt{E_{1cm}^2 - m_1^2}$ with

$$E_{1cm} = \frac{s + m_1^2 - m_2^2}{2\sqrt{s}} \quad . \tag{C.2.9}$$

The integration limits of (C.2.8) are

$$t_0(t_1) = \left(\frac{m_1^2 - m_3^2 - m_2^2 + m_4^2}{2\sqrt{s}} \right)^2 - (p_{1cm} \mp p_{3cm})^2 \quad . \tag{C.2.10}$$

For equal massive initial state particles and equal massive final state particles, one obtains

$$t_0 - t_1 = \sqrt{(s - 4m_1^2)(s - 4m_3^2)} \quad . \tag{C.2.11}$$

Appendix D

Dimensional Regularization

We explain the suppression factors $\frac{1}{16\pi^2}$ arising in loop diagrams. Therefore, we use dimensional regularization. This appendix gives by no means a complete introduction to dimensional regularization.

D.1 Feynman Parameters

In radiative neutrino mass models, light neutrinos become massive at loop level, e.g., in the Zee-Babu model [27], the neutrino mass emerges at two-loop level.
Loop integrals can be divergent. A purely mathematical theory with divergencies is consistent, however, a physical theory with infinities is inconsistent because it will fail to make measurable predictions. Therefore, in physical theories divergencies have to be regularized.
Dimensional regularization is one technique to render the theory finite. One computes loop integrals in d dimensions from the very beginning and treats d as a complex variable. Then one performs the limit $d \to 4$.
To start with, one uses Feynman parameters $x_i\,; i = 1, ..., n$ to combine the propagator terms A_i in the loop integrals $\Pi_{j=1}^{m} \int \frac{d^d p_j}{(2\pi)^d}\,; m \leqq n$ [32]:

$$\frac{1}{A_1 A_2 ... A_n} = \int_0^1 dx_1 dx_2 ... dx_n\, \delta(\sum_{i=1}^{n} x_i - 1) \frac{(n-1)!}{(\sum_{i=1}^{n} x_i A_i)^n} \quad . \tag{D.1.1}$$

D.2 Loop Integrals

Observe that each A_i is quadratic in the integration variables p_j. For each p_j, one completes the square by shifting p_j to l_j, such that in (D.1.1) one is left with a denominator expression of the form $(l_j^2 - \Delta_j)^n$, where Δ_j is independent of p_j.
The remaining integrals are calculable:

$$\int \frac{d^d l_j}{(2\pi)^d} \frac{1}{(l_j^2 - \Delta_j)^n} = \frac{(-1)^n \,\mathrm{i}}{(4\pi)^{\frac{d}{2}}} \frac{\Gamma(n - \frac{d}{2})}{\Gamma(n)} \left(\frac{1}{\Delta_j}\right)^{n - \frac{d}{2}} \quad , \tag{D.2.1}$$

with the Gamma function

$$\Gamma(y) = \int_0^\infty dx\, x^{y-1} e^{-x} \quad .$$

A list of d-dimensional integrals is provided in [32].
If the integral in (D.2.1) converges, one can set $d = 4$. For non-converging integrals one expands $\Gamma(x)$ near its poles $x = -n$, $x = 0$ and takes the limit $d \to 4$ [32].

Appendix E

The Potential 4.2.1 in Terms of Higgs Mass Eigenstates

$$
\begin{aligned}
V(H_1,H_2) \;=\; & \Big(\mu_1^2 cw' + \mu_2^2 sw + \lambda_1 cw'^3 + \lambda_2 sw^3 + \frac{1}{2}\lambda_5 cw^2 w' + \frac{1}{2}\lambda_5 sww'^2 \\
& + \lambda_6 cw' k^{--}k^{++} + \lambda_8 swk^{--}k^{++} + \lambda_7 cw' h^- h^+ \\
& + \lambda_9 swh^- h^+ + \frac{1}{\sqrt{2}}\lambda_\mu \cos\beta k^{++}h^-h^-\Big) H_1 \\
& + \Big(-\mu_1^2 sw' + \mu_2^2 cw - \lambda_1 sw'^3 + \lambda_2 cw^3 - \frac{1}{2}\lambda_5 sw^2 w' + \frac{1}{2}\lambda_5 cww'^2 \\
& - \lambda_6 sw' k^{--}k^{++} + \lambda_8 cwk^{--}k^{++} - \lambda_7 sw' h^- h^+ \\
& + \lambda_9 cwh^- h^+ - \frac{1}{\sqrt{2}}\lambda_\mu \sin\beta k^{++}h^-h^-\Big) H_2 \\
& + \Big(\frac{1}{2}\mu_1^2 c^2 + \frac{1}{2}\mu_2^2 s^2 + \frac{3}{2}\lambda_1 c^2 w'^2 + \frac{3}{2}\lambda_2 s^2 w^2 \\
& + \frac{1}{4}\lambda_5 c^2 w^2 + \lambda_5 csww' + \frac{1}{4}\lambda_5 s^2 w'^2 \\
& + \frac{1}{2}\lambda_6 c^2 k^{--}k^{++} + \frac{1}{2}\lambda_8 s^2 k^{--}k^{++} + \frac{1}{2}\lambda_7 c^2 h^- h^+ + \frac{1}{2}\lambda_9 s^2 h^- h^+\Big) H_1^2 \\
& + \Big(\frac{1}{2}\mu_1^2 s^2 + \frac{1}{2}\mu_2^2 c^2 + \frac{3}{2}\lambda_1 s^2 w'^2 + \frac{3}{2}\lambda_2 c^2 w^2 \\
& + \frac{1}{4}\lambda_5 s^2 w^2 - \lambda_5 csww' + \frac{1}{4}\lambda_5 c^2 w'^2 \\
& + \frac{1}{2}\lambda_6 s^2 k^{--}k^{++} + \frac{1}{2}\lambda_8 c^2 k^{--}k^{++} + \frac{1}{2}\lambda_7 s^2 h^- h^+ + \frac{1}{2}\lambda_9 c^2 h^- h^+\Big) H_2^2 \\
& + \Big(\lambda_1 c^3 w' + \lambda_2 s^3 w + \frac{1}{2}\lambda_5 c^2 sw + \frac{1}{2}\lambda_5 cs^2 w'\Big) H_1^3 \\
& + \Big(-\lambda_1 s^3 w' + \lambda_2 c^3 w + \frac{1}{2}\lambda_5 s^2 cw - \frac{1}{2}\lambda_5 sc^2 w'\Big) H_2^3 \\
& + \Big(\frac{1}{4}\lambda_1 c^4 + \frac{1}{4}\lambda_2 s^4 + \frac{1}{4}\lambda_5 c^2 s^2\Big) H_1^4 + \Big(\frac{1}{4}\lambda_1 s^4 + \frac{1}{4}\lambda_2 c^4 + \frac{1}{4}\lambda_5 c^2 s^2\Big) H_2^4 \\
& + (...)
\end{aligned}
$$

$$
\begin{aligned}
V(H_1,H_2) \;=\;& (...)\\
&+\big(-\mu_1^2 cs+\mu_2^2 cs-3\lambda_1 csw'^2+3\lambda_2 csw^2\\
&-\frac{1}{2}\lambda_5 csw^2+\lambda_5 c^2 ww'-\lambda_5 s^2 ww'+\frac{1}{2}\lambda_5 csw'^2\\
&-\lambda_6 csk^{--}k^{++}+\lambda_8 csk^{--}k^{++}-\lambda_7 csh^- h^+ +\lambda_9 csh^- h^+\big)\, H_1H_2\\
&+\Big(-3\lambda_1 c^2 sw'+3\lambda_2 cs^2 w\\
&+\frac{1}{2}\lambda_5 c^3 w-\lambda_5 cs^2 w+\lambda_5 c^2 sw'-\frac{1}{2}\lambda_5 s^3 w'\Big)\, H_1^2H_2\\
&+\Big(3\lambda_1 s^2 cw'+3\lambda_2 sc^2 w\\
&+\frac{1}{2}\lambda_5 c^3 w'-\lambda_5 cs^2 w'-\lambda_5 c^2 sw+\frac{1}{2}\lambda_5 s^3 w\Big)\, H_2^2H_1\\
&+\left(\frac{3}{2}\lambda_1 c^2 s^2+\frac{3}{2}\lambda_2 c^2 s^2+\frac{1}{4}\lambda_5 c^4-\lambda_5 c^2 s^2+\frac{1}{4}\lambda_5 s^4\right) H_1^2H_2^2\\
&+\left(-\lambda_1 c^3 s+\lambda_2 s^3 c+\frac{1}{2}\lambda_5 c^3 s-\frac{1}{2}\lambda_5 cs^3\right) H_1^3H_2\\
&+\left(-\lambda_1 s^3 c+\lambda_2 c^3 s-\frac{1}{2}\lambda_5 c^3 s+\frac{1}{2}\lambda_5 cs^3\right) H_2^3H_1\\
&+\frac{1}{2}\mu_1^2 w'^2+\frac{1}{2}\mu_2^2 w^2+\frac{1}{4}\lambda_1 w'^4+\frac{1}{4}\lambda_2 w^4+\frac{1}{4}\lambda_5 w^2 w'^2\\
&+\mu_3^2 k^{--}k^{++}+\mu_4^2 h^- h^+\\
&+\lambda_3 (k^{--}k^{++})^2+\lambda_4 (h^- h^+)^2+\lambda_{10} k^{--}k^{++}h^- h^+\\
&+\frac{1}{2}\lambda_6 w'^2 k^{--}k^{++}+\frac{1}{2}\lambda_8 w^2 k^{--}k^{++}+\frac{1}{2}\lambda_7 w'^2 h^- h^+ +\frac{1}{2}\lambda_9 w^2 h^- h^+\\
&+\frac{1}{\sqrt{2}}\lambda_\mu w' k^{++}h^- h^-
\end{aligned}
$$

We have introduced the abbreviations

$$c \equiv \cos\beta \;,\; s \equiv \sin\beta.$$

Bibliography

[1] K. G. Begeman, A. H. Broeils, and R. H. Sanders, "*Extended rotation curves of spiral galaxies: Dark haloes and modified dynamics*", Mon. Not. Roy. Astron. Soc. **249** (1991) 523.

[2] **Supernova Cosmology Project** Collaboration, M. Kowalski *et al.*, "*Improved Cosmological Constraints from New, Old and Combined Supernova Datasets*", Astrophys. J. **686** (2008) 749–778, arXiv:0804.4142 [astro-ph].

[3] R. H. Cyburt, B. D. Fields, and K. A. Olive, "*A Bitter Pill: The Primordial Lithium Problem Worsens*", JCAP **0811** (2008) 012, arXiv:0808.2818 [astro-ph].

[4] **Particle Data Group** Collaboration, C. Amsler *et al.*, "*Review of particle physics*", Phys. Lett. **B667** (2008) 1.

[5] **The CDMS-II** Collaboration, Z. Ahmed *et al.*, "*Results from the Final Exposure of the CDMS II Experiment*", arXiv:0912.3592 [astro-ph.CO].

[6] **CDMS** Collaboration, Z. Ahmed *et al.*, "*Search for Weakly Interacting Massive Particles with the First Five-Tower Data from the Cryogenic Dark Matter Search at the Soudan Underground Laboratory*", Phys. Rev. Lett. **102** (2009) 011301, arXiv:0802.3530 [astro-ph].

[7] E. Armengaud *et al.*, "*First results of the EDELWEISS-II WIMP search using Ge cryogenic detectors with interleaved electrodes*", Phys. Lett. **B687** (2010) 294–298, arXiv:0912.0805 [astro-ph.CO].

[8] E. Aprile *et al.*, "*New Measurement of the Relative Scintillation Efficiency of Xenon Nuclear Recoils Below 10 keV*", Phys. Rev. **C79** (2009) 045807, arXiv:0810.0274 [astro-ph].

[9] V. N. Lebedenko *et al.*, "*Result from the First Science Run of the ZEPLIN-III Dark Matter Search Experiment*", Phys. Rev. **D80** (2009) 052010, arXiv:0812.1150 [astro-ph].

[10] J. R. Ellis, K. A. Olive, Y. Santoso, and V. C. Spanos, "*Update on the direct detection of supersymmetric dark matter*", Phys. Rev. **D71** (2005) 095007, arXiv:hep-ph/0502001.

[11] L. Roszkowski, R. Ruiz de Austri, and R. Trotta, "*Implications for the Constrained MSSM from a new prediction for $b \to s\gamma$*", JHEP **07** (2007) 075, arXiv:0705.2012 [hep-ph].

[12] **DAMA** Collaboration, R. Bernabei *et al.*, "*First results from DAMA/LIBRA and the combined results with DAMA/NaI*", Eur. Phys. J. **C56** (2008) 333–355, arXiv:0804.2741 [astro-ph].

[13] D. Tucker-Smith and N. Weiner, "*Inelastic dark matter*", Phys. Rev. **D64** (2001) 043502, arXiv:hep-ph/0101138.

[14] **XENON10** Collaboration, J. Angle *et al.*, "*Constraints on inelastic dark matter from XENON10*", Phys. Rev. **D80** (2009) 115005, arXiv:0910.3698 [astro-ph.CO].

[15] T. Schwetz-Mangold, *Dark Matter*. Univ. Heidelberg, 2009/2010. Lecture notes.

[16] **Fermi-LAT** Collaboration, A. A. Abdo *et al.*, "*Constraints on Cosmological Dark Matter Annihilation from the Fermi-LAT Isotropic Diffuse Gamma-Ray Measurement*", JCAP **1004** (2010) 014, arXiv:1002.4415 [astro-ph.CO].

[17] R. Gaitskell and F. J., "*The Dark Matter Community Website*". http://dendera.berkeley.edu/plotter/entryform.html.

[18] N. Okada and O. Seto, "*Higgs portal dark matter in the minimal gauged $U(1)_{B-L}$ model*", arXiv:1002.2525 [hep-ph].

[19] F. Zwicky, "*Spectral displacement of extra galactic nebulae*", Helv. Phys. Acta **6** (1933) 110–127.

[20] M. Milgrom, "*A Modification of the Newtonian dynamics as a possible alternative to the hidden mass hypothesis*", Astrophys. J. **270** (1983) 365–370.

[21] D. Clowe *et al.*, "*A direct empirical proof of the existence of dark matter*", Astrophys. J. **648** (2006) L109–L113, arXiv:astro-ph/0608407.

[22] R. Davis, K. Lande, C. K. Lee, B. T. Cleveland, and J. Ullman, "*Results of the Homestake chlorine solar neutrino experiment*",. In *Adelaide 1990, Proceedings, Cosmic ray, vol. 7* 155- 158.

[23] **SNO** Collaboration, F. Zhang, "*Recent results of SNO experiment*", Int. J. Mod. Phys. **A23** (2008) 3352–3357.

[24] **K2K** Collaboration, R. J. Wilkes, "*New results from Super-K and K2K*", arXiv:hep-ex/0212035.

[25] **KamLAND** Collaboration, S. Abe *et al.*, "*Precision Measurement of Neutrino Oscillation Parameters with KamLAND*", Phys. Rev. Lett. **100** (2008) 221803, arXiv:0801.4589 [hep-ex].

[26] E. Ma, "*Z_3 Dark Matter and Two-Loop Neutrino Mass*", Phys. Lett. **B662** (2008) 49–52, arXiv:0708.3371 [hep-ph].

[27] K. S. Babu, "*Model of 'Calculable' Majorana Neutrino Masses*", Phys. Lett. **B203** (1988) 132.

[28] K. Cheung and O. Seto, "*Phenomenology of TeV right-handed neutrino and the dark matter model*", Phys. Rev. **D69** (2004) 113009, arXiv:hep-ph/0403003.

[29] R. Schabinger and J. D. Wells, "*A minimal spontaneously broken hidden sector and its impact on Higgs boson physics at the Large Hadron Collider*", Phys. Rev. **D72** (2005) 093007, arXiv:hep-ph/0509209.

[30] E. W. Kolb and M. S. Turner, *The Early Universe*. Westview Press.

[31] M. Bohm, A. Denner, and H. Joos, "*Gauge theories of the strong and electroweak interaction*",. Stuttgart, Germany: Teubner (2001) 784 p.

[32] M. E. Peskin and D. V. Schroeder, *An Introduction to Quantum Field Theory*. Westview Press.

[33] N. Cabibbo, "*Unitary Symmetry and Leptonic Decays*", Phys. Rev. Lett. **10** (1963) 531–533.

[34] M. Kobayashi and T. Maskawa, "*CP Violation in the Renormalizable Theory of Weak Interaction*", Prog. Theor. Phys. **49** (1973) 652–657.

[35] N. Schmitz, *Neutrinophysik*. Teubner Stuttgart.

[36] T. Lasserre, "*LAUNCH 09: Neutrinos and Beyond*", in *Neutrinos Oscillations: Status, on-going and up-coming experiments*.

[37] M. C. Gonzalez-Garcia, M. Maltoni, and J. Salvado, "*Updated global fit to three neutrino mixing: status of the hints of theta*$13 > 0$", JHEP **04** (2010) 056, arXiv:1001.4524 [hep-ph].

[38] W. Rodejohann, "*On Non-Unitary Lepton Mixing and Neutrino Mass Observables*", Phys. Lett. **B684** (2010) 40–47, arXiv:0912.3388 [hep-ph].

[39] **KATRIN** Collaboration, J. A. Formaggio, "*Probing the absolute neutrino mass scale with the KATRIN experiment*",. Prepared for 18th International Conference on Particles and Nuclei (PANIC 08), Eilat, Israel, 9-14 Nov 2008.

[40] C. Kraus *et al.*, "*Final Results from phase II of the Mainz Neutrino Mass Search in Tritium β Decay*", Eur. Phys. J. **C40** (2005) 447–468, arXiv:hep-ex/0412056.

[41] D. Larson *et al.*, "*Seven-Year Wilkinson Microwave Anisotropy Probe (WMAP) Observations: Power Spectra and WMAP-Derived Parameters*", arXiv:1001.4635 [astro-ph.CO].

[42] S. Weinberg, "*Baryon and Lepton Nonconserving Processes*", Phys. Rev. Lett. **43** (1979) 1566–1570.

[43] E. Ma, "*Pathways to Naturally Small Neutrino Masses*", Phys. Rev. Lett. **81** (1998) 1171–1174, arXiv:hep-ph/9805219.

[44] M. E. Peskin and T. Takeuchi, "*Estimation of oblique electroweak corrections*", Phys. Rev. **D46** (1992) 381–409.

[45] G. Cacciapaglia, C. Csaki, G. Marandella, and A. Strumia, "*The minimal set of electroweak precision parameters*", Phys. Rev. **D74** (2006) 033011, arXiv:hep-ph/0604111.

[46] T. Appelquist, B. A. Dobrescu, and A. R. Hopper, "*Nonexotic neutral gauge bosons*", Phys. Rev. **D68** (2003) 035012, arXiv:hep-ph/0212073.

[47] M. S. Carena, A. Daleo, B. A. Dobrescu, and T. M. P. Tait, "*Z' gauge bosons at the Tevatron*", Phys. Rev. **D70** (2004) 093009, arXiv:hep-ph/0408098.

[48] D. Hilbert, "*Die Grundlagen der Physik*", Konigl. Gesell. d. Wiss. Goettingen, Nachr. Math.-Phys. Kl. (1915) 395.

[49] S. Blondin *et al.*, "*Time Dilation in Type Ia Supernova Spectra at High Redshift*", arXiv:0804.3595 [astro-ph].

[50] W. J. Percival *et al.*, "*Baryon Acoustic Oscillations in the Sloan Digital Sky Survey Data Release 7 Galaxy Sample*", Mon. Not. Roy. Astron. Soc. **401** (2010) 2148–2168, arXiv:0907.1660 [astro-ph.CO].

[51] R. Kessler *et al.*, "*First-year Sloan Digital Sky Survey-II (SDSS-II) Supernova Results: Hubble Diagram and Cosmological Parameters*", Astrophys. J. Suppl. **185** (2009) 32–84, arXiv:0908.4274 [astro-ph.CO].

[52] K. A. Olive, D. N. Schramm, and G. Steigman, "*Limits on New Superweakly Interacting Particles from Primordial Nucleosynthesis*", Nucl. Phys. **B180** (1981) 497.

[53] M. Taoso, G. Bertone, and A. Masiero, "*Dark Matter Candidates: A Ten-Point Test*", JCAP **0803** (2008) 022, arXiv:0711.4996 [astro-ph].

[54] P. Gondolo and G. Gelmini, "*Cosmic abundances of stable particles: Improved analysis*", Nucl. Phys. **B360** (1991) 145–179.

[55] B. W. Lee and S. Weinberg, "*Cosmological lower bound on heavy-neutrino masses*", Phys. Rev. Lett. **39** (1977) 165–168.

[56] R. J. Scherrer and M. S. Turner, "*On the Relic, Cosmic Abundance of Stable Weakly Interacting Massive Particles*", Phys. Rev. **D33** (1986) 1585.

[57] G. Bertone, D. Hooper, and J. Silk, "*Particle dark matter: Evidence, candidates and constraints*", Phys. Rept. **405** (2005) 279–390, arXiv:hep-ph/0404175.

[58] G. Jungman, M. Kamionkowski, and K. Griest, "*Supersymmetric dark matter*", Phys. Rept. **267** (1996) 195–373, arXiv:hep-ph/9506380.

[59] S. Bridle, "*The Matter and CMB Power Spectra*", Univ. College London .

[60] J. R. Primack, "*Whatever happened to hot dark matter?*", SLAC Beam Line **31N3** (2001) 50–57, arXiv:astro-ph/0112336.

[61] P. Peebles, *Principles of Physical Cosmology*. Princeton University Press.

[62] F. Bezrukov, H. Hettmansperger, and M. Lindner, "*keV sterile neutrino dark matter in gauge extensions of the standard model*", Phys. Rev. **D81** (2010) 085032, arXiv:0912.4415 [hep-ph].

[63] D. Hooper and E. A. Baltz, "*Strategies for Determining the Nature of Dark Matter*", Ann. Rev. Nucl. Part. Sci. **58** (2008) 293–314, arXiv:0802.0702 [hep-ph].

[64] P. Agrawal, Z. Chacko, C. Kilic, and R. K. Mishra, "*A Classification of Dark Matter Candidates with Primarily Spin-Dependent Interactions with Matter*", arXiv:1003.1912 [hep-ph].

[65] C. Munoz, "*Dark matter detection in the light of recent experimental results*", Int. J. Mod. Phys. **A19** (2004) 3093–3170, arXiv:hep-ph/0309346.

[66] G. Belanger, F. Boudjema, A. Pukhov, and A. Semenov, "*Dark matter direct detection rate in a generic model with micrOMEGAs2.1*", Comput. Phys. Commun. **180** (2009) 747–767, arXiv:0803.2360 [hep-ph].

[67] D. Tucker-Smith and N. Weiner, "*The status of inelastic dark matter*", Phys. Rev. **D72** (2005) 063509, arXiv:hep-ph/0402065.

[68] S. Chang, G. D. Kribs, D. Tucker-Smith, and N. Weiner, "*Inelastic Dark Matter in Light of DAMA/LIBRA*", Phys. Rev. **D79** (2009) 043513, arXiv:0807.2250 [hep-ph].

[69] E. A. Baltz and L. Bergstrom, "*Detection of leptonic dark matter*", Phys. Rev. **D67** (2003) 043516, arXiv:hep-ph/0211325.

[70] J. Lavalle, Q. Yuan, D. Maurin, and X. J. Bi, "*Full Calculation of Clumpiness Boost factors for Antimatter Cosmic Rays in the light of Λ CDM N-body simulation results*", arXiv:0709.3634 [astro-ph].

[71] J. F. Navarro, C. S. Frenk, and S. D. M. White, "*The Structure of Cold Dark Matter Halos*", Astrophys. J. **462** (1996) 563–575, arXiv:astro-ph/9508025.

[72] B. Moore, F. Governato, T. R. Quinn, J. Stadel, and G. Lake, "*Resolving the Structure of Cold Dark Matter Halos*", Astrophys. J. **499** (1998) L5, arXiv:astro-ph/9709051.

[73] J. Einasto, "*Influence of the atmospheric and instrumental dispersion on the brightness distribution in a galaxy*", Alma-Ata **51** (1965) .

[74] A. Klypin and F. Prada, "*Testing gravity with motion of satellites around galaxies: Newtonian gravity against Modified Newtonian Dynamics*", Astrophys. J. **690** (2009) 1488–1496, arXiv:0706.3554 [astro-ph].

[75] P. Ullio, L. Bergstrom, J. Edsjo, and C. G. Lacey, "*Cosmological dark matter annihilations into gamma-rays: A closer look*", Phys. Rev. **D66** (2002) 123502, arXiv:astro-ph/0207125.

[76] M. Boylan-Kolchin, V. Springel, S. D. M. White, A. Jenkins, and G. Lemson, "*Resolving Cosmic Structure Formation with the Millennium- II Simulation*", arXiv:0903.3041 [astro-ph.CO].

[77] J. S. Bullock *et al.*, "*Profiles of dark haloes: evolution, scatter, and environment*", Mon. Not. Roy. Astron. Soc. **321** (2001) 559–575, arXiv:astro-ph/9908159.

[78] M. Weber and W. de Boer, "*Determination of the Local Dark Matter Density in our Galaxy*", arXiv:0910.4272 [astro-ph.CO].

[79] M. J. Reid and A. Brunthaler, "*The Proper Motion of Sgr A*: II. The Mass of Sgr A**", Astrophys. J. **616** (2004) 872–884, arXiv:astro-ph/0408107.

[80] A. M. Ghez *et al.*, "*Measuring Distance and Properties of the Milky Way's Central Supermassive Black Hole with Stellar Orbits*", Astrophys. J. **689** (2008) 1044–1062, arXiv:0808.2870 [astro-ph].

[81] S. E. Koposov, H.-W. Rix, and D. W. Hogg, "*Constraining the Milky Way potential with a 6-D phase- space map of the GD-1 stellar stream*", Astrophys. J. **712** (2010) 260–273, arXiv:0907.1085 [astro-ph.GA].

[82] C. McCabe, "*The Astrophysical Uncertainties Of Dark Matter Direct Detection Experiments*", arXiv:1005.0579 [hep-ph].

[83] A. Cuoco, A. Sellerholm, J. Conrad, and S. Hannestad, "*Anisotropies in the Diffuse Gamma-Ray Background from Dark Matter with Fermi LAT: a closer look*", arXiv:1005.0843 [astro-ph.HE].

[84] E. A. Baltz, M. Battaglia, M. E. Peskin, and T. Wizansky, "*Determination of dark matter properties at high-energy colliders*", Phys. Rev. **D74** (2006) 103521, arXiv:hep-ph/0602187.

[85] J. van der Bij and M. J. G. Veltman, "*Two Loop Large Higgs Mass Correction to the rho Parameter*", Nucl. Phys. **B231** (1984) 205.

[86] K. L. McDonald and B. H. J. McKellar, "*Evaluating the two loop diagram responsible for neutrino mass in Babu's model*", arXiv:hep-ph/0309270.

[87] K. S. Babu and C. Macesanu, "*Two-loop neutrino mass generation and its experimental consequences*", Phys. Rev. **D67** (2003) 073010, arXiv:hep-ph/0212058.

[88] D. Aristizabal Sierra and M. Hirsch, "*Experimental tests for the Babu-Zee two-loop model of Majorana neutrino masses*", JHEP **12** (2006) 052, arXiv:hep-ph/0609307.

[89] S. L. Glashow and S. Weinberg, "*Natural Conservation Laws for Neutral Currents*", Phys. Rev. **D15** (1977) 1958.

[90] J. T. Ruderman and T. Volansky, "*Decaying into the Hidden Sector*", JHEP **02** (2010) 024, arXiv:0908.1570 [hep-ph].

[91] W. Grimus, L. Lavoura, O. M. Ogreid, and P. Osland, "*A precision constraint on multi-Higgs-doublet models*", J. Phys. **G35** (2008) 075001, arXiv:0711.4022 [hep-ph].

[92] S. Profumo, M. J. Ramsey-Musolf, and G. Shaughnessy, "*Singlet Higgs Phenomenology and the Electroweak Phase Transition*", JHEP **08** (2007) 010, arXiv:0705.2425 [hep-ph].

[93] Y. B. Zeldovich, I. Y. Kobzarev, and L. B. Okun, "*Cosmological Consequences of the Spontaneous Breakdown of Discrete Symmetry*", Zh. Eksp. Teor. Fiz. **67** (1974) 3–11.

[94] A. Vilenkin, "*Cosmic strings and other topological defects*",. In *Kyoto 1985, Proceedings, Quantum Gravity and Cosmology*, 269-302.

[95] Y. Chikashige, R. N. Mohapatra, and R. D. Peccei, "*Are There Real Goldstone Bosons Associated with Broken Lepton Number?*", Phys. Lett. **B98** (1981) 265.

[96] A. S. Joshipura and J. W. F. Valle, "*Invisible Higgs decays and neutrino physics*", Nucl. Phys. **B397** (1993) 105–122.

[97] V. Barger, P. Langacker, M. McCaskey, M. Ramsey-Musolf, and G. Shaughnessy, "*Complex Singlet Extension of the Standard Model*", Phys. Rev. **D79** (2009) 015018, arXiv:0811.0393 [hep-ph].

[98] G. B. Gelmini and M. Roncadelli, "*Left-Handed Neutrino Mass Scale and Spontaneously Broken Lepton Number*", Phys. Lett. **B99** (1981) 411.

[99] P. Langacker, "*Electroweak physics beyond the standard model*",. Invited talk given at Int. Workshop on Electroweak Physics Beyond the Standard Model, Valencia, Spain, Oct 2-5, 1991.

[100] L. Ackerman, M. R. Buckley, S. M. Carroll, and M. Kamionkowski, "*Dark Matter and Dark Radiation*", Phys. Rev. **D79** (2009) 023519, arXiv:0810.5126 [hep-ph].

[101] N. F. Bell, J. B. Dent, T. D. Jacques, and T. J. Weiler, "*Electroweak Bremsstrahlung in Dark Matter Annihilation*", Phys. Rev. **D78** (2008) 083540, arXiv:0805.3423 [hep-ph].

[102] A. Semenov, "*LanHEP - a package for the automatic generation of Feynman rules in field theory. Version 3.0*", Comput. Phys. Commun. **180** (2009) 431–454, arXiv:0805.0555 [hep-ph].

[103] M. Abramowitz and I. A. Stegun, eds., *Handbook of Mathematical Functions*. Dover Publications, Inc., New York, 1972.

[104] K. Griest and D. Seckel, "*Three exceptions in the calculation of relic abundances*", Phys. Rev. **D43** (1991) 3191–3203.

[105] M. Nebot, J. F. Oliver, D. Palao, and A. Santamaria, "*Prospects for the Zee-Babu Model at the LHC and low energy experiments*", Phys. Rev. **D77** (2008) 093013, arXiv:0711.0483 [hep-ph].

[106] P. Langacker, "*The Physics of Heavy Z' Gauge Bosons*", Rev. Mod. Phys. **81** (2008) 1199–1228, arXiv:0801.1345 [hep-ph].

[107] **CDF** Collaboration, A. Abulencia *et al.*, "*Search for $Z' \to e^+e^-$ using dielectron mass and angular distribution*", Phys. Rev. Lett. **96** (2006) 211801, arXiv:hep-ex/0602045.

[108] M. Maggiore, *A Modern Introduction to Quantum Field Theory*. Oxford University Press.

[109] H. E. Haber and G. L. Kane, "*The Search for Supersymmetry: Probing Physics Beyond the Standard Model*", Phys. Rept. **117** (1985) 75–263.

Index

Acknowledgment

I would like to express my acknowledgment to those I was accompanied by during the course of this work: to my supervisor Manfred Lindner; to my collaborators Thomas Schwetz-Mangold and Pei-Hong Gu; to secretary Anja Berneiser; to my former and current colleagues Hans Hettmansperger, Michael Dürr, Nico Kronberg, Felix Kahlhöfer, Alexander Dück, Angnis Schmidt-May, Julian Heeck, Joachim Kopp, Tom Underwood, Adisorn Adulpravitchai, Martin Holthausen, Alexander Merle, Alexander Kartavtsev, Andreas Hohenegger, Viviana Niro, Ryo Takahashi, James Berry, Werner Rodejohann, Fedor Bezrukov and Evgeny Akhmedov; to my friends Julia & Heinrich Klein and Sebastian Meuren; and to my parents Rita & Michael Schmidt.
It was an honor for me to carry out this thesis in Manfred Lindner's Particle and Astroparticle Physics Division because the working research topics challenge exactly the problems which aroused my interest in physics. I am cordially thankful to Manfred Lindner for his encouragement and guidance.
Special thanks go to Thomas Schwetz-Mangold and Pei-Hong Gu for nice collaboration.
I thank Alexander Merle for providing advice on Mathematica; and Michael Dürr, Nico Kronberg and Alexander Kartavtsev for computer assistance.
For proofreading this work I am indebted to Michael Dürr, Nico Kronberg and Andreas Hohenegger.
I am deeply grateful to Manfred Lindner for granting me permission to attend the Summer School in Cosmology at the Abdus Salam International Centre for Theoretical Physics (ICTP) in Miramare, Trieste. At the ICTP I gained important scientific experiences and became friends with interesting people.

Ewige Dankbarkeit schulde ich meinen Eltern Rita & Michael Schmidt.

Liebe Mama, Lieber Papa,

Ich bin sehr stolz, euch als Eltern zu haben.
Ihr fördert immer meine Interessen; vor allem,
Ihr habt es mir ermöglicht, Physik in Heidelberg zu studieren.
Ihr steht mir immer zur Seite mit guten Ratschlägen für alle Lebensbereiche.
Ihr seid immer da, wenn Eure Hilfe gebraucht wird.

Danke!

Erklärung:

Ich versichere, dass ich diese Arbeit selbständig verfasst und keine anderen als die angegebenen Quellen und Hilfsmittel benutzt habe.

Heidelberg, den 01.09.2010

.....
(Daniel Schmidt)